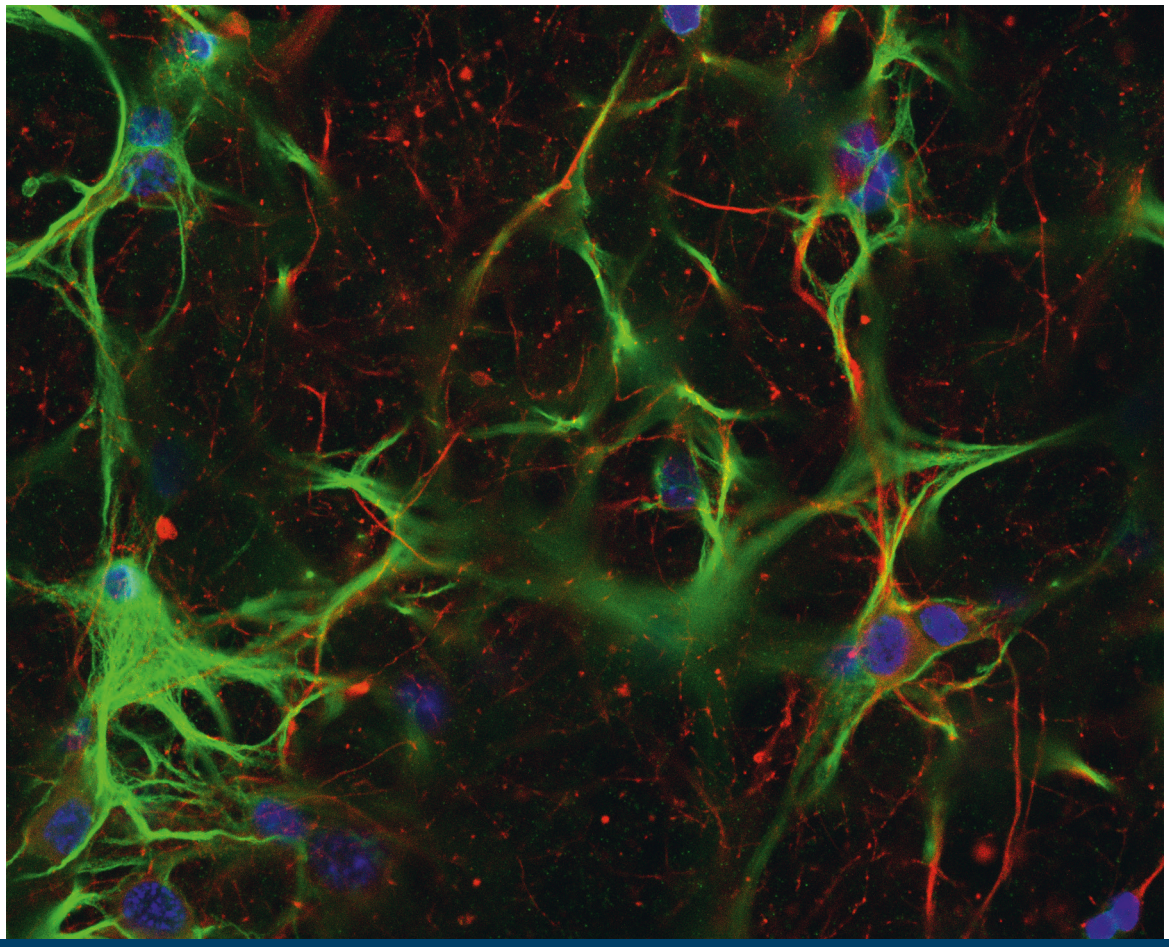

Hybrid hydrogels promote physiological functionality of long-term cultured primary neuronal cells in vitro

Corinna Meeßen

Information
Band / Volume 83
ISBN 978-3-95806-643-4

Mitglied der Helmholtz-Gemeinschaft

JÜLICH
Forschungszentrum

Schriften des Forschungszentrums Jülich
Reihe Information / Information Band / Volume 83

Forschungszentrum Jülich GmbH
Institut für Biologische Informationsprozesse (IBI)
Bioelektronik (IBI-3)

Hybrid hydrogels promote physiological functionality of long-term cultured primary neuronal cells in vitro

Corinna Meeßen

Schriften des Forschungszentrums Jülich
Reihe Information / Information Band / Volume 83

ISSN 1866-1777 ISBN 978-3-95806-643-4

Bibliografische Information der Deutschen Nationalbibliothek.
Die Deutsche Nationalbibliothek verzeichnet diese Publikation in der
Deutschen Nationalbibliografie; detaillierte Bibliografische Daten
sind im Internet über http://dnb.d-nb.de abrufbar.

Herausgeber und Vertrieb:	Forschungszentrum Jülich GmbH Zentralbibliothek, Verlag 52425 Jülich Tel.: +49 2461 61-5368 Fax: +49 2461 61-6103 zb-publikation@fz-juelich.de www.fz-juelich.de/zb
Umschlaggestaltung:	Grafische Medien, Forschungszentrum Jülich GmbH
Druck:	Grafische Medien, Forschungszentrum Jülich GmbH
Copyright:	Forschungszentrum Jülich 2022

Schriften des Forschungszentrums Jülich
Reihe Information / Information, Band / Volume 83

D 82 (Diss. RWTH Aachen University, 2021)

ISSN 1866-1777
ISBN 978-3-95806-643-4

Vollständig frei verfügbar über das Publikationsportal des Forschungszentrums Jülich (JuSER)
unter www.fz-juelich.de/zb/openaccess.

Eidesstattliche Erklärung

Ich, Corinna Meeßen, erkläre hiermit, dass diese Dissertation und die darin dargelegten Inhalte die eigenen sind und selbstständig, als Ergebnis der eigenen originären Forschung, generiert wurden.
Hiermit erkläre ich an Eides statt

- Diese Arbeit wurde vollständig oder größtenteils in der Phase als Doktorand dieser Fakultät und Universitätangefertigt;
- Sofern irgendein Bestandteil dieser Dissertation zuvor für einen akademischen Abschluss oder eine andere Qualifikation an dieser oder einer anderen Institution verwendet wurde, wurde dies klar angezeigt;
- Wenn immer andere eigene- oder Veröffentlichungen Dritter herangezogen wurden, wurden diese klar benannt;
- Wenn aus anderen eigenen-oder Veröffentlichungen Dritter zitiert wurde, wurde stets die Quelle hierfür angegeben. Diese Dissertation ist vollständig meine eigene Arbeit, mit der Ausnahme solcher Zitate;
- Alle wesentlichen Quellen vonUnterstützung wurden benannt;
- Wennimmer ein Teil dieser Dissertation auf derZusammenarbeit mit anderen basiert, wurde von mir klar gekennzeichnet, was von anderen und was von mir selbst erarbeitet wurde;
- Kein Teil dieser Arbeit wurde vor deren Einreichung veröffentlicht.

Die Dissertation hat keiner anderen Prüfungsbehörde vorgelegen.

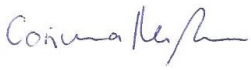

Abstract

This study aimed to develop and establish a modular system for the 3D cultivation of primary neuronal cells, with the desirable tuneability in mechanical and chemical properties, while enhancing the cell viability for long-term studies. It could be shown that the novel Collagen-PVP-*co*-$GMA_{3}mol\%$ biohybrid hydrogel promote physiological development of functional cortical networks. Primary cortical cells had been transfected with GCaMP6f to record spontaneous neuronal activity over 40 days *in vitro*. Network dynamics had been estimated based on generalized transfer entropy (GTE), showing the development of a functional network of balanced segregation and integration, with a strong emerging ability for resilience over 40 days in culture. Synchronous network activity could be observed already at *day in vitro* (DIV) 8-9 in absence of external stimuli. Further, a correlation of network maturation as well as functional development with increasing molecular weight of PVP could be shown. With decreasing polymer chain length, neurite outgrowth and network maturation are significantly promoted. The addition of PVP to collagen was demonstrated to not only support network functionality and growth, but also prevent the degradation of the hydrogel.

Zusammenfassung

Ziel dieser Dissertation ist die Entwicklung und Etablierung eines modularen Systems mit der gewünschten Abstimmbarkeit der mechanischen und chemischen Eigenschaften, zur Langzeitkultivierung von primären neuronalen Zellen. Es konnte gezeigt werden, dass das neue biohybride Gel aus Kollagen-PVP-*co*-GMA$_{3}mol\%$ die physiologische Entwicklung funktioneller kortikaler Netzwerke fördert. Zellen wurden mit GCaMP6f transfiziert, um die spontane Aktivität über 40 Tage *in vitro* (DIV) zu beobachten. Die Netzwerkdynamik wurde basierend auf der "generalized Transfer Entropy" (GTE) berechnet. Dabei konnte die Entwicklung eines funktionalen Netzwerks mit ausgewogener Segregation und Integration sowie der Ausbildung einer starken Widerstandsfähigkeit gegen äußere Beeinträchtigungen gezeigt werden. Eine synchrone Aktivität der Zellen konnte bereits an DIV8-9 ohne die Reizung durch externe Stimuli beobachtet werden. Desweiteren zeigte sich eine negative Korrelation der der morphologischen und funktionellen Netzwerkentwicklung mit zunehmendem Molekulargewicht des PVP. Mit abnehmender Polymerkettenlänge werden das Neuritenwachstum und die Netzwerkreifung signifikant gefördert. Außerdem wurde gezeigt, dass die Zugabe von PVP zu Kollagen nicht nur die Netzwerkfunktionalität und das Netzwerkwachstum unterstützt, sondern auch den Abbau des Hydrogels verhindert.

Contents

1. Introduction

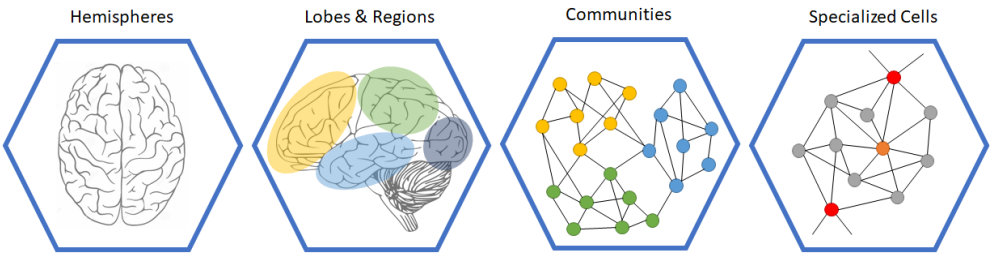

Figure 1.1.: Schematic representation of different levels of human brain organization. Brain icons are modified from [1, 2].

The human brain is the most complex organ in the human body, consisting of about 86 billion neurons, and is probably one of the least understood organs. [3] The brain is spatially and functionally organized in different levels (see fig. 1.1), and can be classified into three main parts: (1) the cerebrum, (2) the cerebellum and (3) the brain stem. The cerebrum again separates up into two hemispheres, each consisting of four lobes. These lobes comprise different areas, specialized in their function. The networks, comprised in these areas, are optimized in performance based on subdividing into interconnected clusters. Special cell types within these communities affect the networks' ability for fast and specialized processing (see chapter 2.5, p.17).

In neurodegenerative diseases, dysfunctions of these complex organized networks are caused. Fifty neurodegenerative diseases are assigned to dementia, such as Alzheimer, which is the most abundant and incurable form. In Germany every year about 200.000 new infections add.[4] Certainly, the repair of neurodegenerative diseases is still challenging. The characteristic neural loss causes ataxia and dementia. Neurons in the central nervous system (CNS) cannot replace themselves naturally due to cell-secreted molecules that inhibit regeneration.[5] So far, treatments of such diseases include a detailed disease pathogenesis and a long-term prevention of further tissue damage.[6] Current research focuses on the understanding of the molecular and cellular reasons of neuronal dysfunction, injury but also understanding physiological functionalities.

From literature it is known that cell adhesion molecules (CAMs) affect intracellular signaling pathways.[7] At that point CAMs can display properties way beyond the simple adhesion of cells to their surrounding matrix and other cells.[8, 9, 10, 11] For example, ECM and integrin aberrations are thought to cause synaptic dysfunctions in Alzheimer and also Epilepsy.[12, 13, 14] Sheng et al. obtained the indirect activation of Ca^{2+} channels by CAMs.[7] Calcium is a secondary signaling messenger, regulated by voltage gated ion channels in the neuronal cell membrane.[15] The influx of calcium ions into the cells is known to initiate the release of neurotransmitters, in order to transmit action potentials to the next neuron (see section 2.2, p. 4). One of the most well-known neurotransmitters are gamma-aminobutyric acid (GABA) and Glutamate.[16] However, the majority of common neurological or psychiatric drugs act on other signaling molecules, without even knowing their way of transmission.[3]

Although 2D cell cultures revealed essential knowledge about the functionalities of neurons, there is a growing demand for experiments of higher complexity, as present *in vivo*. During the past years, researchers came up with different approaches of three dimensional (3D) models of the human brain (see chapter 2.3, p.7).[17] Hydrogels, as a powerful tool to mimic the natural ECM (see chapter 2.3, p. 7), facilitate the physiological development of neuronal networks. They became the most prominent and versatile used scaffolds in tissue engineering, i.a. due to their high-water content and physiological promoting characteristics. These include e.g. the support of cell survival, differentiation, and proliferation due to tissue like properties, which are based on the chemistry of the chosen polymer.[18]

Other approaches, such as spheroids or organoids, also support the physiological growth and function of neuronal networks, almost without the need of scaffold support (see chapter 2.3, p.7). Nevertheless Hydrogels entail the possibility of specifically designing the desired environment.

The presented work focuses on the development of a biohybrid hydrogel system, which is tunable in the desired chemical and rheological properties. The established model allows the growth of physiological functioning primary neuronal networks over 40 days *in vitro* (DIV). Thus enabling studies on drug development, and permitting clinical relevant research. The present study shows the improvement in persistence of networks grown in natural hydrogels by the addition of the synthetic polymer polyvinylpyrrolidone (PVP). Besides the ability for long-term cultivation, also physiological network development could be shown and analyzed using calcium imaging technology. Furthermore, it allows specific modification by biofunctionalization of the gel. Thereby e.g. distinct adhesion ligands and their influence on signal processing can be evaluated. Also applications beyond neurobiological research may be of great interest. For instance hydrogels used as coatings for chronically implanted devices make full use of the potential revealed by the presented new biohybrid hydrogel (see chapter 10, p. 83).

2. Background

2.1. The extracellular matrix of the central nervous system

Generally, the human brain's extracellular matrix (ECM) consists of water ions, glycoproteins, proteoglycans, hyaluronic acid and fibrous proteins, [19] and comprises 10-20% of the brains volume [20, 21, 22]. It is secreted from a complex network of proteins and glycans, serving as structural and chemical support of cells. Structural promotion is defined by cell adhesion points and allowing the formation of distinct CNS regions. Chemical support instead provides cell guidance by various molecular signals which also improves viability and functionality of the network.[23] According to Lau et al. the structure of the CNS ECM consists of three compartments (see fig. 2.1): the basal lamina, perineural nets and the neural interstitial matrix.

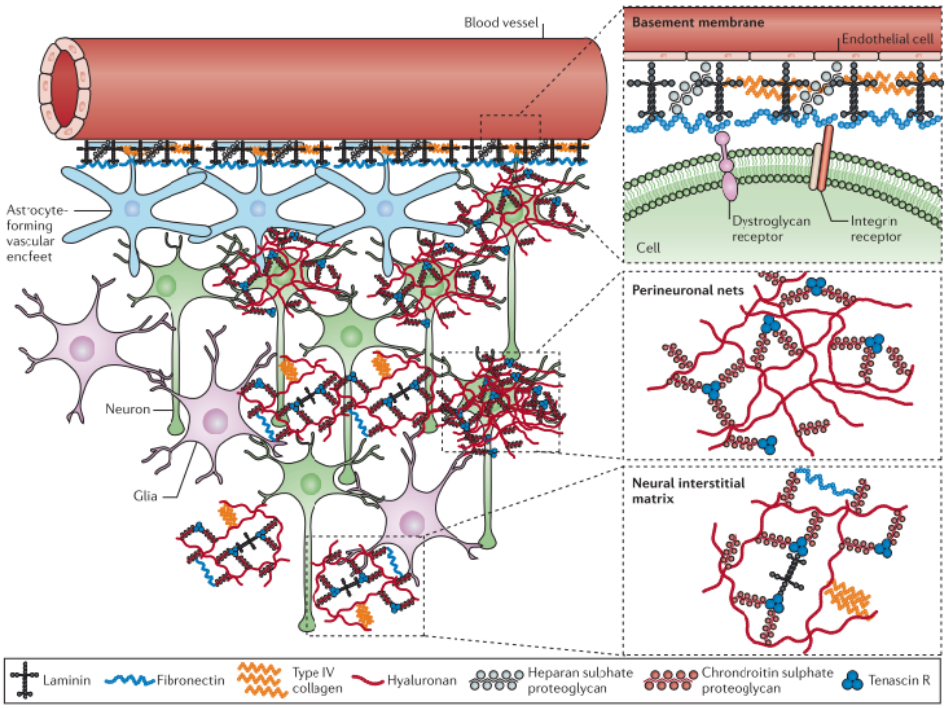

Figure 2.1.: ECM compartements of the central nervous system. Figure from [23].

Basal lamina

The basal lamina is the functional link between endothelial cells and the CNS parenchymal tissue, spanning the pial surface of the CNS. Its main components are collagen, laminin-nidogen complexes, fibronectin, dystroglycan and perlecan.

Perineural nets (PNNs)

PNNs are mesh structures surrounding neuronal cell bodies and proximal dendrites. Its main components are hyaluronan, link proteins, chondroitin sulfate proteoglycans and tenascin-R.[24, 25, 26, 27] It has been shown that these complex matrices play a substantial role in the control of CNS plasticity. According to several research groups, PNNs surround highly active neurons, are emphasizing its functional support features.[28, 29, 30, 31]

Neural interstitial matrix

The neural interstitial matrix represents the matrix between cells in the CNS. It is composed of proteoglycans, hyaluronan, tenascins and link proteins. Besides small amounts of fibrous proteins, such as collagen and elastin, adhesive glyco- proteins like laminin and fibronectin are present.[23]

2.2. Basics of neuronal communication

Neurons are the functional elements of the nervous system and can be divided into three main parts: the axon, cell body and dendrites (see fig. 2.2). The electrical excitability allows the transmission of information, as action potentials (APs), between neurons via synapses. Dendrites gather most of synaptic input with respect to its degree of arborization. From the dendrites the information is transferred through the cell body, containing the nucleus and organelles, to the axon hillock for further processing. According to the level of depolarization, an AP is generated and transmitted to the axon terminals. Synapses allow to pass the information from an axon terminal to the dendritic process of another neuron using neurotransmitters. Incoming APs cause the influx of calcium ions through voltage gated ion channels and Ca^{2+} binds to the soluble N-ethylmaleimide-sensitive-factor attachment receptor (SNARE) complex. Thus, neurotransmitter filled vesicles merge into the presynaptic membrane and empty into the synaptic cleft. Released neurotransmitter diffuse towards the postsynaptic membrane and bind to ion channel gated receptors, causing a depolarization, termed postsynaptic potential.[32]

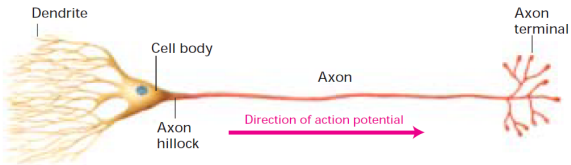

Figure 2.2.: Schematic structure of a neuron. A neuron is a polarized cell, composed of dendrites on one side and an axon on the other. Dendrites receive information and transmit the action potential through the axon to the axon terminals. There signal is transmitted to the following neuron via synapses. Figure from [33].

2.2.1. Action potential

Neurons communicate via the transmission of changes in the membrane potential. In resting state an electrical potential, resting potential, of about -70 mV is caused by a concentration gradient between intra- and extracellular space. The rise of an action potential (AP) requires a sufficient voltage change to overcome the threshold of about -55 mV in the cell membrane. Once the threshold is exaggerated, a membrane depolarization occurs. Voltage gated sodium channels open and sodium ions enter the neuron according to the concentration gradient, until overvalue the relative potassium efflux. The AP peak is reached and the sodium channels close and the phase of repolarization begins. Sodium channels close and potassium channels open, allowing K^+ influx right up to a membrane hyperpolarization. The resting potential then will be restored by a sodium/potassium pump. After an AP occurred the neuron is in a state of almost non-excitability, the refractory period (RP). While an absolute RP precludes a further excitation, a relative RP allows APs in case of stronger stimuli appearing.[32]

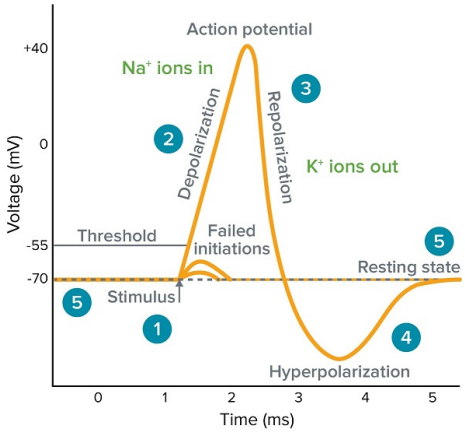

Figure 2.3.: Schematic of an action potential. Details given in text. Figure from [33].

2.2.2. Chemical synapse

At a chemical synapse, the electrical AP is transformed into a chemical signal via the release of neurotransmitters into the synaptic cleft. The synaptic cleft is defined as a narrow region, of about 20μm, between an axon terminal of the presynaptic neuron and the dendrite of the postsynaptic neuron. Incoming AP cause the influx of Calcium ions by activating voltage gated ion channels. These Ca^{2+} ions bind to the SNARE-complex, which is responsible for the fusion of vesicles with the membrane. Synaptic vesicles comprise neurotransmitters, as GABA or Glutamate, which are then released into the synaptic cleft. These neurotransmitter diffuse to the dendritic membrane of the postsynaptic neuron and bind to ion channel coupled receptors. These channels open, causing a depolarization and probably an AP.[34, 32]

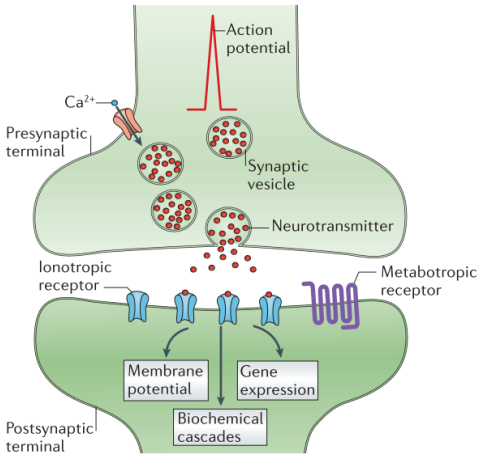

Figure 2.4.: Schematic of a chemical synapse. At the chemical synapse the electrical action potential is translated into a chemical signal and transferred from the axon of the presynaptic cell to the following postsynaptic dendrite. Details are given in text. Figure adapted from [34].

2.3. Mimics of the human brain

Over the last decades 3D cell cultures became of great interest, as depicted in figure 2.5, showing the increased number of publications on 3D cultures.[35] The focus on 3D environments, rather than traditional 2D cell cultures, arises from the growing interest for more clinical relevant studies. Nonetheless 2D cell cultures revealed substantial knowledge about basic functionalities of the human brain. Mina J. Bissell presented a major milestone with emphasizing the crucial role of the ECM, surrounding tissues and organs, in her work published in the Journal of Theoretical Biology, 1982.[36] Roughly eleven years later, the concept of tissue engineering emerged and PEG hydrogels had been used for cell cultures.[37, 38, 39] Since then, constantly new approaches of 3D cell cultivation methods and materials are developed. Of these numerous methods around, the three main ones will be introduced in the following, in respect to neuroscientific applications.

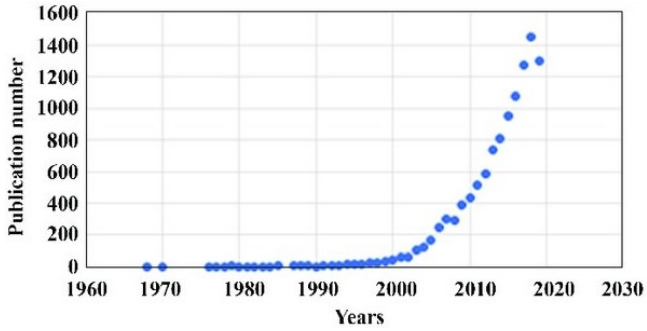

Figure 2.5.: Schematic showing the growing urge for more complex and physiological relevant environments *in vitro*, by depicting the number of publications on 3D cultures. Figure from [35].

2.3.1. Organoids

Organoids are *in vitro* mimics of organs derived from stem cells with addition of specific growth factors to the medium at certain time points. Prof. Dr. Hans Clever, of the Hubrecht Institute in Utrecht, the Netherlands, invented these 3D constructs in 2009. For this purpose Toshiro Sato used Matrigel as initiating growth scaffold, facilitating the de novo development of intestinal crypt tissue.[40] This breaking through discovery was the inspiration for Prof. Dr. Madeline Lancaster, of the MRC Laboratory of Molecular Biology in Cambridge, UK, to use Matrigel for developing cerebral organoids.[41]

Her work, published 2013 in Nature, impelled organoid research in neuroscience. The grown cerebral organoids exhibited distinct regions similar to the developing human brain. Even the development of retinal tissue could be shown. Furthermore they could model some aspects of the neurological disease microcephaly, defined by a dramatic loss of neural tissue volume. Subsequently there was a significant increase in research published on brain organoids.[42]

Inevitable leading to the question: "How well do brain organoids capture your brain?"[43] This question is the caption of a recently published critical view on the scientific relevance of brain organoids, by Kim et al. in iScience - CellPress. They formulate challenges and potentialities

of brain organoids from various aspects, regarding the applicability of research results onto medical issues. Figure 2.6 graphically shows limitations and similarities with the human brain of current brain organoids. To conclude, brain organoids, at the current stage, are a powerful tool to investigate early stage development and modeling neurological diseases emerging at early stages. Future work needs to scope especially gyrification and the lack of a fully functional microenvironment, among others. For a more detailed review the reader is referred to the publication of Kim et al. (2021).[43]

In order to overcome topographic limitations, a method of organoid fusion was invented recently. Therefore, separate organoids, patterned for specific brain regions are grown and then merged.[44] Applications in neuroscience, such as brain organoid vascularization and brain tumor research, already showed promising potentials of this new method.[44]

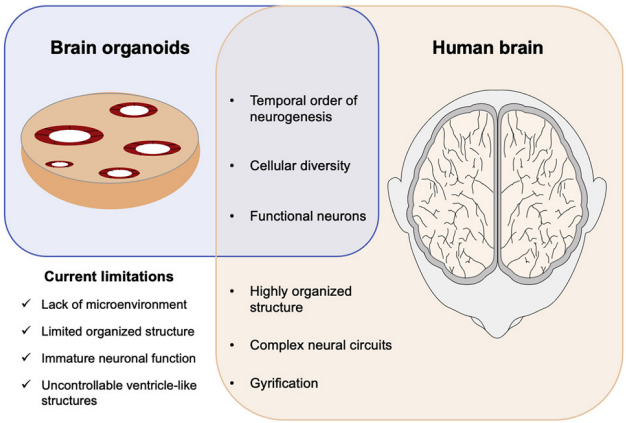

Figure 2.6.: Comparability of brain organoids with the human brain. Details given in text. Figure from [43].

2.3.2. Spheroids

Spheroids are commonly scaffold-free 3D cell cultures, originating from self-assembly (see fig. 2.7). In this case, cells in suspension innately form loose aggregates due to integrin-ECM interactions. This causes an upregulation of cadherin expression and accumulation. Finally, cadherin-cadherin bindings cause the formation of strong aggregates, termed multi-cellular spheroids (MCS). The cell-ECM interaction can be supported by the addition of a hydrogel. The formation of spheroids requires a low adhesion environment, e.g. via repellent culture plates or the popular hanging drop model.[45]

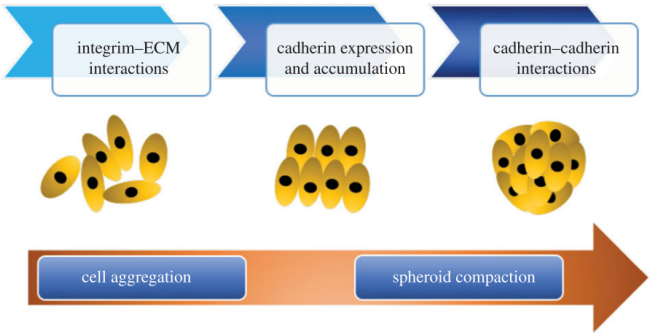

Figure 2.7.: Schematic of spheroid formation. The formation of spheroids can be distinguished into two phases: (1) cell aggregation and (2) spheroid compaction. Figure from [45].

Figure 2.8 depicts the spatial organization of spheroids into different metabolic zones. These zones are significantly influenced by the size of the aggregate. The necrotic core is commonly a hypoxic area, due to insufficient nutrient and oxygen supply. The lack of vasculature causes a reduced diffusion of substances towards the core, initiating with a size of about 1 to 2 mm. Instead cells at the outer zone have a high oxygen and nutrient supply, enhancing growth and proliferation. The establishment of this metabolic zones make spheroids to the most powerful tool to mimic the physical tumor microenvironment.[46]

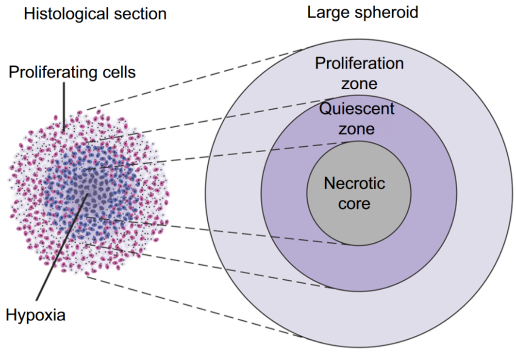

Figure 2.8.: Spatial organization of a spheroid. Spheroids can be distinguished into three metabolic zones: (1) necrotic core, (2) quiescent zone and the (3) proliferation zone. Figure from [46].

In neuroscience, spheroids are used as a tool to mimic partial tissue components. Herein, commonly the forebrain or cerebral development is investigated.[47, 48, 49, 50] Also applications in disease modeling and drug screening had been reported.[51, 52, 53]

As well as organoids, spheroids highly suffer from heterogeneity and reproducibility. A huge lack constitutes the varying sizes of aggregates, leading to distinct stages of cell differentiation and cell types within one batch.[17]

2.3.3. Hydrogels

Compared to previously introduced biologically driven approaches, hydrogels reflect the more engineering way of mimicking the ECM *in vitro*. Hydrogels are a beneficial environment to build a matrix close to the native tissue, due to its high water content similar to biological tissues.[54] Furthermore they comprise a high biocompatibility owing to it's native origin. The latter also promotes a good biodegradability, important for many regenerative basic approaches. Also they share mechanical properties with soft tissues.

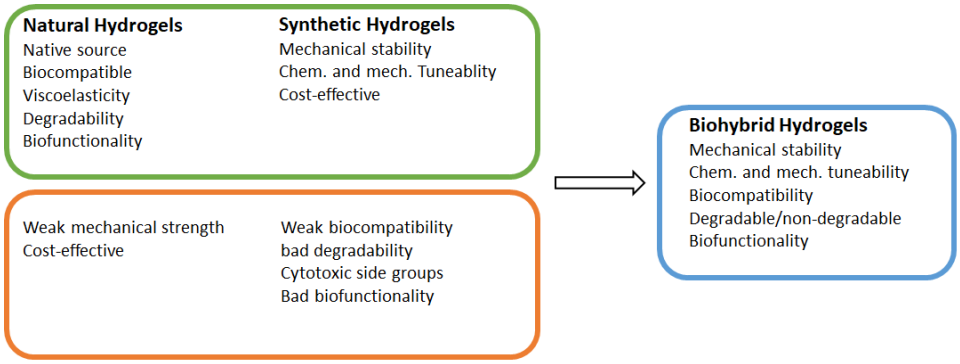

Figure 2.9.: Hydrogel classification by its sources, showing their advantages and disadvantages.

Hydrogels can be classified into three major groups: naturally and synthetically derived scaffolds, and hybrid materials (see fig. 2.9). **Synthetic Hydrogels** generally promote strong rheological properties. Their main advantage is the controllability in their mechanical and chemical properties. Besides, the fabrication is mostly more cost-effective compared to natural polymers derived from animal or human sources.[55] Most popular synthetic polymers are: polyvinylpyrrolidone (PVP), polylactic adid (PLA), polyethylene glycol (PEG) and polyvinyl alcohol (PVA). Despite the compelling advantage of controllability, synthetic hydrogels also carry some disadvantages. Especially, they inherently show low cell adhesiveness.[55] Functionalization with adhesive motifs can enhance cell attachement, thus increasing cell viability and functionality.

Naturally derived hydrogels are able to mimic the components of the native ECM and enhance the cell viability due to a larger cell-surface contact area. They are usually based on proteins (e.g. collagen, fibrin, gelatin) or polysaccharides (e.g. chitosan, alginate, hyaluronic acid) of the native ECM.[56] Besides biofunctionality these hydrogels possess biocompatibil-

ity, degradability and low cytotoxicity.[56] Additionally cell adhesion is provided through integrin binding domains.[57] Well investigated scaffold materials are alginate, chitosan, fibrin and collagen.[58, 59, 60, 61, 62, 63] Also decellularized tissue is used as natural matrix especially in tissue engineering applications.[64, 65, 66]

Hybrid hydrogels combine the advantageous properties of natural and synthetic polymers. While the latter increases the mechanical strength of the hydrogel, natural polymers contribute great cell adhesiveness.[67]

As the brain lacks the capacity of self-regeneration, hydrogels are attracting widespread interest in fields of CNS repair and neuroprotection. Thereby its main application is as a reservoir of i.a. neurotrophic factors or drugs.[68] Neural tissue engineering faces four strategic categories: "(a) incorporation of guidance cues, (b) factors to promote cell adhesion and proliferation, (c) drug delivery components, and (d) electrical conductivity of the tissue supporting matrix".[69] Also the ordinary modeling of neurodegenerative diseases, such as Alzheimer's disease and epilepsy, generated considerable research interest in hydrogel-based cultivation systems *in vitro*. The investigation of neuronal network communication exposed to higher complexity, became of great interest during the past years.

Also the presented work aims the development of a proper cultivation environment for the investigation of complex neuronal networks *in vitro*, of a higher biological relevance. The following section elaborates requirements and challenges related to the development of hydrogel-based cultivation systems, which have to be faced in neuroscience.

2.4. Requirements and challenges of Hydrogels for neuroscience

This section will introduce the requirements and challenges that have to be faced in engineering hydrogels for neuroscientific applications (see fig. 2.10). Thereby, only physiological relevant issues will be discussed. Environmental properties in diseases can significantly differ from healthy tissue, as e.g. in brain tumors.[70, 71]

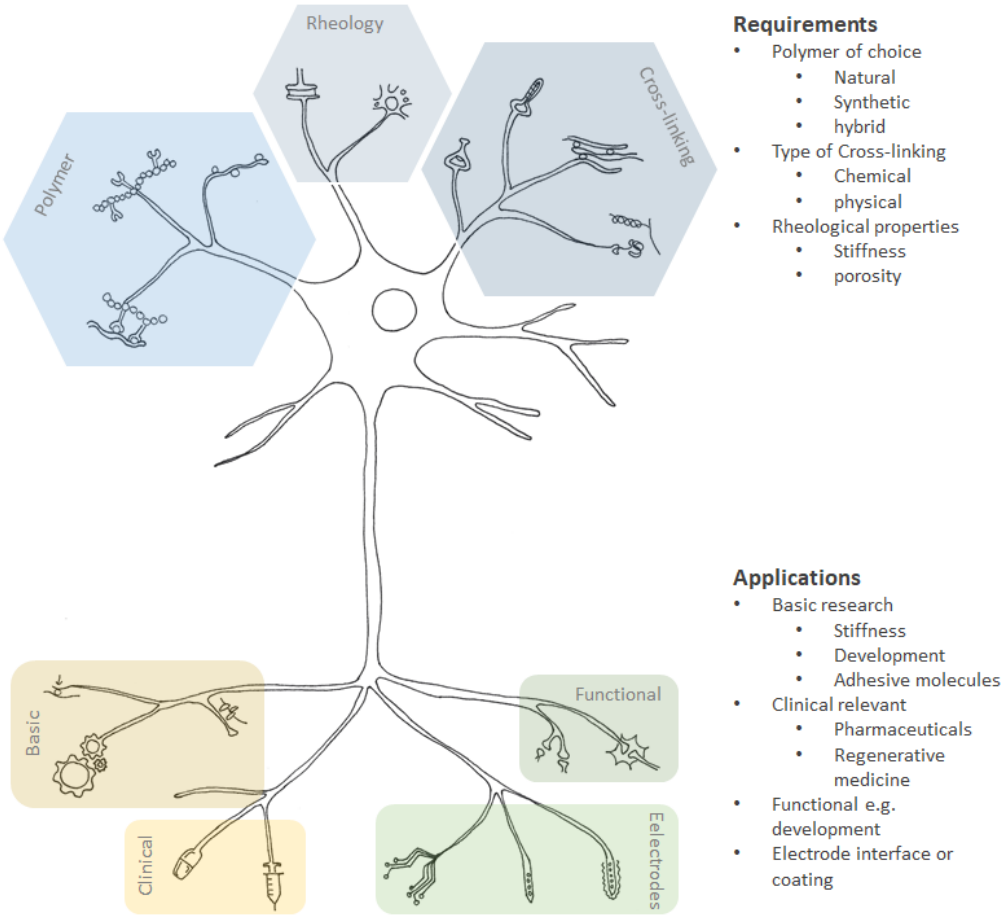

Figure 2.10.: Schematic showing the main requirements of hydrogel engineering for neuroscientific applications.

The design of a hydrogel can drastically affect the health and functionality of the underlying cell culture. Aside from biological functionality, such as cell adhesiveness, also physical characteristics play an important role in tissue function and structural integrity in the CNS. Cells sense and react to mechanical cues, a process called mechanotransduction.[72] Thereby, mechanical force is translated into biochemical signals, affecting tissue specific differentiation and homeostasis.[73]The rodent and human brain is assumed to be a viscoelastic material with a Poisson's ratio of 0.5 and an elastic modulus ranging from 0.1 to 16 kPa.[74] Recently it has been shown that physical and chemical cues of a scaffolds can control cell viability, differentiation, outgrowth and function. These include mechanical properties, topography, surface chemistry and biological ligands.[75] In order to convey and maintain a physiological behavior of the cultured cells, it is a crucial step to mimic their natural environment at best.

Therefore, the careful design, individually tailored for the tissue of interest, is of high importance. The presented work aims to mimic the environmental conditions of the CNS, likewise remaining variable in chemical and mechanical properties. Figure 2.10 shows schematically the requirements and inputs, affecting the network growth and functionality for various applications. Mechanical behavior, such as elasticity, can be influenced by the type of cross-linking (see fig. 2.11). Chemical cross-linking is formed by covalent bonding, which is known to support elasticity. Instead, physical cross-linking emerges from non-covalent interactions, resulting in viscoelastic behavior (see fig. 2.11).[18] Photopolymerization became an attractive method for regenerative medicine, in particular for hydrogels which are cross-linked directly in the body. Advantage of this method is the fast polymerization time and homogeneous hydrogels formed. Nevertheless, the photoinitiator has to be chosen carefully, as some are highly toxic.[76]

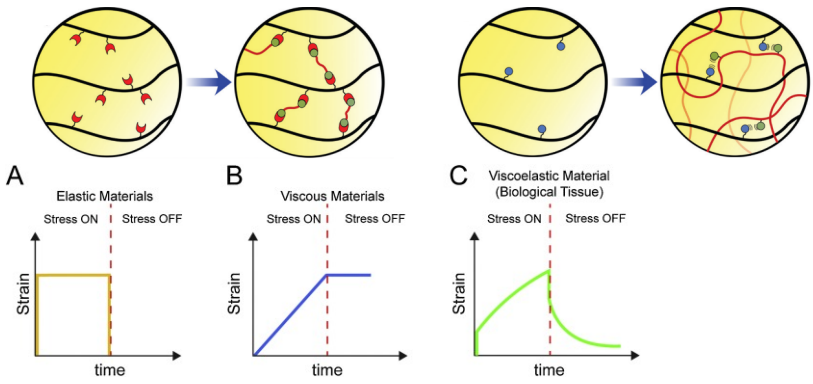

Figure 2.11.: Chemical and mechanical properties of hydrogels. Hydrogels can be distinguished by its type of cross-linking. Chemical cross-linking is formed by covalent bonds, while physical cross-linked by molecular entaglement and non-covalent bonds. Figure adapted from [18]. Besides chemical categorization, also mechanical properties characterizes hydrogels. Natural polymer show viscoelasticity, as well as native tissue. Figure from [77].

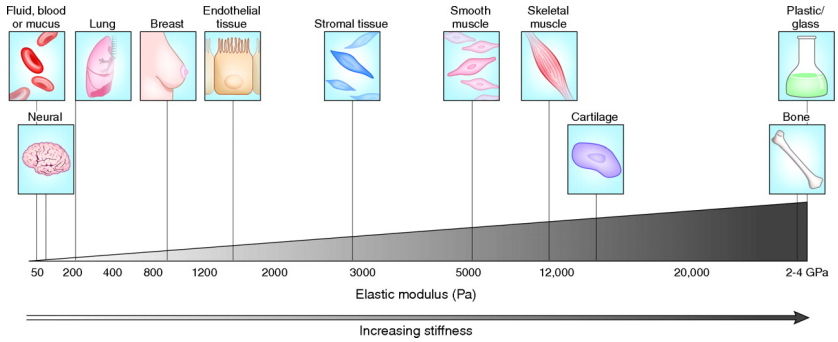

Figure 2.12.: Scale of varying stiffness between tissues. The brain is one of the softest tissues in the human body. Depending on the measurement, it's stiffness ranges from 0.1 to 16 kPa.[74] This behavior arises from different mechanical loads affecting the tissues. While bones experience high mechanical loads, the brain is a mechanical static tissue. Figure from [78].

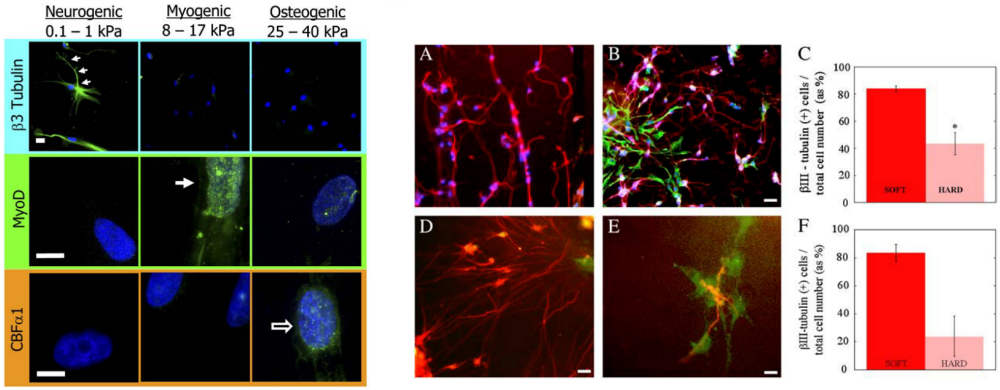

Figure 2.13.: Influence of environmental stiffness on cell behavior. Stiff substrates promote the differentiation of hMSCs into osteogenic cells, and soft environment supports the differentiation of hMSCs into neuronal cells. (left) Figure from [79]. Astrocytes prefer, contrary to neruons, stiffer environments to grow. (right) Figure from [80].

The human brain is known to be one of the softest organs in the human body (see fig. 2.12). Depending on the method applied, the stiffness of the human brain varies between 0.1 and 16 kPa.[74] As the main component of the CNS' ECM is non-fibrillar, the elastic modulus is decreased.[71] Up to now, most cell cultivation environments of neuronal cells did not consider both, stiffness and viscoelastic properties, leading to opposing cell behavior compared to *in vivo*.[81]

Numerous experiments have shown that neurons are highly sensitive to their surrounding environment. The drastic effect of matrix stiffness on cell behavior was shown most imposing by the pioneering work of Engler et al..[79] Human mesenchymal stem cells differentiated spontaneously into neuronal cells on soft substrates, while moderate stiffness supported muscular cell growth and stiffer environments promoted the differentiation into osteogenic cells (see fig. 2.13, left).[79, 81] With increasing stiffness, cell viability, differentiation, migration and axonal length are enhanced. In comparison, astrocytes show opposing behavior (see fig. 2.13, right). With increasing substrate stiffness, astrocytes show more physiological morphology and growth.[80]This controversy makes it challanging to find the proper balance of mechanical propterties, suitable for multi-cellular cultures in hydrogels. Nevertheless, astrocytes are important feeding cells for neuronal networks.[82] It was clearly shown, that neurons in the presence of astrocytes, show enhanced cell viability and functionality.[83, 84]

A straight forward way to increase the mechanical strength of a hydrogel, is to increase the degree of cross-linking or the molecular weight of the polymer.[81]Thereby, the handling of the hydrogel system should also be covered regarding the application of interest, as extremely soft hydrogels tend to be very fragile. Hydrogels designed for e.g. on-chip evaluation should be considered to promote a strong adhesiveness to the substrate coating, rather than a floating culture. In case of dynamic medium flow, e.g. supported by a pumping system, hydrogels should provide sufficient mechanical strength to withstand the shear forces generated in the cultivation environment.

The cross-linking degree also affects the viscoelastic properties of a hydrogel, as the stress relaxation time increases with stronger cross-linking.[81] As previously mentioned, the brain exhibits strong viscoelastic behavior. Many naturally occurring polymers share this properties, making e.g. collagen a widely recognized polymer in neuroscience.[81] Comparable to stiffness, viscoelasticity positively influences neuronal cell growth. It was shown, that with constant stiffness and enhanced viscoelasticity, cell spreading, proliferation and differentiation are supported.[81, 85] However, it has to be noted that most literature mainly rely on viscoplastic substrates instead of viscoelastic materials.[85] Viscoplasticity, contrary to viscoelasticity, does not fully recover from deformation (see fig. 2.14, top).[86]

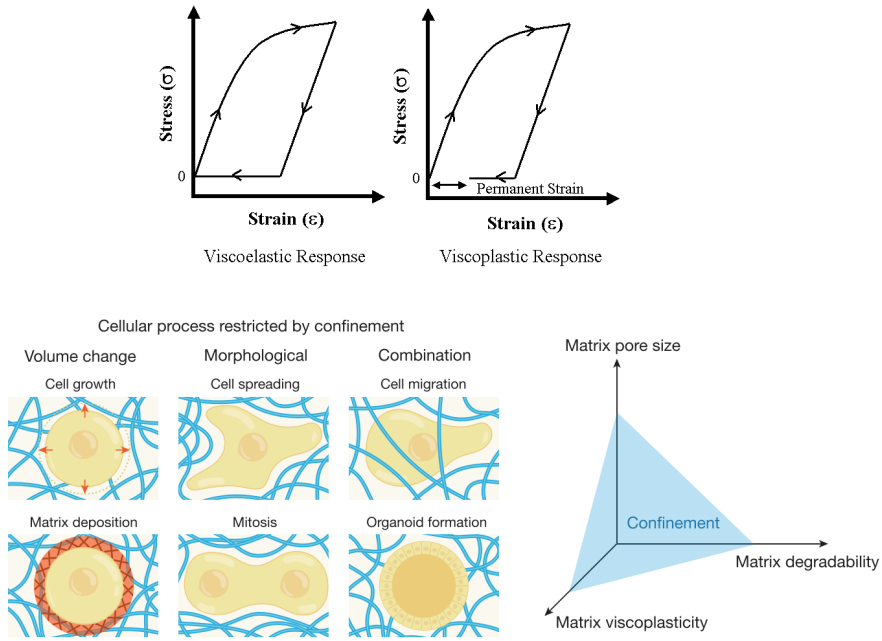

Figure 2.14.: Viscoelasticity and mechanical confinement. Charts of viscoelasticity and viscoplasticity (top). Schematic illustration of dynamic cell behaviors and mechanical confinement (bottom). Figures from [85, 86].

However, some cellular processes are restricted by mechanical confinement, which is regulated by the matrix pore size, viscoplasticity and degradability (see fig. 2.14, bottom). The porosity of a hydrogel has influence on diverse issues of a healthy cell culture. A high porosity enhances the diffusion of nutrients and oxygen. Pores smaller than 10 μm restrict cell movement and negatively influence cell viability. Another issue affecting diffusion, is the size of the substrate. It was shown in organoids, that sufficient nutrient and oxygen supply, without the support of a dynamic medium flow, is limited by 1 to 2 mm.[87] Matrix degradability plays a key role in those cellular processes, especially in case of rigid or elastic pores [85], providing a dynamic environment. It was shown that matrix remodeling is a key property in maintaining the stemness of neuronal progenitor cells.[88] Further, Schultz et al. (2015) revealed the mechanical importance of dynamic hydrogel environments. They observed the change of an elastic hydrogel into a viscoelastic fluid by cellular remodeling.[85, 89] Changes in viscoelasticity are known to be a key regulative factor in many diseases, such as Alzheimer's disease.[90, 91] However, a detailed understanding of mechanotransduction and developmental cellular behavior in viscoelastic materials is limited.[85]

2.5. Network analysis and graph theory

Graph theory became the conventional mathematical tool for the description of complex real-life brain networks. It is based on the distinction between **nodes and edges**. Depending on which scale (macro-, meso- or microscale) we consider the brain network, the definition of nodes and edges is different. In the presented work, the mesoscale network functioanlity was examined. Therefore nodes are defined as single neurons and edges, also called links, are characterizing the connection between two different nodes. Graphs can be classified as **weighted or binary** and **directed or undirected** graphs (see fig. 2.15). While weighted graphs preserve information about the presence or absence of connections, as well as their strength, binary graphs miss the latter information.[92] Further complexity can be reached by adding the preferred information flow direction, called directed graphs (see fig. 2.15).

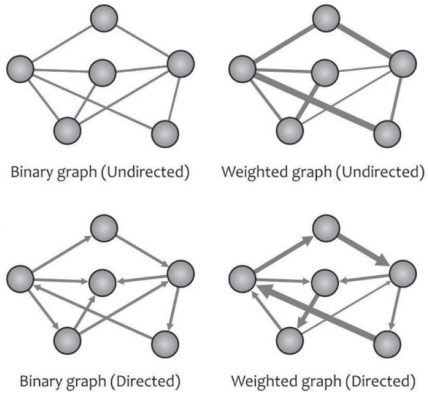

Figure 2.15.: Schematic showing the difference between binary directed and undirected and weighted directed and undirected graphs. Figure from [93].

When analyzing complex network behavior, one has to carefully differentiate the underlying **network types**. The definition of network connectivity is highly influencing the interpretation of analysis. **Anatomical or structural networks** reflect the physical characteristics of regional information. In contrast **functional networks** are defined by cross-correlations between spike time-series of different nodes. **Effective networks**, instead, reflect causal dependencies between two neurons, where the activity of a neuron directly affects another network component (see fig. 2.16).[92, 94]

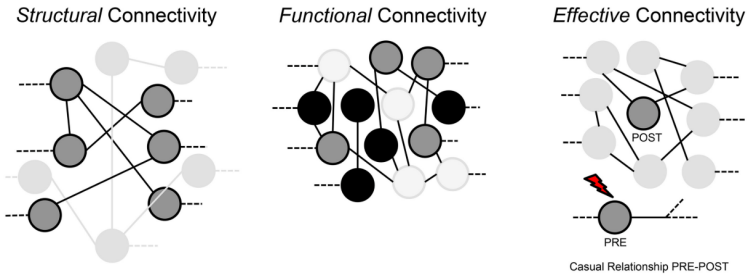

Figure 2.16.: Differentiation of structural, functional and effective connectivity. Figure from [94].

2.5.1. Functional connectivity estimation

Complex network activity can be described and estimated by so called connectivity matrices. These matrices reflect the dependency of two neurons in a network with values ranging from zero to one. Correlations of one imply a connectivity of node i and j in a network. As described in the previous section 2.5, it is important to define the type of network to be analyzed. In this project functional connectivity was of interest. Figure 2.17 depicts the most common algorithms used in literature. The computation of functional connectivity can be divided into model-free and model-based methods, relating to their type of estimate.[95, 96] This thesis focuses on directed estimates, while introducing the most commonly used model-based and model-free method respectively.

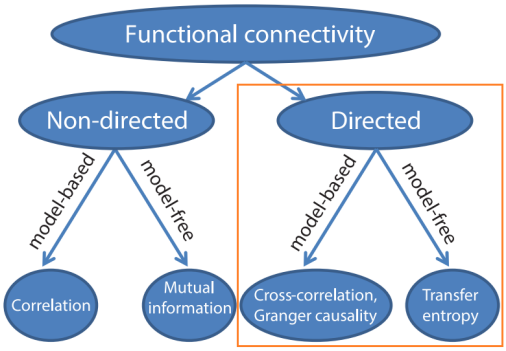

Figure 2.17.: Most common methods used to estimate functional connectivity and it's differentiation. Figure adapted from [95].

One of the most well-known statistical, model-based approach is Cross correlation (CC), whereas Transfer Entropy (TE) is the most widely established information theoretic, model-free estimate of functional connectivity. Both methods will be briefly introduced in the following. Exemplary matrices shown below had been computed using a sample data set with simultaneously high synchronized and single events (see fig. 2.18), for illustrative purposes. The eventual data analysis will be presented in section 8, p.59 .

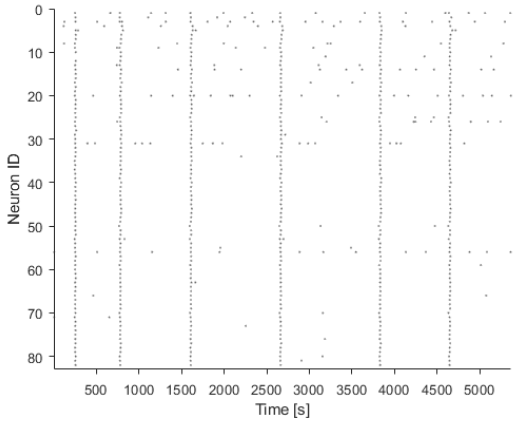

Figure 2.18.: Rasterplot of sample data used for testing different approaches to infer functional connectivity.

Cross correlation (CC) is a modification of the Pearson's correlation coefficient (PCC), which denotes the time-domain linear measure of two random nodes. CC finds the maximum correlation between two time series of which one has the lag τ as a function of τ [96, 97, 98], giving a connectivity matrix with the weighted connection strength between two given nodes (see fig. 2.19). A high correlation value indicates a strong functional connectivity between two given nodes.

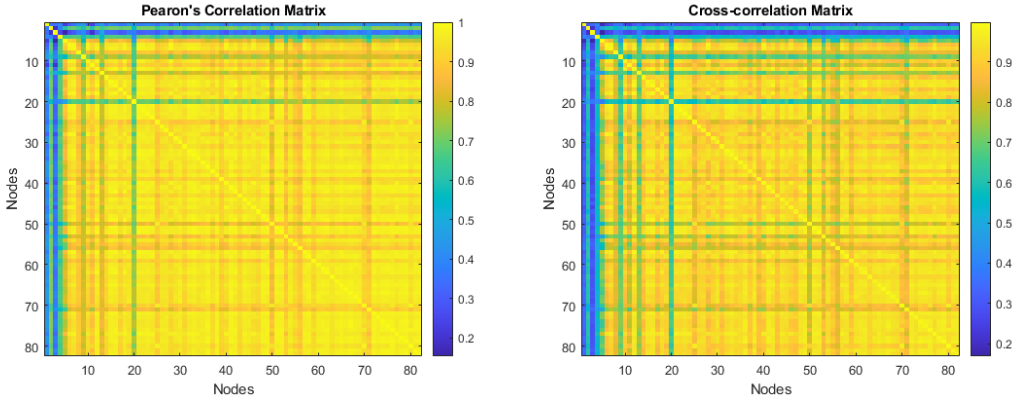

Figure 2.19.: Connectivity matrix derived from pearson's correlation (left) and cross correlation(right).

Although CC, as a causal indicator, is able to imply the direction of connectivity, it suffers from indirect connections and external inputs.[96] Furthermore the range of τ, taking the maximum value, can be different for each node.[96] The coincidence index (CI) approaches this issue by using a coincidence interval and different ranges of τ, indicating a higher reproducibility with increasing CI value.

Transfer Entropy (TE) measures the directed causal relationship between two signals, while considering both linear and non-linear information flow [97], as it is a model-free approach. This implies that the model is not dependent on any assumptions about the underlying network interconnectivity, setting it apart from other model-based approaches for computing connectivity. The eventuated matrix ranges between zero and one (see fig. 2.20), while high values denote a strong causal relationship and low values vice versa.

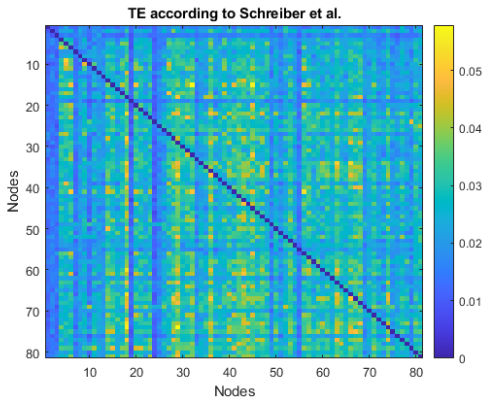

Figure 2.20.: Transfer Entropy connectivity matrix according to Schreiber et al.[99] The diagonal representing auto-correlation of nodes was removed, resulting in a value of zero instead of one.

Drawback of this method is the unknown true topology of a given network, leading to uncertainties in reconstruction quality.[97] The missing ground-truth topology can be substituted by well-known simulated network connectivities, also named *surrogates*. Thereby the quality of the computed network connectivity can be determined by comparison to the defined topology results.[97] Surrogate data are usually characterized by similar properties as the experimental data. Light scattering artifacts and noise is added to make the surrogates more realistic.[97, 100, 101]

TE was originally formulated by Schreiber et al.in 2000 [99]. Thereupon the field of neuroscience discovered this approach utilized in different experimental designs. In this way TE found its application in multimodal functional neuroimaging like e.g. fMRI and EEG/MEG.[102] But also in vitro cultures of neuronal networks made good use of this approach.[103] Stetter et al. refined TE to be more suitable for calcium imaging data sets by two additional features and named it **generalized transfer entropy (GTE)** [97], giving it a further boost in laboratory applications. The two main challenges of calcium imaging tackled are the difference of low frame rates and synaptic activity by using same bin interactions, as well as changing dynamical states of the network by introducing a thresholding variable.[97] Although GTE has huge advantages over common approaches regarding calcium imaging data, not trivial uncertainties, besides lacking the true topology, of this method will be specified in section 5 (p. 41).

2.5.2. Network Measures

Different levels of network modularity and functionality can be described by distinct measures. A detailed description of more network measures was written by Rubinov et al..[92] In the following only the measures used in this project will be introduced.

Network development can be distinguished straight forward through morphological changes. In simplified terms, a higher connectivity to neighbored neurons indicates an eventual developmental phase. The measure of a node's **degree** reflects the number of connected links to a given node. Thus depicting a consistent measure of network development when examining the mean degree, also named density or total wiring cost. The weighted variant is termed **strength**. Another version of the degree is the **within-module z-score**, reflecting the number of nodes connected within the module to the given node.

Besides the general peculiarity of simple connectivity, complex networks preserve distinct manifestations of the ability for local specialized information processing, **functional segregation**, and the fast combination of specialized information globally, **functional integration**. Integration and segregation enable sophisticated communication of the brain, as a result of rapid classification of huge amounts of incoming signals and the capability of allocating information into specialized communities (see fig. 2.21).[92, 104] It was shown that during childhood the human brain increasingly specializes, developing from an integrated towards a more segregated system (see fig. 2.22)[105], remaining in a balanced condition. In psychiatric disorders, the balance between integration and segregation in a brain can differ from its physiological state[104], affecting physiological functionality. For example, increased segregation is an indicator for focal epilepsy.[106]

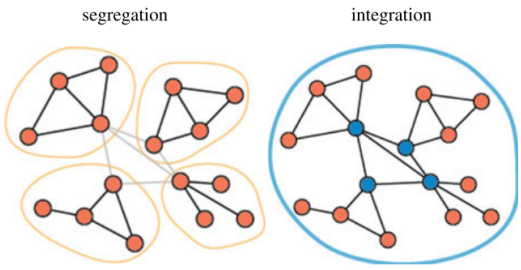

Figure 2.21.: Schematic showing segregation (specialized processing) and integration (efficient processing). Figure from [104].

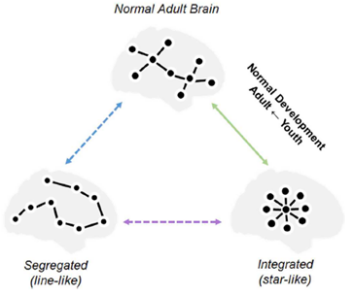

Figure 2.22.: Developmental behavior of segregation and integration. Figure from [105].

With the help of graph theory it is possible to measure these traits, as introduced in the following. **Modularity** describes the level of network subdivision into non-overlapping clusters, termed modules or communities. High values of modularity emphasize the prevalence of segregation in the observed network.[92] Initial drivers of modularity are **connector hubs**, which play a key role in integration and inter-modular segregation, since they access communities and transmit information between sub-populations (see fi.2.23).[92, 104] In contrast **provincial hubs**, also local hubs, are crucial for segregated processing. High connectivity within their own module yields specialization, which can cause definite functional loss after injury.[104] Graph theoretic measures are able to characterize different hub types. The most common measures are the node degree/within-module z-score or strength (see p.21), centrality and the participation coefficient.[92] **Betweenness centrality** (bc) describes the fraction of all shortest paths that pass through a given node. Thus important nodes with a high value of bc participate in a huge number of shortest paths, indicating a hub cell. The **participation coefficient** (Pcoeff) instead reflects the inter-modular connectivity.[92] Minor roles are taken over by **peripheral hubs** with on average low degree, bc and Pcoeff.[92]

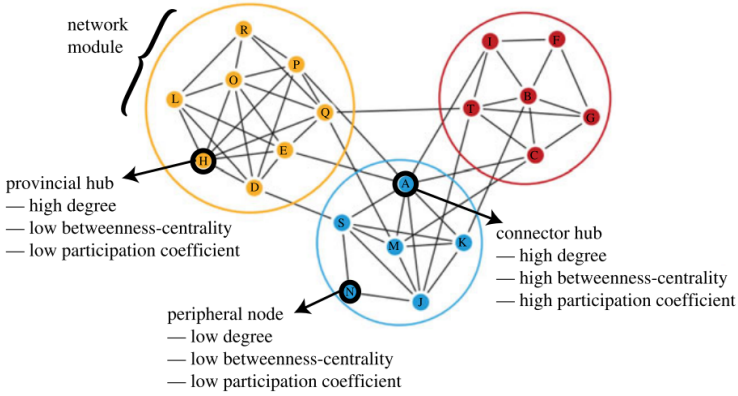

Figure 2.23.: Depiction of the classification of hubs into: provincial, peripheral and connector hubs in community structures. Figure from [104].

Besides the presence of specific hub types, integration and segregation can be measured by further variables. Segregation e.g. is, in addition to a high modularity, indicated by an increased transitivity.[92] **Transitivity** is a variant of the clustering coefficient, which reflects the average degree of clustered connectivity around individual nodes. Unlike the mean clustering coefficient, transitivity is globally normalized which prevents the negative influence of low degree nodes.[92] Whereas functional integration needs traits enhancing the network's efficiency. Functional short paths between communicating nodes improve the performance of a information flow. The **characteristic path length** is an estimate of the average shortest path length occurring in a network. In comparison the **global efficiency** (Eglob), which is the inverse of it, is not misproportioned by disconnected nodes, leading to infinite large contributions. Another measure of efficiency is the **local efficiency** (Eloc), which is simply the Eglob computed on the neighborhood of the given node.[92]

The balance of integration and segregation in the healthy human brain is known to show **small-worldness** behavior.[107] Small-worldness is defined by significantly high clustering, compared to random networks, while having roughly the same **characteristic path length**.[92] These networks are in an optimal balance of local and global efficiency (see fig. 2.24).

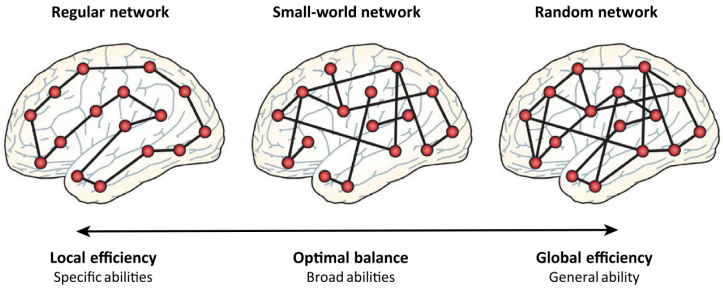

Figure 2.24.: Schematic showing the balance of small-world networks and its relation to efficiency. Figure adapted from [107].

As depicted in figure 2.24, efficiency can be described by regular and random networks. [104, 107] While regular networks follow an ordered lattice behavior, where each node connects to an equal number of other nodes. Instead, random networks equal disordered graphs, where randomness decreases integration due to shorter path lengths.[104, 107]

This balance is exceedingly important for healthy brain functionality. Epileptic seizures for example cause an excess of integration. An aberrant number of brain regions begin to fire synchronously, leading to an inefficient information processing.[104]

Another important feature of the human brain is the ability for **network resilience**.[92, 93] As explained above, special hubs assume particular tasks in a network, enabling e.g. special behaviors or functions. In case of an injury, it is possible that hubs take over the function of damaged hub nodes. This resistance of a network against damage of such nodes can be measured by **assortativity**.[93] Figure 2.25 depicts the difference between an assortative and dissortative network. While the performance in an assortative network can be maintained by a strong intermodular connectivity, a dissortative network is not able to sustain functionality due to excessive modularity.

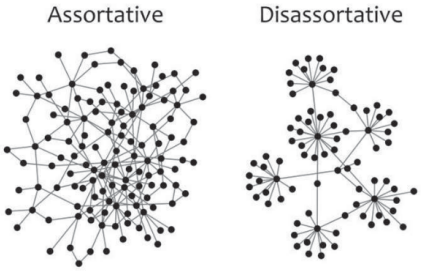

Figure 2.25.: Schematic of an assortative and dissortative network. Figure adapted from [93].

3. Materials and Methods

3.1. Natural Hydrogels

3.1.1. Fibrin

Fibrin is a natural polymer with versatile applications in tissue engineering and contributes significantly to wound healing, angiogenesis, inflammation and many more. [108, 109] The polymerization of fibrinogen is initiated by thrombin, forming fibrin.

The ability to extract fibrinogen from patients blood, where it occurs at 2 - 4 g/L, made it famous as an autologous scaffold. [58, 110] Besides, it is often used in tissue engineering due to its high biocompatibility, biodegradability and cell binding affinity. [57, 58] Cells in direct contact to a fibrin matrix progressively degrade fibrin and replace the scaffold by a mature extracellular matrix. Its ability to behave as a reservoir of growth factors enhances the tissue-specific matrix development. [57]

Fibrin is well known in wound repair as a sealing agent. But also in other clinical and bioengineering applications fibrin scaffolds acquires renown, e.g. skin tissue, vascular tissue, heart valve replacements as well as drug delivery, cell delivery and differentiation.[57, 111] Furthermore in neuroscience fibrin-based matrices fade into spotlight. Especially in the research of spinal cord injury fibrin caught recently close attention. It was shown successfully that aligned fibrin fibers promote the regeneration of spinal cord injuries and support locomotion function recovery.[75, 112, 113]

In the presented work, human derived fibrinogen (plasminogen-, vWF- and fibronectin-depleted, Milan Analytica AG) was used in a stock solution of 40 mg/mL in 1xPBS. Initially, 5.8% v/v $CaCl_2$ (50 mM)(Carl Roth GmbH + Co.KG) and 19.3% v/v 1xPBs were mixed. Afterwards 3% v/v of 40 mg/mL fibrinogen were added and 69.7% v/v of the cell suspension was re-suspended. As fibrinogen starts to spontaneously polymerize after some time at RT, it is necessary to store it on ice and reduce the working time as much as possible. Subsequently, 2.2% v/v human plasma derived thrombin (20 U/L)(Sigma-Aldrich) was added to initiate the polymerization. After the addition of $CaCl_2$ and thrombin, gelation occurs fast, presuming a fast practiced working. Since polymerization starts promptly, it is important to add the cell suspension prior the addition of Thrombin.

3.1.2. Collagen

Collagen is the most abundant protein in connective tissue and native extra cellular matrix of living animals, comprising 25% of the total protein in vivo.[114, 115] Thus, being the most occupied protein intissue engineering applications.[116] It is an already well proven biomaterial in medical applications like bone or cartilage reconstruction, wound healing, drug delivery and cell encapsulation in scientific applications. Its main advantages are the ability of storing large amounts of water molecules, its high biocompatibility, and biodegradability. Although Collagen does not occur naturally in the brain it has shown various positive effects on neurons. Besides collagen type I is present in the dura mater [117], which is surrounding the CNS, it promotes neuronal cell attachment, axonal outgrowth, proliferation, and guidance during development.[118]

Collagen fibrils can be formed by type I, II, III, V and XI collagen, whereby collagen I is the most prevailing scaffold material in biomedical applications.[114] It is mainly produced by fibroblasts and can be extracted from e.g. tendon or tails.[119, 120] Usually, collagen I is solubilized in acidic solution and mostly derived from rat tail tendon. In the human brain collagen IV is a component of the basal lamina and the neural interstitial matrix.[23] In *in vitro* cultures collagen IV was shown to provide cell attachment and neurite outgrowth capacities.[121]

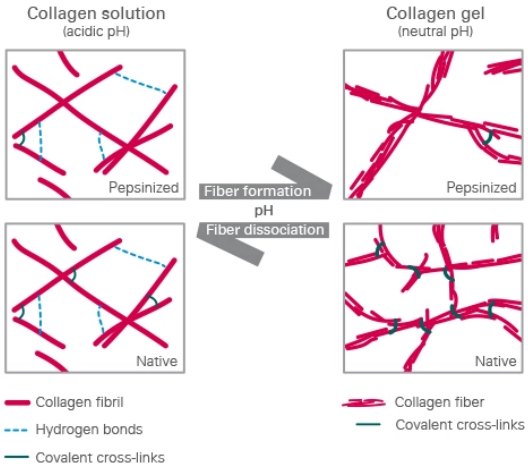

Figure 3.1.: Schematic of collagen fiber formation, influenced by pH variation. Figure from [122].

Hydrogel formation is commonly performed by increasing the temperature and pH to physiological values, thus initiating collagen-fibril self assembly.[123] Solubilized collagen, in an acidic environment, shows characteristic viscous properties, due to loose hydrogen bonds formed between fibrils. Collagen gel formation is initiated by neutral pH, while non-pesinized collagen form an *in vivo*-like, strong cross-linking and vice versa (see fig. 3.1).[122] Despite its high biomimetic properties, collagen has some major drawbacks. For example, the degradability by matrix metalloproteinases (MMPs; cell mediated proteases) and its low stiffness, which is usually below 1 kPa.[124]

Also collagen got of particular interest in neurological research, beside outstanding success as injectable hydrogel in e.g. cartilage, bone tissue or CNS repair.[125, 126, 127] For instance Gil et al. used collagen type I hydrogel constructs for the study of axonal regrowth and migration of embryonic mouse CNS tissue.[128] Furthermore collagen was shown to promote the differentiation of CNS stem and progenitor cells into neurons forming a functional network in vitro.[129]

In the presented work rat tail collagen type I (Gibco^{TM} Fisher Scientific GmbH) was used. At first, 38.6% v/v Dulbecco's Buffered Saline (DPBS) and 7.1% v/v HEPES (Carl Roth GmbH + Co.KG) were mixed. Then 17.1% v/v of 3 mg/mL collagen and 11.4% v/v of Milli-Q was added. Eventually, 25.7% v/v of the cell suspension was re-suspended. Unlike aqueous solutions, the collagen mixture does not mix itself by diffusion. Therefore it is crucial to properly mix the hydrogel solution. As Collagen is highly sensitive a proper buffering system is necessary after increasing the pH for gelation. The stock solution of collagen has a pH of 3.5. The optimal pH for polymerization lays at about 7 (6.5 to 7.5). Moreover it is important to protect collagen from light and reduce the working time as much as possible. To prevent eventual polymerization of collagen, it is necessary to work on ice.

3.2. Biohybrid Hydrogels

Using reversible addition−fragmentation chain-transfer (RAFT) polymerization, PVP-*co*-GMA was synthesized by the working group of Prof. Dr. Pich of the DWI (Leibniz-Institut für Interaktive Materialien e.V., Aachen). They developed a fibrin-based composite hydrogel, as depicted in fig. 3.2 on the left.[130] Based on the work of Peng et al.[131], they used polyvinylpyrrolidone-*co*-glycidyl methacrylate (PVP-*co* -GMA-Copolymers) to enhance the mechanical properties of fibrin-based hydrogels (see fig. 3.2, right). The glycidyl methacrylate (GMA) is conjugated to the amine groups of the lysines, and thiols of cystein and methionine, on the fibrinogen. In the presented work, PVP-*co*-GMA$_{3mol\%}$ was diluted in 1xPBS at a concentration of 1 mg/mL. In order to examine the proper biohybrid hydrogel conditions for the successful encapsulation of primary neuronal cells, different molecular weights of PVP were tested: 6662 g/mol, 8118 g/mol, 11100 g/mol and 65000 g/mol.

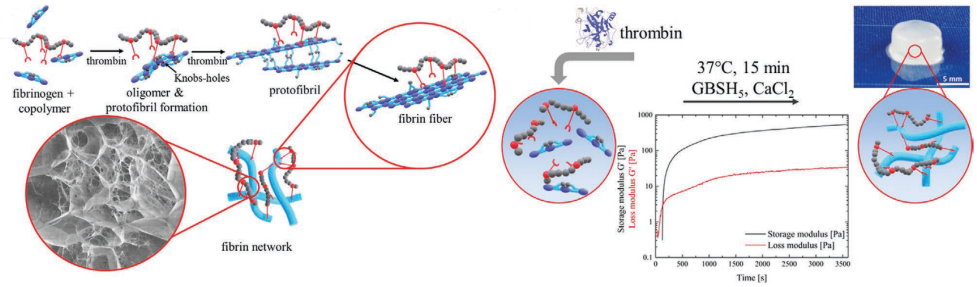

Figure 3.2.: Schematic of the polymerization of Fibrin-PVP-*co*-GMA and its rheological properties. Figure adapted from [130].

3.2.1. Fibrin-PVP-*co*-GMA$_{3mol\%}$

As fibrinogen is spontaneously polymerizing after some time at room temperature, it is necessary to hold this component on ice. All components were aliquoted and thawed in the fridge prior usage. For the synthesis of Fibrin-PVP-*co*-GMA$_{3mol\%}$, 14.5% v/v of 40 mg/mL human fibrinogen (plasminogen-, vWF- and fibronectin-depleted, Milan Analytica AG) was mixed with 4.3% v/v $CaCl_2$ (50m mM)(Carl Roth GmbH + Co.KG), which is needed for the activation of thrombin. Following, 8.5% v/v of 1 mg/mL PVP-*co*-GMA$_{3mol\%}$ and 70.9% v/v of cell suspension were added and carefully re-suspended. The Polymerization was then initiated by the addition of 1.8% v/v thrombin (20 U/L)(Sigma-Aldrich). After the addition of thrombin, polymerization is directly initiated, requiring fast work. Therefore, the cell suspension should always be added prior thrombin. Complete polymerization was then allowed at 37°C in the incubator for about 20 min. Next, medium was added and changed the following day.

3.2.2. Collagen-PVP-*co*-GMA$_{3mol\%}$

Collagen-PVP-*co*-GMA$_{3mol\%}$ requires the entire hydrogel synthesis on ice. Therefore also all components were pre-chilled, to avoid too early polymerization (see section 3.1.2, p. 26). Cold neurobasal medium (NB, 52.4% v/v)(Life Technologies GmbH) was mixed with 7.1% v/v of 0.1 M sodium hydroxide (NaOH). Following, 17.1% v/v of 3 mg/mL collagen was added, while making sure that collagen was properly mixed, as collagen is not mixing itself by diffusion (see section 3.1.2, p.26). Then 11.4% v/v of 1mg/mL PVP and 11.9% v/v of the cell suspension were added. Complete polymerization was then allowed at 37°C in the incubator for about 50 min. Then NB medium was added and changed the following day.

3.3. Cell culture

Primary rat cortical cells of E18 Wistar rat embryos were used to engineer 3D neuronal networks *in vitro*. Therefore cortices were isolated from the brain in Hank's Balanced salt Solution (HBSS, Gibco^{TM}). Following, cells were dissociated by incubating the tissue in 0.05% Trypsin Ethylenediaminetetraacetic acid (EDTA)(Life Technologies GmbH) for about 15 min at 37°C. The suspension was centrifuged and cells counted.

In this study, cell concentrations close to the physiological densities in the CNS were aimed. The maximum cell density feasible was about 11 820 cells/mm^2. In comparison the human neocortex comprises about 20 000 cells/mm^2. The maximum possible cell desnities, in respect to the used hydrogels, are listed in table 3.1.

Table 3.1.: Cell densities in respect to hydrogels.

Hydrogel	final cell density [cells/mm^3]
Fibrin	11.615
Collagen	11.615
Fibrin-PVP-*co*-GMA$_{3mol\%}$	11.820
Collagen-PVP-*co*-GMA$_{3mol\%}$	8.503

Hydrogels were cultivated in ibidi dishes containing 2 mL Neurobasal medium (NB, Life Technologies GmbH) at 37°C, 5% CO_2 and 95% humidity. The NB medium was supplemented with 1% heat inactivated fetal bovine serum (FBS, Life Technologies GmbH), 2% B-27 (Life Technologies GmbH) and 1% N2 (Thermo Fisher Scientific GmbH) were used. B-27 is a serum-free supplement, known to enhance neuronal cell viability.[132] N2 is associated to enhance neuronal cell growth, and was added to support long-term studies.[133] In order to prevent contamination, 0.5 mM L-glutamine (Life Technologies GmbH) and 50 μg/mL gentamicin (Sigma-Aldrich) were added. In case of fibrin-based hydrogels, Tranexamic Acid (TA) has to be added, in order to prevent matrix degradation. The medium was changed completely, twice a week.

3.4. Cell viability

Live/dead stainings were performed using Calcein-AM (ThermoFisher Scientific Inc.) and Ethidium Homoder-1 (EthD-1, ThermoFisher Scientific Inc.). Both agents were used in a concentration of 1:1000 diluted in NB medium. Prior staining, the culture medium was removed. Following, the samples were incubated for 15 min at 37°C. Afterwards the gels was rinsed carefully 3 times for five minutes each. In total ten images were taken from all samples, while N=3 for each DIV. The live/dead ratios were evaluated with the help of ImageJ.

3.5. Immunostaining

Cell morphology was explored by fluorescent labeling of cellular structures via antibodies at different maturational stages (at about DIV9, DIV22, DIV41). Prior fixation, hydrogels were rinsed carefully three times with pre-heated 1xPBS, for five minutes respectively. Networks were then fixated with 4% paraformaldehyde (Sigma-Aldrich) in 1xPBS for 15 minutes at 37°C, 5% CO_2 and 95% humidity. Subsequent rinsing (3x 5 minutes) with 1xPBS stopped the fixation process. Permeabilization of the cell membrane was initiated by the incubation of 0.1% Triton x-100 (Sigma-Aldrich) for 6 hours at room temperature (RT), again followed by 3x rinsing for 5 minutes each. Following, unspecific binding sides were blocked by the incubation of 5% bovine serum albumin (BSA, Gibco^{TM}) in 1xPBS for 3 hours at RT or over night at 4°C. Neuronal dendrites and somata were stained with the primary antibody β-III-tubulin (rabbit, CellSignaling Technology) at a dilution of 1:500. Astrocytes were visualized using glial fibrillary acidic protein (GFAP, mouse, CellSignaling Technology) at a dilution of 1:500. Primary antibodies were incubated over night at 4°C. Nuclei were stained with 4',6-diamidino-2-phenylindole (DAPI, 2.5 mg/mL, Life Technologies) at a dilution of 1:1000. As secondary antibodies Alexa Fluor anti-rabbit 546 and Alexa Fluor anti-mouse 488 (Invitrogen) were incubated over night at 4°C, with a dilution od 1:500.

3.6. Microscopy

3.6.1. Confocal imaging

As described in section 3.5 (p.29), cell morphology was studied at different maturational stages: early (DIV9), intermediate (DIV22) and advanced (DIV41). Hydrogels were imaged at the Institute of Biological Information Processing (IBI), Mechanobiology (IBI-2) at Forschungszentrum Jülich (Germany). Microscopy was done using a confocal laser scanning microscope (LSM 710; Carl Zeiss MicroImaging GmbH) equipped with an argon ion laser (488 nm) and a red helium-neon laser (633 nm).

3.6.2. Calcium imaging

Calcium imaging is one of the most popular approaches to record neuronal network activity *in vivo* and *in vitro* since protein based calcium indicators (GCaMP) had been established.[134, 135, 136] Based on rapid changes of intracellular free calcium during action potentials (see section 2.2, p.4), the activity of neuronal populations can be visualized using fluorescent calcium indicators. With the introduction of the green fluorescent calcium indicator GCaMP6 by Chen et al.[137], calcium imaging reached a new qualitative level due to its high temporal sensitivity. Before, protein-based indicators could not compete with common synthetic ones, as e.g. Oregon Green Bapta-1-AM (OGB1-AM), owing to low sensitivity and slow kinetics.[137] GCaMP6f, developed by Chen et al., became apparent to be the fastest calcium indicator with a comparable sensitivity to OGB1-AM.

A variant of this genetically-encoded indicator was used in this project, purchased from Addgene (USA). The cells were transduced with adeno-associated viruses (AAVs) containing Syn.GCaMP6f.WPRE.SV40 at a concentration of 104gc/cell. AAVs were added to the cell suspension prior encapsulation. Before start imaging, fresh medium should be prepared for the ongoing culture of the hydrogels after imaging. Medium was changed directly after recordings.

3.7. Data processing

This section addresses the steps of data processing used to characterize the developing neuronal networks and raises the critical view on the selection process of suitable algorithms. The presented evaluation sequence can be divided into four different parts: (1) Signal extraction and data preprocessing (2) connectivity estimation (3) network analysis and (4) functional reconstruction.

3.7.1. Signal extraction and data preprocessing

The recorded calcium imaging movies are analyzed using parts of the **Suite2p** pipeline (version: v0.9.2)[138], regarding cell detection and signal extraction. Suite2p was established by M. Pachitariu and C. Stringer et al. in 2017 and is continuously being optimized. It is capable of detecting 10,000 neurons simultaneously and offers an individual customizable classifier that detects cells by weighting properties, based on biological structure and microscope optics [139]. The classifier can be trained by manual adjustment of detected real cells. After running the

classification manually for a few data sets, a new optimized classifier can be build and applied to the given data, while manual interventions are remain possible.

As input Suite2p takes the raw calcium imaging movie as e.g. TIFF formatted file. The graphical user interface (GUI) enables the adjustment of different settings according to the given data before running the pipeline. All settings can be found in the following figure 3.3.

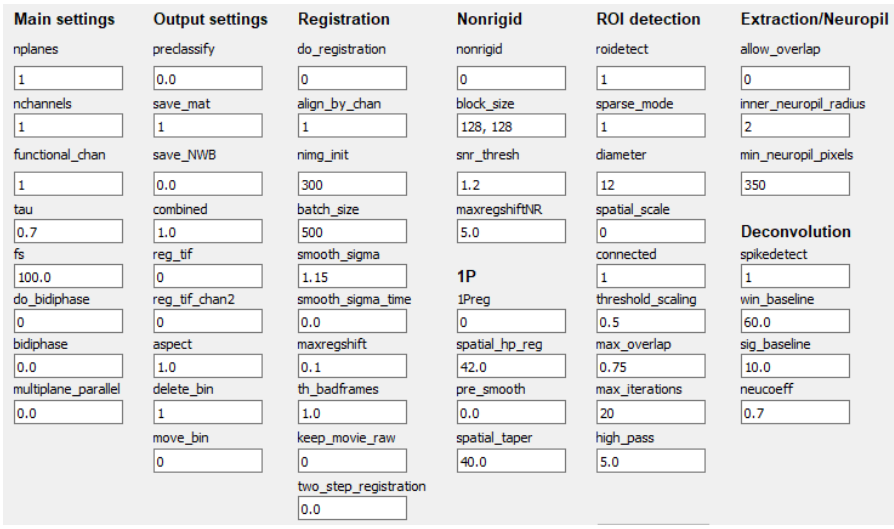

Figure 3.3.: Screenshot of the settings used in Suite2p.

Furthermore Suite2p detects signals originating from neuropil, which can severely contaminate the signals from regions of interest (ROIs).[138] Neuropil are defined as the amorphous mesh in the central nervous system, located between the cell bodies, composed of dendrites, axons and glial processes.[140] These areas lead to diffuse signals of the average fluorescence activity of out-of-focus dendrites and axons. In 3D recordings, cells, assumed as the only structure in focus, can be negatively influenced in its recorded activity, by neuropil signals. This effect relies on the microscopic acquisition characteristics, which displays the average signal of several microns across the z-direction. Despite other common approaches, M. Pachitariu and C. Stringer et al. account a **neuropil correction**, considering these signals as potentially high correlative with the cell's activity.[138] As Output Suite2p gives six different arrays ([139]):

1. array of fluorescence traces (ROIs by timepoints)
2. array of neuropil fluorescence traces (ROIs by timepoints)
3. array of deconvolved traces (ROIs by timepoints)
4. array with a list of statistics computed for each cell (ROIs denoted by 1)
5. array with options and intermediate outputs (dictionary)
6. array that specifies whether an ROI is a cell, first column is 0/1, and second column is the probability that the ROI is a cell based on the default classifier

While the array of fluorescence traces already implements the neuropil correction. For a more detailed description of the Suite2p pipeline please check out: `https://suite2p.readthedocs.io/en/latest/index.html`. The entire code is available on GitHub: `https://github.com/mouseland/suite2p`.

Further **preprocessing** steps have been performed in MATLAB R2020b (licensed by RWTH Aachen). As a next step, the raw signal traces were normalized. Therefore, the **baseline correction** by P. Patel et al. was adjusted to the given data. The relative fluorescence change $\Delta F/F$ was calculated using the common percentile method. Therefore, a five second sliding window was used to categorize the fluorescence trace into sections and subtract the mean of the lower 50% of the preceding five second section.[141]

Finally, to extract further information about the underlying network functionality, **peak detection** based on MinPeakHeight and MinPeakProminence was performed. Previously, the data was smoothed using a butterfly filter with a 7 Hz cutoff frequency and a filter order 5. Then, a threshold was calculated according to the absolute median deviation, in order to get the minimum peak height and prominence necessary for peak detection. ROIs without any detected activity had been excluded from further processing.

3.7.2. Network analysis

Section 2.5.2 (p.21) already introduced the network measures applied in this project. All functions had been used from the *'Brain Connectivity Toolbox (BCT)'* established by Rubinov et al.[92] The detection of hub cells was applied according to Karrer et al..[142] Thus nodes need to fulfill at least two of the following criteria to be defined as a hub cell: above average nodal strength, betweenness centrality and/or local efficiency. A further classification is thresholded through the participation coefficient (Pcoeff). While connector hubs usually show an above average Pcoeff, provincial hubs are characterized by a below-average value.[101] Beside the previously mentioned network measures, also the average number of active cells, the mean network firing rate and synchronicity was observed. As a measure of synchrony, the frobenius norm of the connectivity matrix was calculated.

3.7.3. Cross-correlation

The corss-correlation was calculated by applying the standard function 'xcorr', using the normalization option 'coeff', of MATLAB.[143]

3.7.4. Statistical evaluation

Statistical significance was tested using one-way ANOVA with bonferroni multicomparison for normal distributed data. In case of a non-normal distribution a kruskal-wallis test was applied instead of ANOVA. P-values of 0.001(***), 0.01(**) and 0.05(*) had been used as significance levels.

4. Engineering of a suitable hydrogel system for primary neuronal cell encapsulation

This chapter discusses the development of the eventually used hydrogel formulations from the more engineering point of few. Herein emerging issues and requirements, some of which had been already introduced in section 2.4 (p.12), and possible solutions are revealed.

4.1. Commercial hydrogels

There are many commercially available hydrogel kits for 3D cell cultivation. However, as described in section 2.3 (p.7) neurons are highly sensitive to their surrounding environment.

The most well known hydrogel is **Corning**^{TM} **Matrigel**^{TM}, which is derived from Engelbreth-Holm-Swarm mouse sarcoma. It is mainly composed of Laminin, making it a favorable scaffold for various cell types.[144] The probably largest drawback about Matrigel is its inconsistency from batch to batch. The exact composition of proteins is never known. Nevertheless, due to its high biocompatibility and adhesive properties, Matrigel remains to be the state of the art. Therefore, it was also considered as environment for the cultivation of primary neuronal cells in the presented work. Further, the alternative **ECM Gel (e1270)**, purchased from Sigma-Aldrich, was tested. ECM Gel is also derived from Engelbreth-Holm-Swarm mouse sarcoma, however, having a relatively low protein concentration of about 8-12 mg/mL compared to Corning Matrigel matrix, which is also available with 18-21 mg/mL.[144, 145]

Different concentrations had been evaluated, as shown in table 4.1. Initially without cells to spot good cross-linking gels, before including a cell suspension with a high cell density of about 33 000 cells/μL.

Table 4.1.: Neuronal cell viability in commercial available hydrogels.

	Matrigel I	Matrigel II	ECM
Concentration	5 mg/mL	10 mg/mL	8-12 mg/mL
Viability	79%	90%	74%

Working with Matrigel/ECM requires the constant execution of each step on ice to prevent spontaneous polymerization, as it is a temperature sensitive material. Additionally, all labware working with, has to be pre-chilled. Thermal polymerization of ECM is initiated at 20-40°C, instead Matrigel is already polymerizing at temperatures above 4°C, according to the suppliers notes. Both solutions should be thawed over night in the fridge and then vortexed, to ensure a complete, homogeneous thawed and mixed substance. A final dilution below 4 mg/mL should

be avoided, as polymerization is limited due to protein content. Further, as Matrigel/ECM is a very high viscous material, a positive displacement pipet should be used to avoid distorted volumes used. It is important to note, that Matrigel and ECM should be stored in the very back of the freezer to ensure a constant temperature, as good as possible.[146]

Figure 4.1 shows exemplary grown neuronal networks in different concentrations and sources respectively. Living cells are labeled green fluorescent, by Calcein-AM, and dead cells are labeled red, using Ethidium-Homodimer (see section 3.4, p.29).

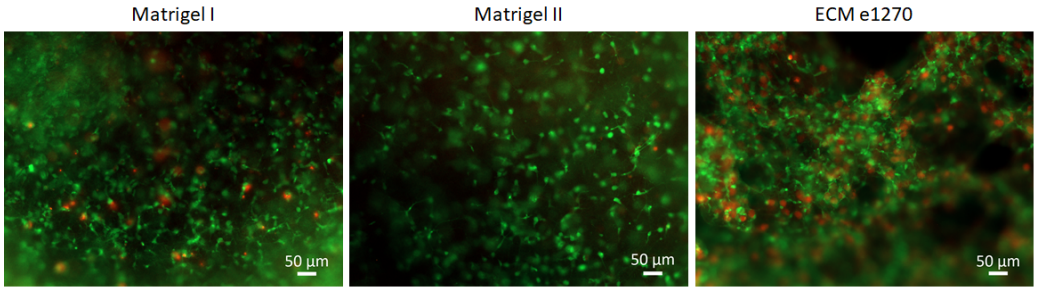

Figure 4.1.: Live/dead images of neuronal cells cultured in5 mg/mL and 10 mg/mL Matrigel, and ECM at DIV7. (green:vital cells, red:dead cells)

Another commercially available hydrogel tested, was **VitroGel3D** (TheWell Bioscience), an xeno-free polysaccharide hydrogel system.[147] According to the suppliers notes, it is room temperature stable, thus not requiring the consequent work on ice. Additional features are neutral pH, transparency and good permeability.[147] Nevertheless, this hydrogel, at that date (2018), was not tested with primary neurons before. The fabrication of cell encapsulated hydrogels was performed following the provided standard protocol by TheWell Bioscience.

Figure 4.2 shows exemplary bright field images of cells grown in VitroGel. The cell encapsulation had been very bad, as many cells had not been captured by the gel. Further, all hydrogels showed inhomogeneous gel topography, as seen in figure 4.2 (left). Additionally, cells highly tend to form clusters and died already at DIV2.

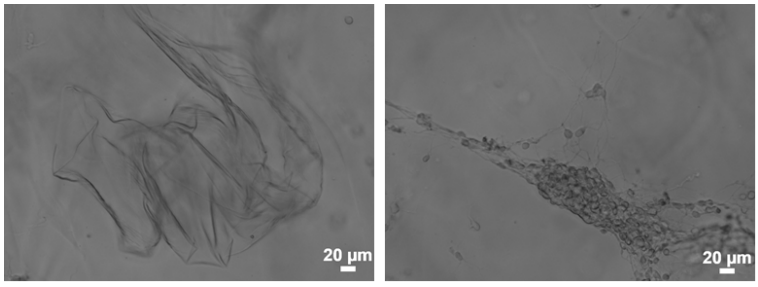

Figure 4.2.: Bright field images of primary neuronal cells cultured in VitroGel at DIV2. VitroGel shows inhomogeneous gel topography and enhances cell clustering.

To conclude, all commercially available hydrogel kits tested, did not satisfy the aim of the presented study. Insecurity about the detailed composition of Matrigel and ECM, as well as bad reproducibility within and throughout batches, outweighed advantages mentioned earlier. VitroGel, although owing very good transparency and easy handling, suffered from bad cell viability and inhomogeneous gel topography. Therefore, the engineering of an individual hydrogel, with mechanical and chemical controllability, as well as a promotive environment for long-term cultivation was aimed.

4.2. Natural hydrogels

As mentioned in section 3.1.1 (p.25), fibrin is a well-known polymer in biomedical applications.. Fibrin hydrogel polymerization is a straight forward process, initiated by thrombin. Also mechanical properties can be easily influenced, by varying the fibrin, thrombin or $CaCl_2$ concentration. Lee et al. (2019) showed the strong dependency of hydrogel stiffness with the fibrin concentration (see fig. 4.3). With increasing fibrin concentration, also the Young's Modulus rises.[148]

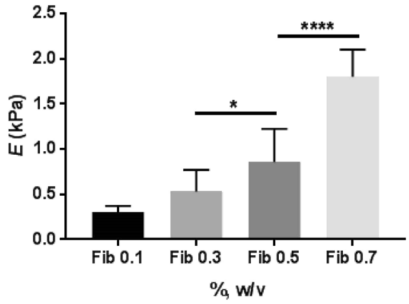

Figure 4.3.: Graph showing the dependency of the fibrin concentration on the Young's Modulus. Figure from [148].

While keeping the fibrin concentration constant and increasing the thrombin concentration, thin fibers are formed and vice versa.[149] Resulting pore sizes affect the diffusion of nutrients and oxygen, as well as cell movement. Stiffness was shown to be strongly correlated with the fibrin and thrombin concentration, while high stiffness is associated with increased fibrin concentrations.[149, 150] Another factor influencing the stiffness, is fibrinolysis. Collet et al. (2000) observed faster degradation of fibrin hydrogels, composed of thin fibers, compared to hydrogels out of thick fibrin fibers.[151] In the presented work fibrinolysis was prevented by the addition of tranexamic acid (TA) into the medium (see section 3.3, p. 28).

The effects of different fibrinogen concentrations on cell viability and morphology are discussed in section 6.1 (p.45).

Another well known polymer in biomedical applications is **collagen**. As described in section 3.1.2 (p.26), the collagen used is derived from rat tail tendon and solubilized in acidic acid. The decision to use rat tail collagen rather than bovine derived collagen was accounted for

various compelling advantages. These benefits are, besides a fast gelation, which ensures cell encapsulation during gelation, also the high purity. This is achieved by non-pepsinized extraction of collagen, as described earlier see section 3.1.2 (p.26), leading to the formation of a more *in vivo*-like hydrogel.

Polymerization is initiated by increasing the pH to physiological values. Thereby temperature plays a critical role regarding the hydrogel architecture. In order to get a collagen hydrogel with thick fibers, it is necessary to incubate all solutions previous to temperature rise, in order to allow molecular assembly.[152] Thick fibers had been associated with increased cell survival of human mammary fibroblasts.[152] However, temperature rises above 38.5°C should be avoided, as collagen will denature. Jansen et al. (2018) extensively studied the influence of network architecture on the mechanical properties of collagen gels.[153] They also showed the significant dependence of fibril formation on polymerization temperature (see fig. 4.4). Accordingly, physiological temperature (37°C) promotes the formation of homogeneous and less bundled networks. Further they observed the significant decrease in fiber diameter with increasing temperature (∼300 nm at 22°C and ∼150 nm at 37°C). Also the collagen concentration, at a constant polymerization temperature of 37°C, influences the network topography (see fig. 4.5). Therefore, they evaluated collagen concentration ranging from 0.2 to 4 mg/mL. Thus, showing a constantly more homogeneous and dense network formation with increasing collagen concentrations.[153]

The choice of medium should be considered carefully, as divalent cations may act as flocculants. Experiments had shown, that a high cell concentration, of about 8 503 cells/μL (see section 3.3, p.28), in $CaCl_2$ containing medium does not significantly affect the gelation, as the cells take most of the volume. Instead, when fabricating collagen hydrogels for e.g. rheological measurements without cells, it is of high importance to use divalent ion-free medium or a proper buffer, as e.g. 4-(2-hydroxyethyl)-1-piperazineethanesulfonic acid (HEPES), in order to ensure full and homogeneous gelation. Another issue affecting gelation quality is the behavior of collagen in solution itself. Unlike aqueous solutions, collagen requires careful mixing prior to usage, as it does not mix itself by diffusion. The detailed analysis of cell growth and functionality in collagen hydrogels can be found in chapter 6.2 (p.48).

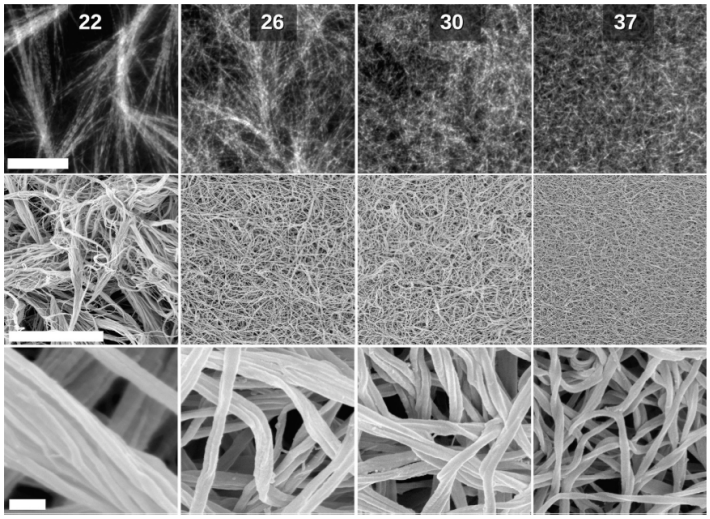

Figure 4.4.: Micro-structural analysis of collagen hydrogel formation, in dependence of temperature, using SEM. With increasing temperature, fiber thickness decreases and a homogeneous network formation is supported. (scale bar upper rows 20 μm, bottom row 200 nm) Figure from [153].

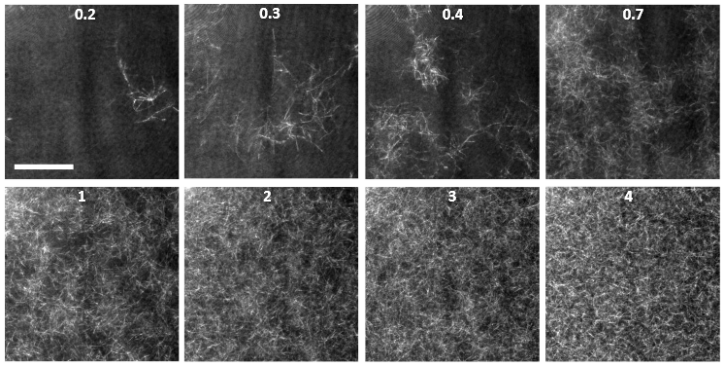

Figure 4.5.: Collagen hydrogels, polymerized at 37°C, show a strong dependency on collagen concentration regarding network topology. Higher concentrations promote dense and homogeneous network formation. (scale bar 20 μm) Figure from [153].

4.3. Biohybrid hydrogels

The development of presented biohybrid hydrogels was conducted in close collaboration with the group of Prof. Dr. A. Pich of the DWI Aachen, as part of an ERS seed funded project (OPSF412). Miriam Al-Enezy Ulbrich (PhD candidate) developed and investigated the Fibrin-PVP-*co*-$GMA_{3mol\%}$ hydrogel published in [130], which was the basis for presented further developments. The engineering of Collagen-PVP-*co*-$GMA_{3mol\%}$ had been part of an external research project of Nicole Terefenko (DWI Aachen, RWTH Aachen). Chemical and rheological characterizations of the established polymers had been performed by Miriam Al-Enezy Ulbrich and coworkers (Nicole Terefenko, Shannon Jung).

Biohybrid hydrogels had been fabricated using PVP-*co*-$GMA_{3mol\%}$ as synthetic polymer, and fibrin and collagen respectively, as biological component. The hydrogel synthesis is the same for fibrin and collagen. The epoxid group of GMA reacts with the amino group of the biopolymer (see fig. 4.6). However, both systems are completely different in their handling and behavior, as described in the following.

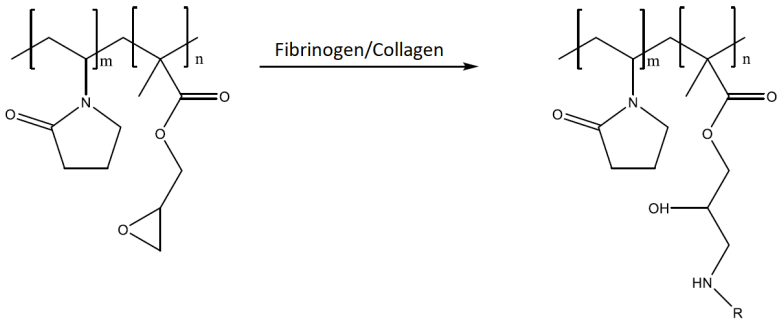

Figure 4.6.: Schematic of the biohybrid hydrogel synthesis.

The most obvious difference between both variants is the temperature during hydrogel preparation, and the final gelation time required for a proper cross-linking. Fibrin-based hybrid hydrogels had been fabricated at RT, Collagen-based gels required the entire work on ice, as discussed earlier (section 4.2 p.35). The final polymerization process was performed at 37°C for both variants. Herein, fibrin-based hydrogels needed a significantly shorter time of 20 min for full gelation, compared to collagen-based gels with 50 min. The different cell behaviors in respect to the hybrid hydrogel systems mentioned, is discussed in chapter 7 (p.51).

Al-Enezy Ulbrich et al. showed the dependency of **Fibrin-PVP-*co*-GMA** copolymer concentration on the fibrin hydrogel stiffness (see fig. 4.7). With increasing copolymer concentration up to 2wt %, the amount of inter-fiber cross-link rises, as well as the storage modulus. Further, physiological characteristic strain stiffening can be induced by varying the molecular weight of the copolymer.

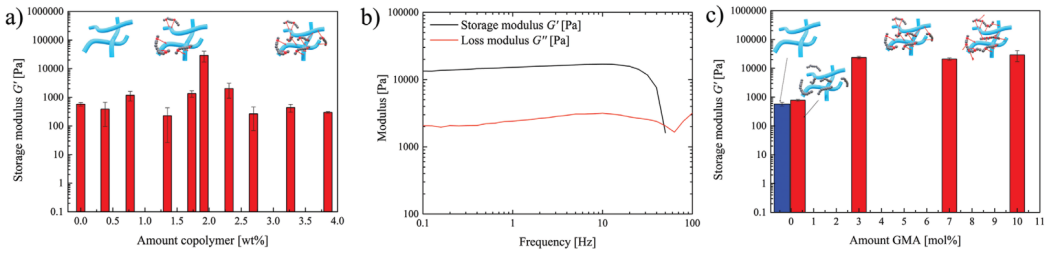

Figure 4.7.: Rheology: Fibrin-PVP-*co*-GMA shows mechanical dependency on copolymer concentration and molecular weight. Figure adapted from [130]

Also the morphology of the biohybrid hydrogel can be tuned by the copolymer concentration. A high concentration of copolymer induced thicker fiber formation, and vice versa (see fig. 4.8). Additionally, they showed a good biocompatibility, despite the presence of epoxy groups in the copolymer structure.[130]

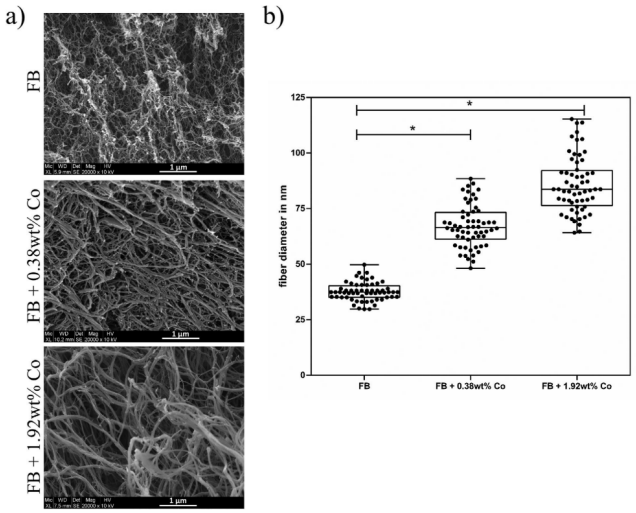

Figure 4.8.: Analysis of the topography of Fibrin-PVP-*co*-GMA gels by SEM. Fiber formation in biohybrid hydrogels show a strong dependency on the copolymer concentration. Figure from [130]

However, **Collagen-PVP-*co*-GMA**$_{3mol\%}$ showed completely different behaviors. In this context the main issue had been the adjustment of the pH level during polymerization. Basic cross-linking evaluations had been performed without cells. Therefore the volume of cell suspension needed to be replaced. As mentioned earlier, the amount of $CaCl_2$ containing medium is influencing the hydrogel polymerization. Therefore different buffering systems and NB/Buffer ratios were evaluated at the DWI (Aachen) and the pH of resulting hydrogels was measured (see tbl. 4.2). HEPES revealed to be the best buffering system.

Table 4.2.: Buffers tested for cross-linking of Collagen-PVP-*co*-GMA gels.

Volume ratio (NB:Buffer) [μL]	Morality [mM]	Buffer	pH
-	-	Water	12
9.5:85.1	25	HEPES	8
37.8:56.7	25	HEPES	7
9.5:85.1	15	HEPES	11
37.8:56.7	15	HEPES	11
9.5:85.1	10	PBS	10
37.8:56.7	10	PBS	11
9.5:85.1	-	DPBS	12
37.8:56.7	-	DPBS	12

As well as the investigation of Fibrin-PVP-*co*-GMA$_{3mol\%}$, collagen-based biohybrid hydrogels were screened for mechanical properties influenced by copolymer concentrations or molecular weight. No influences of PVP polymer chain length and copolymer concentration on the mechanical behavior of collagen-based biohybrid hydrogels, could be observed

However, significant differences compared to Fibrin-based biohybrid hydrogels could be observed in the cellular behavior, discussed in chapter 7 (p.51) and chapter 8 (p.59).

5. Implementation of generalized transfer entropy (GTE) and its pitfalls

As described in section 2.5.1 TE estimates the directed causality between two nodes, while the GTE is fitted to the challenges of calcium imaging. In the following, some issues regarding different TE estimation methods will be addressed briefly and the chosen algorithm will be depicted. In order to test the method, the same sample data as described previously was used (see 2.18, p. 19). The implementation of GTE was evolved with countenance of Prof. Dr. M. Pieper, FH Aachen.

The execution of GTE is accompanied by challenges of probability estimation and binning methods. Hlaváckova-Schindler et al. [154] and Lee et al. [155] showed previously that each method can lead to significantly different results, making a straight comparison with literature data difficult, without a detailed revision of used algorithms. Further, the screening of data processing in depth is difficult - if not often impossible - as provided information about data processing pipelines are not that profound, if published at all.

Nonetheless, GTE was the algorithm of choice in this project, due to compelling advantages mentioned earlier (see section 2.5.1). GTE was implemented according to Stetter et al. [97] by means of the calculation method according to Lee et al. [155], including ordinal sampling and quantization. Furthermore, GTE was applied to all networks having more than five active nodes.

Here, the **histogram method** was applied, which is the most common approach with low computational cost.[154] The data are quantized into fixed bins (b), with a defined width. Stetter et al. recommends a bin width close to twice of the standard deviation of the fluorescence signal.[97] Figure 5.1 depicts the importance of choosing a proper bin width. While setting b too low, small fluctuations in the fluorescence signal might get lost. However, in this study a fixed bin of four was evaluated as being recommendable for the underlying data.

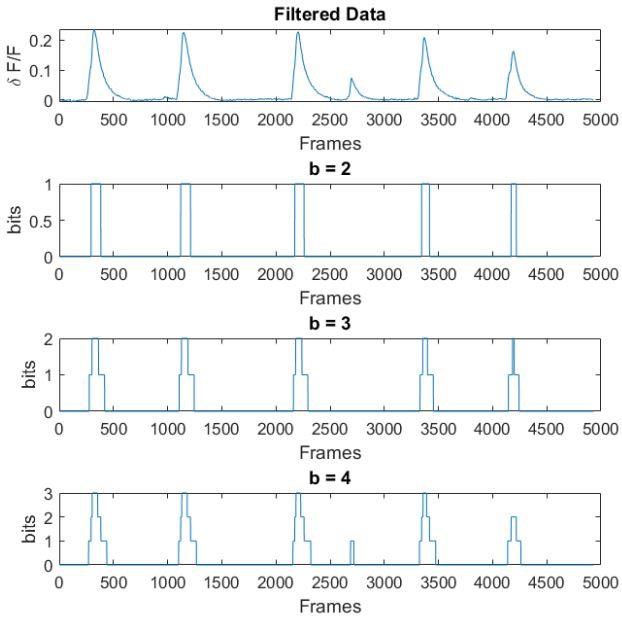

Figure 5.1.: Influence of the binning width onto the quantization quality.

In order to make the algorithm robust against outliers and sparse regions, **ordinal sampling** was added previously to quantization of the signal, as implemented by Lee et al..[155] Ordinal sampling describes the ranking and sorting of the original signal according to their magnitude of order. In detail, the data trace is first sorted from min to max, resulting in a vector IX (see fig. 5.2). Then, a new data vector X is computed by assigning the data values according to their ranks (X(IX)). Figure 5.3 shows the original filtered signal compared to the ordinal sampled data X as a function of IX.

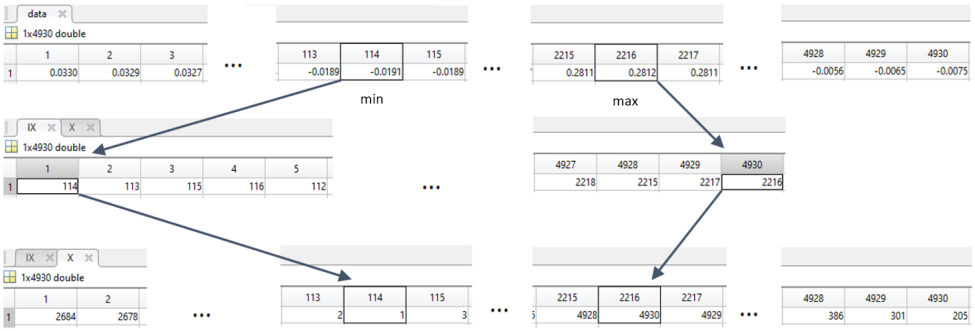

Figure 5.2.: Ordinal sampling depicted by stages.

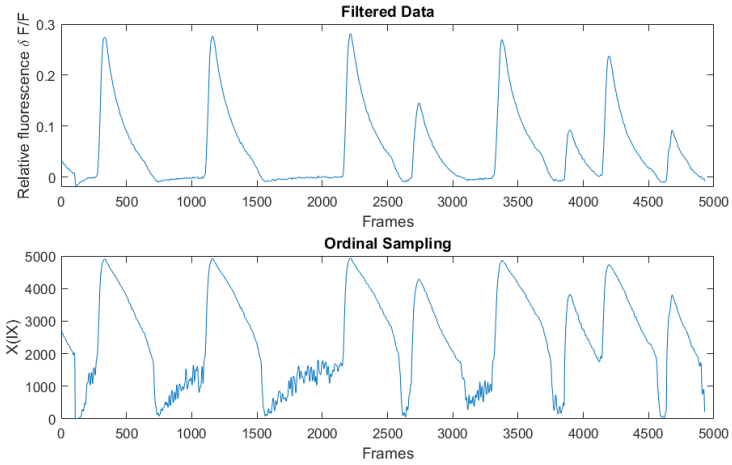

Figure 5.3.: Signal trace before and after ordinal sampling and quantization.

6. Natural hydrogels lack long-term cultivation properties

This chapter focuses on the evaluation of the biocompatibility and morphology of the encapsulated cells in natural hydrogels. The natural polymers of choice were fibrin (see section 3.1.1, p. 25) and collagen (see section 3.1.2, p. 26).

6.1. Fibrin concentrations in hydrogels affect cell viability

As has been stated before, polymer concentrations have major influence on the mechanical behavior of hydrogels, affecting cell viability and functionality (see section 2.4, p. 12). Therefore, different fibrinogen concentrations were evaluated (5 mg/ml, 2.5 mg/ml and 1.25 mg/ml), to figure out the most suitable hydrogel composition for encapsulated primary neuronal cell culture (see section 3.1.1, p. 25). Results presented in this section were part of a bachelor thesis completed by Joscha Graeve (RWTH Aachen, March 2018).

Biocompatibility was tested with a simple live-dead staining, using Ethidium Homodimer (EthD) and Calcein-AM. This assay was applied at DIV8, 15 and 22. Figure 6.1 clearly shows the negative influence of increasing fibrinogen concentration on the cell viability. The lowest concentration, of 1.25 mg/mL, outstandingly supported a viability of about 85% over three weeks.

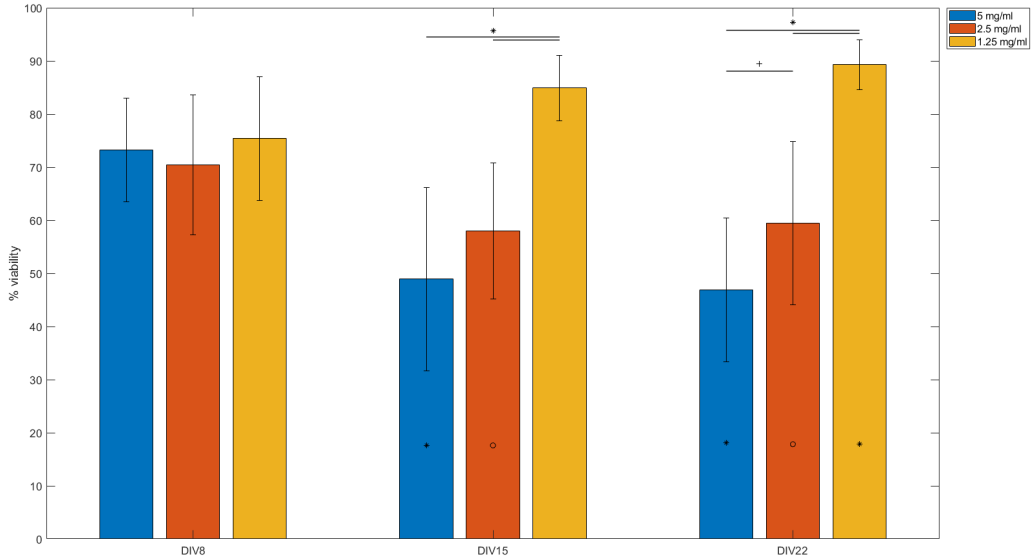

Figure 6.1.: Viability of primary neuronal cells cultured in fibrin hydrogels over three weeks. (N=3, $p \leq 0.05^{o}, p \leq 0.01^{+}, p \leq 0.001^{*}$; error bars denote the standard deviation.)

Increasing fibrinogen concentration is known to enlarge the substrate stiffness, whereby the axonal outgrowth is attenuated.[156] These findings are in complete agreement with the observed results. As shown in figure 7.2, with increasing fibrinogen concentration, neurite length decreased (exemplary indicated by arrows) beyond an intensive clustering behavior respectively. This could be explained by the decreasing porosity of fibrin hydrogels with increasing concentration [156], combined with the high cell density used. High cell densities initiate attraction of cells to each other, before being distributed. As the accumulation of cells decreased with the fibrinogen concentration, causes of cell dissociation can be excluded, due to consistency within cell batches. Another reason could be an inconvenient culture environment, although the most common problem is a lack of cell adhesion points. This should not be the case here, as fibrin hydrogels provide Arg-Gly-Asp (RGD) groups as binding sites for the cells. However, in the latter case, cells take more advantage of forming a cluster for the purpose of maintenance of viability. Interesting observations were reported by Lee et al., who introduced a new measure to quantify the rate of cell adhesion to hydrogels. They hypothesize that on the microscopic scale, the biopolymer fiber chain flexibility highly influences the cell adhesion behavior. Since fibrin possesses more flexible chains it is more difficult for the cells to keep adhesion points.[148] This hypothesis further emphasizes the behavior of cell cluster formation observed.

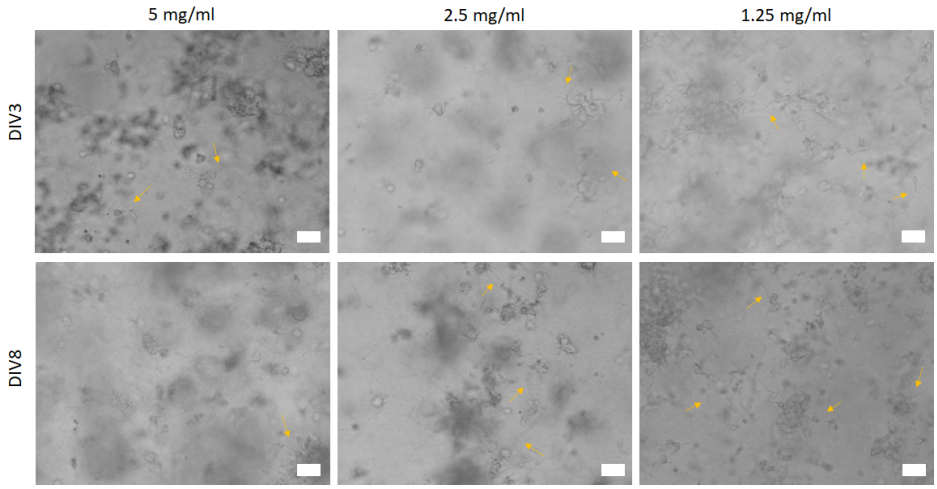

Figure 6.2.: Bright-field images of neuronal networks cultured in hydrogels with different fibrinogen concentrations. Cells in higher concentrations are more likely to cluster, while neurite growth is enhanced in lower fibrinogen concentrations. Scale bar 10 μm.

Further suspicious behaviors are depicted in figure 6.3. Cells started to escape from the hydrogel (exemplary indicated by arrows) by DIV22, thus implying an adverse cultivation environment, as the cells favored to grow on an even stiffer cell culture plate surface than a hydrogel offering greater amounts of cell adhesion points.

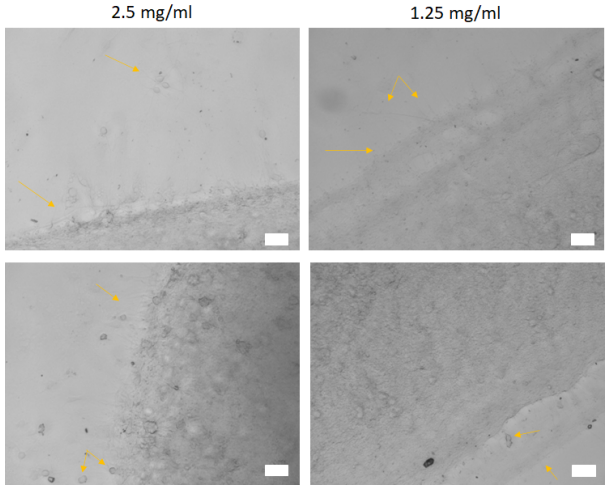

Figure 6.3.: Bright-field images at DIV22 depicting escaping cells from fibrin hydrogels. Scale bar 10 μm.

6.2. Collagen hydrogels enhance neuronal cell viability

Primary neuronal cells were encapsulated in collagen (see section 3.1.2). As shown in figure 6.4 the cell viability decreased significantly from about 73% ± 18.2 at DIV8 to 50% ± 12.2 at DIV37. This decreasing trend in viability is in common with results shown by O'Connor et al., who also reported a significant drop in viability through the first five days in culture with an ongoing declining trend.[157]

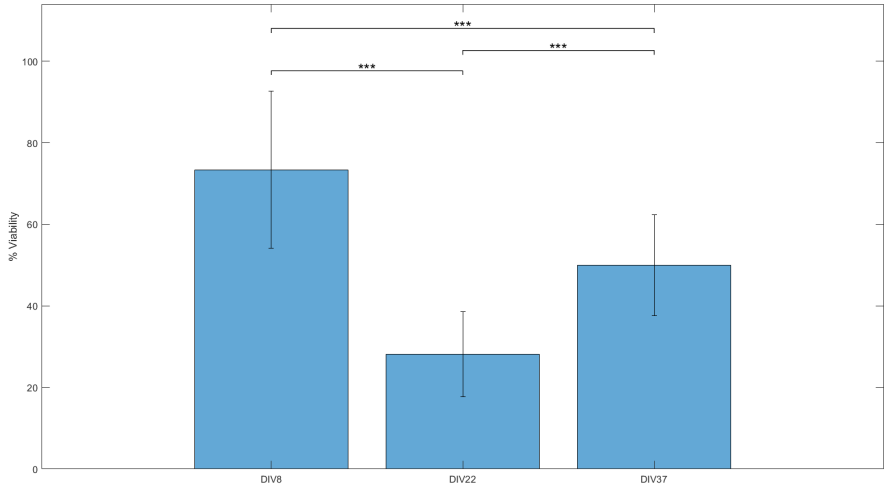

Figure 6.4.: Viability of primary neuronal cells cultured in collagen hydrogels over five weeks. (N=3, $p \leq 0.05^{*}, p \leq 0.01^{**}, p \leq 0.001^{***}$; error bars denote the standard deviation.)

Figure 6.5 shows representative confocal microscope images of cultured networks in collagen hydrogels at DIV8. A complex network of neurons could be observed in the presence of supportive astrocytes. Both cell types showed physiological morphology.[158, 159] Results imply a good cell-material interaction, as network formation was allowed by dynamical cell migration and neurite outgrowth. The low amount of present astrocytes imply a low stiffness of the material, as astrocytes favor to grow on stiff substrates.[160] Besides, figure 6.6 shows representative the homogeneous distribution of neuronal cells throughout the hydrogel.

Xie et al. described that cell spreading, proliferation and migration is highly correlated with fibrillar micro-architectures.[161] The structure of collagen hydrogels can be influenced by the polymerization temperature, polymer concentration or pH as described previously in section 3.1.2 (p.26). With increasing polymerization temperature and constant polymer concentration, it is known that the collagen stiffness is decreasing.[148, 161] Further Xie et al. showed that lower fiber stiffness enhances cell spreading dynamics, completely in agreement with results observed in this study.

As introduced previously in section 6.1 (p.45), Lee et al. showed the influence of fiber chain flexibility on the cell adhesion. Thus, cells are more likely to adhere to semi-flexible chains, as the case for collagen hydrogels.[148] Due to the low collagen concentration (see section 3.1.2, p.26) and a polymerization at 37°C, it can be assumed that same behaviors, as described above by Lee and Xiu, can be applied here.

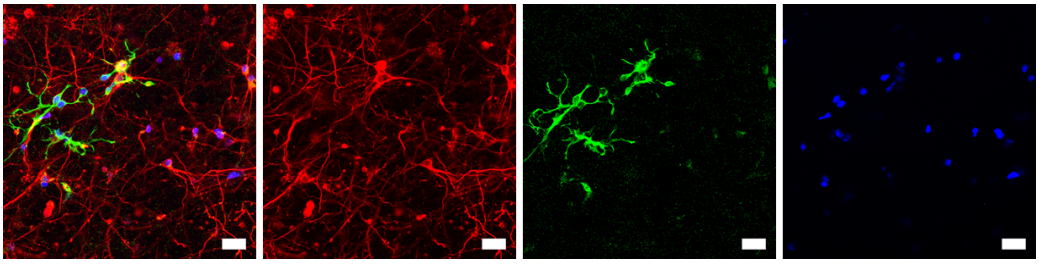

Figure 6.5.: Network maturation in collagen hydrogels at DIV8. Scale bar 20 μm. (DIV8, red:ß-III-tubulin, green:MAP-2, blue:DAPI)

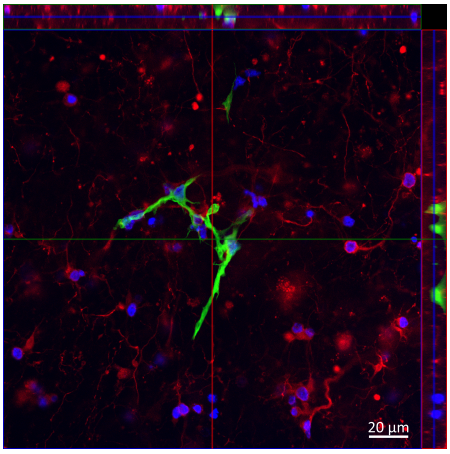

Figure 6.6.: Networks in collagen hydrogels show a homogeneous cell distribution throughout the hydrogel. (DIV8, red:ß-III-tubulin, green:MAP-2, blue:DAPI)

7. Biohybrid hydrogels enhance physiological development for long-term cultivation

Objective of this project was the development and establishment of a modular system with the desirable tuneability in mechanical and chemical properties. In the following, the two hybrid hydrogel systems: Fibrin-PVP-*co*-GMA$_{3}$*mol*% and Collagen-PVP-*co*-GMA$_{3}$*mol*%, will be introduced and examined. It has to be noted that PVP polymers with 65000 g/mol suffer from inconsistencies in fabrication. Thus, the exact molecular weight is not known and may vary a lot.

In contrast to the considered natural hydrogels introduced in the previous section, experiments presented in the following aim for long-term cultivation. Therefore experiments were elongated to about 40-41 days of culture. In order to examine the morphology of cultured networks, immunostainings will be shown (see section 3.5, p. 29). The hybrid hydrogels evaluated are based on the work of Miriam Al-Enezy Ulbrich, who established the previously introduced Fibrin-PVP-*co*-GMA$_{3}$*mol*% hydrogel.[130] They showed that the addition of PVP to fibrin hydrogels increase the stiffness and prevents the degradation of the hydrogel. Also they showed the successful cultivation of human mesenchymal stem cells for seven days *in vitro*. It has to be noted that the presented work applied cell encapsulation, while Miriam Al-Enezy Ulbrich et al. applied cell cultures on top of the biohybrid hydrogels.

7.0.1. Fibrin-PVP-*co*-GMA$_{3mol\%}$

According to observations elaborated by Miriam al-Enezy Ulbrich et al., different molecular weights of PVP were tested. Resulting from observations described in section 6.1 (p.45), a fibrinogen concentration of 1.25 mg/ml was chosen for further experiments.

Deviating from reported prevention of degradation by the addition of PVP-*co*-GMA, tranexamic acid had to be included in the cell culture medium (see section 3.3, p. 28). This might be the reasons of the direct cell encapsulation inside the hydrogel (mixing with cells previous to gelation), compared to subsequent addition [130], and/or the significantly higher cell concentration used.

However, the cell viability at DIV8 is similar in all tested polymer chain length: 6662 g/mol 52% ± 11, 8118 g/mol 64% ± 7, 65000 g/mol 66% ± 12 (see fig. 7.1). In comparison to simple fibrin hydrogels, there was no improvement in cell viability, if not even slightly diminished.

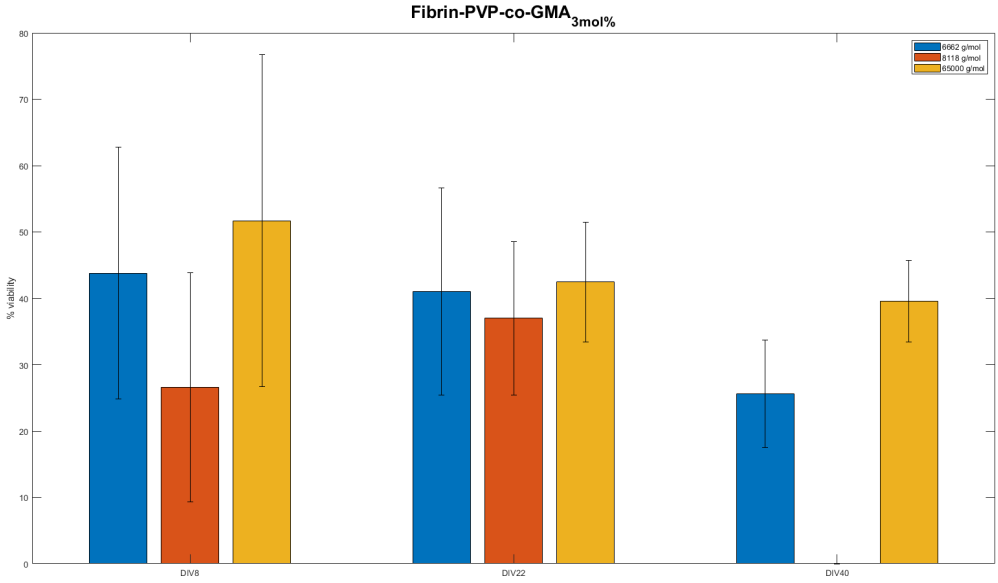

Figure 7.1.: Viability of primary neuronal cells cultured in Fibrin-PVP-*co*-GMA$_{3mol\%}$ hydrogels of different polymer chain length over six weeks. Error bars denote the standard deviation.

Similar to results obtained for simple fibrin hydrogels, Fibrin-PVP-*co*-GMA$_{3mol\%}$ suffered from escaping cells in low molecular weight gels (see fig. 7.2 and fig. 7.3). In contrast, a high polymer chain length kept the cells entrapped, while forming a 'cell-free border 'at the edge of the gel (indicated by arrow). Besides, the neuron morphology changed from a physiological to a stellar-like appearance with increasing polymer chain length (fig. 7.2 bottom row).

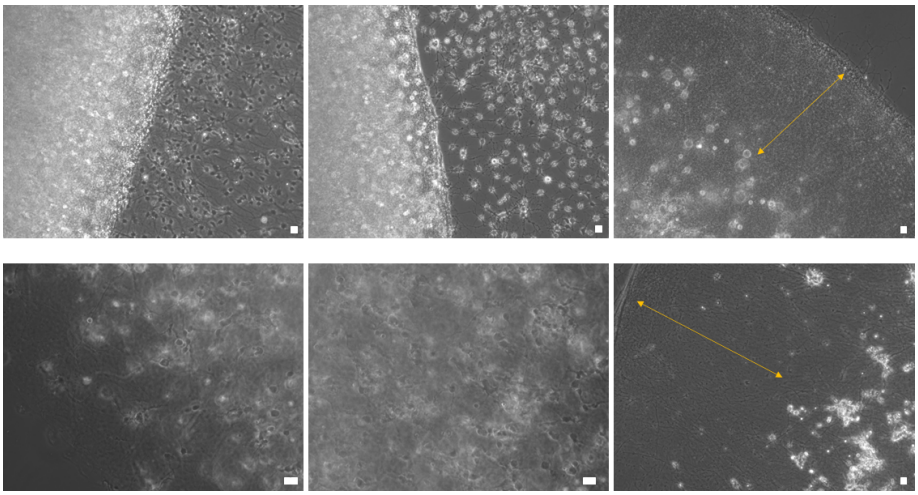

Figure 7.2.: Influence of the different molecular weights on the cell growth dynamics. Varying polymer chain length 6662 g/mol (left), 8118 g/mol (middle) and 65000 g/mol (right) show significant influence on the neuronal network formation. Scale bar 20 μm.

Immunostainings showed that both neurons and astrocytes escape from the hydrogels (see fig. 7.3). Besides, in case of the highest molecular weight, rod-like formations of astrocytes was observed at the edges of the hydrogel (fig. 7.3, bottom row). This was thought to be based on the relatively slow polymerization time and probably faster settling of the cells due to gravitation. Therefore, polymerization was carried out upside down after half time of polymerization and from the beginning, without any beneficial effects. Also the addition of OptiPrep^{TM} (Stemcell Technologies) did not solve the problem. The cause of this phenomenon lies elsewhere. Literature reports effects of leaking cells in case of insufficient adhesion points offered to the cells or disintegration of the hydrogels structure.[162, 163] As a portion of the cells grow inside the hydrogel, this hypothesis was discarded. Further analysis of the network was carried out, as described in the following.

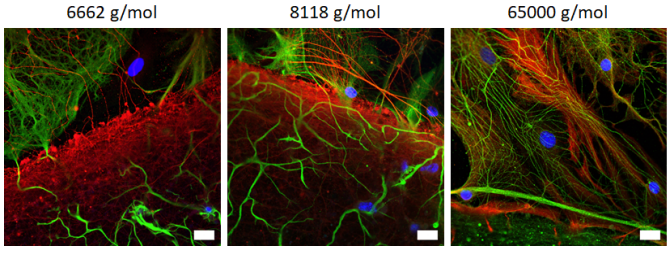

Figure 7.3.: Neuronal cells escape from Fibrin-PVP-*co*-GMA$_3$*mol*% hydrogels of polymers with different molecular weights at DIV9. Scale bar 20 μm. (red:ß-III-tubulin, green:MAP-2, blue:DAPI)

Figure 7.4 shows the network dynamics from early to advanced matured networks inside the hydrogels. It is noticeable that for lower molecular weights strong neuronal networks established in comparison to the sparse network in 65000 g/mol hydrogels. On the contrary, astrocytes showed a consistent growth in all testes hydrogels. This implies an excessive stiffness of the hydrogels for neurons, as astrocytes prefer higher stiffness environments.[160] These findings are in accordance with reported results of Al-Enezy Ulbirch et al., who showed an increased stiffness of hydrogels with increasing molecular weights.[130] Nevertheless, no significant differences in astrocyte ratios among different molecular weights could be observed. On the other hand at DIV41, networks in all molecular weights slightly declined, correlated with the decreasing viability described earlier.

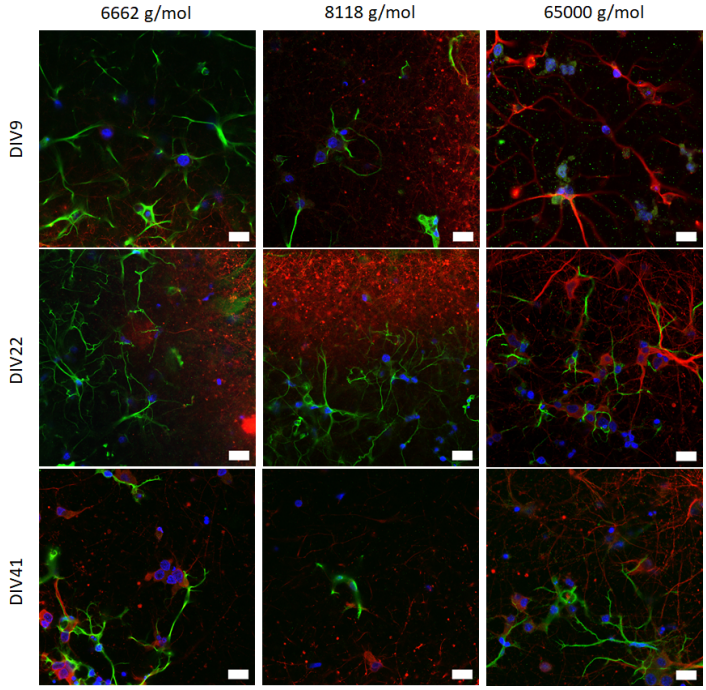

Figure 7.4.: Network maturation in Fibrin-PVP-*co*-GMA$_3$*mol*% hydrogels of different molecular weights over time. Scale bar 20 μm. (red:ß-III-tubulin, green:MAP-2, blue:DAPI)

Moreover, it was observed that astrocytes and neurons tend to separate within Fibrin-PVP-*co*-GMA$_3$*mol*% hydrogels (see fig. 7.5). While astrocytes preferably grew at the bottom of the gel, neurons sprouted at the top. This phenomenon may arise from the porous structure of the hydrogel, since cell bodies of astrocytes comprise a diameter of around 10 to 20 μm, while neurons instead have cell body diameter of about 20 to 30 μm. In order to better understand the observed cell behaviors, cryo-field emission scanning electron microscopy (cryo-FESEM) images were taken at the DWI, Aachen (see fig. 7.6). It could be observed, that Fibrin-PVP-*co*-GMA$_3$*mol*% hydrogels preserved a high porous structure of large pores, composed of walls with

even smaller pores, without any significant differences between polymer chain length. Additionally, an increased structural order with increasing molecular weight was examined.

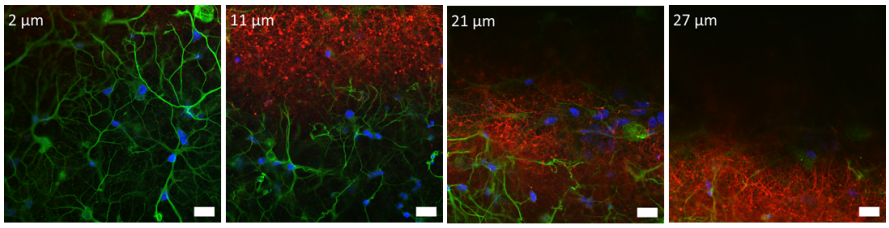

Figure 7.5.: Neurons and astrocytes separate into regions when cultured in Fibrin-PVP-*co*-GMA$_3$*mol*%. Scale bar 20 μm. (DIV22, red:ß-III-tubulin, green:MAP-2, blue:DAPI)

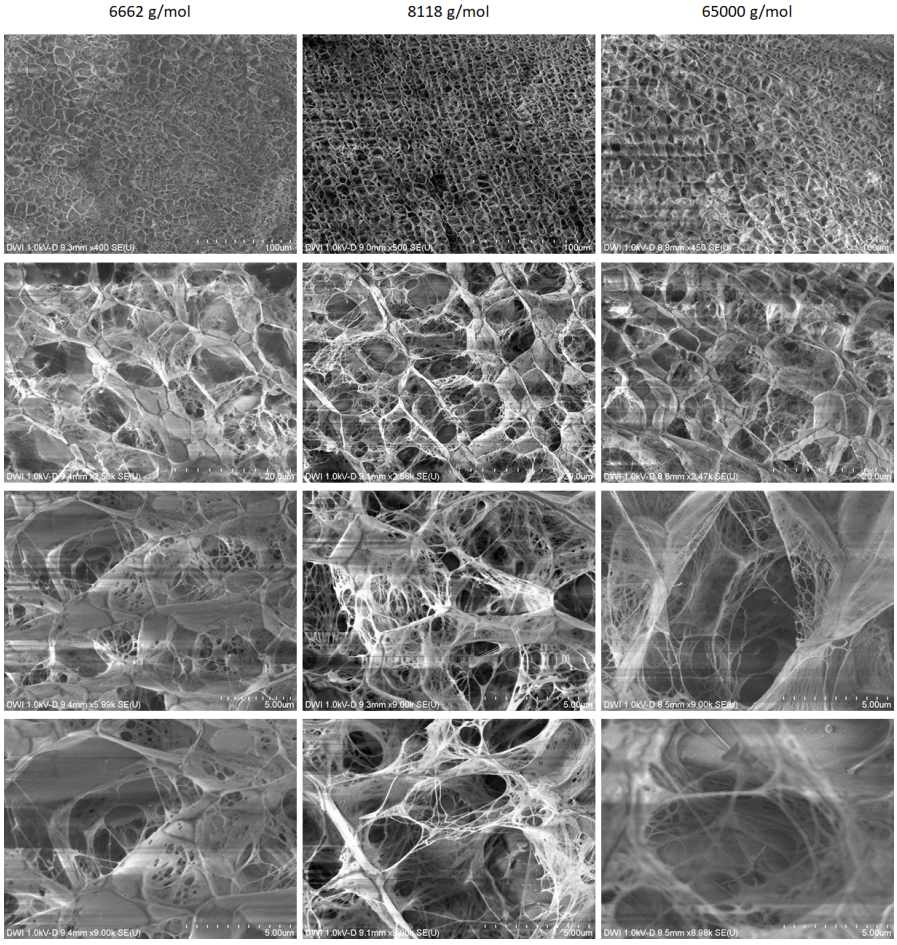

Figure 7.6.: Cryo-FESEM images of the pore structure and distribution of different molecular weights of Fibrin-PVP-*co*-GMA$_{3mol\%}$

7.0.2. Collagen-PVP-*co*-GMA$_{3mol\%}$

As fibrin is rarely present in the ECM of the CNS, collagen was evaluated as the biopolymer component. According to the distinct results presented in the previous section different molecular weights were tested, with addition of 11100 g/mol. The latter showed better reproducibility during fabrication and outstanding results in the application of human mesenchymal stem cells.[130]

A significant increase in viability was observed with the exchange of fibrinogen with collagen (see fig. 7.7), and in comparison with simple collagen hydrogels. Besides, higher molecular weights negatively influenced the cell viability over time. Especially in 11100 g/mol, cells died already after DIV22. In contrast, networks cultured in lower polymer chain length showed a constant viability of about 66-75%.

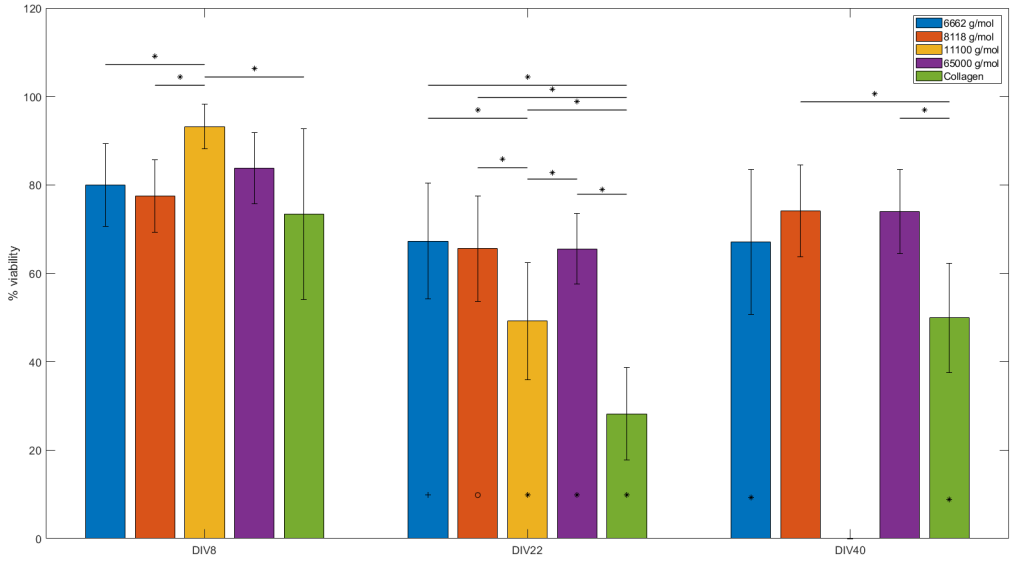

Figure 7.7.: Viability of primary neuronal cells cultured in Collagen-PVP-*co*-GMA$_{3mol\%}$ hydrogels of different polymer chain length over six weeks. (N=3, $p \leq 0.05^{o}, p \leq 0.01^{+}, p \leq 0.001^{*}$; error bars denote the standard deviation)

Figure 7.8 shows the network development over time cultured in hydrogels with different polymers of different molecular weight, while distinct behaviors were observed. Whereas low polymer chain length supported a balanced growth of neurons and astrocytes, in high molecular weight gels no specific astrocyte labeling could be observed. The latter can be a consequence of poor aliquots of antibodies. The complex network growth of neurons already at DIV8-9 imply physiological development, if comparing to observations of organotypic cultures.[164]

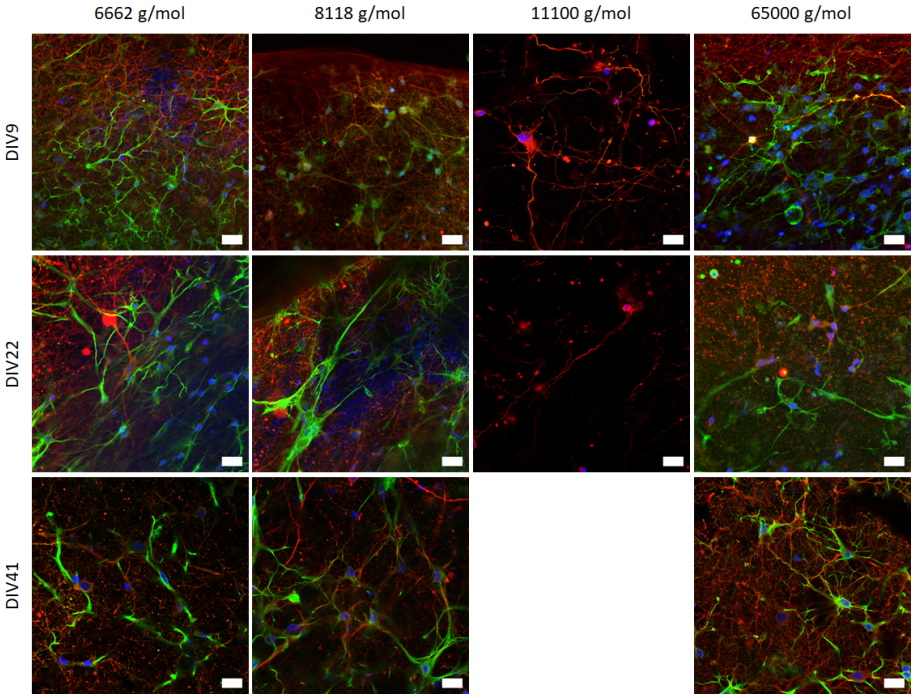

Figure 7.8.: Network maturation in Collagen-PVP-*co*-GMA$_3$*mol*% hydrogels of polymers with different molecular weights over time. Scale bar 20 μm. (red:ß-III-tubulin, green:MAP-2, blue:DAPI)

Significant differences in neurite morphology were observed for 11100 g/mol chain length. Neurites showed wormed-like appearance in comparison to cultures in other hydrogels. A change of porosity (size or structure) might be a plausible explanation of this phenomenon. This can also be a reason for the reduced network development in higher molecular weight gels.

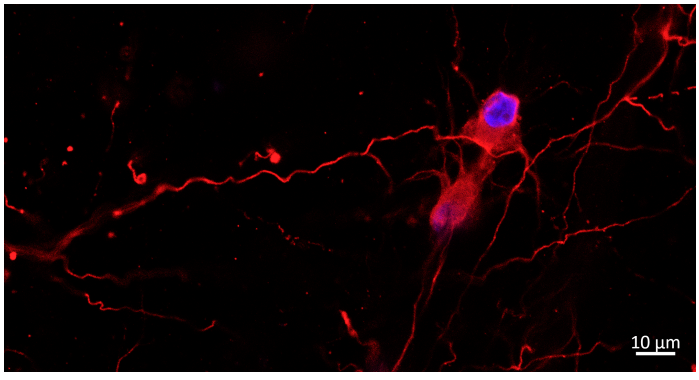

Figure 7.9.: Neurons in Collagen-PVP$_1$1100*g*/*mol*-*co*-GMA$_3$*mol*% exhibit wormed neurites. (DIV9, red:ß-III-tubulin, blue:DAPI)

In contrast to Fibrin-PVP-*co*-GMA$_3$*mol*% hydrogels, collagen-based gels exhibited a homogeneous distribution of cells throughout the gel (see fig. 7.10), implying a more favorable environment for both, neurons and glial cells.

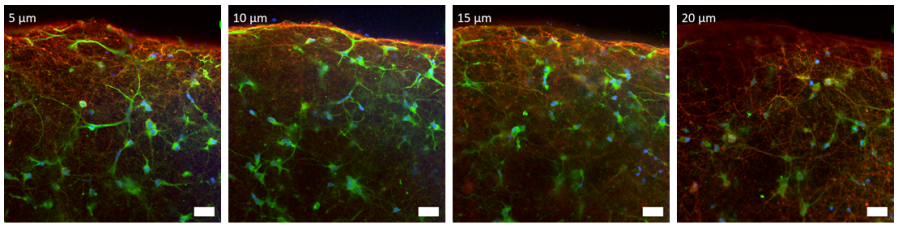

Figure 7.10.: Neurons and astrocytes homogeneously distribute in Collagen-PVP-*co*-GMA$_3$*mol*% hydrogels. The figure shows exemplary network behavior in 8118 g/mol, while being representative also for 6662 g/mol and 65000 g/mol hydrogels. Scale bar 20 μm. (DIV9, red:ß-III-tubulin, green:MAP-2, blue:DAPI)

7.0.3. Conclusion

Within this chapter the development of suitable hybrid hydrogels for primary neuronal cell culture was described and evaluated. It was shown that collagen is advantageous over fibrin as biopolymer of choice. Outstanding results shown by Collagen-PVP-*co*-GMA$_3$*mol*% have to be further analyzed regarding the micro-structural influences of hydrogel properties by e.g. rheological measurements. However a distinct behavior of PVP added to collagen in comparison with fibrin can be clearly stated. Beside the prevention of degradation and superior viability of long-term cultures, complex network maturation is enhanced by Collagen-PVP-*co*-GMA$_3$*mol*% hydrogels.

8. Development of spontaneous network activity over time

This chapter will discuss the development and differences of grown network functionality over a time period of about six weeks and within different environmental conditions (see section 3.2, p. 27), based on spontaneous network activity. First, an introduction to methods used is given. This includes general remarks about calcium imaging and the experiment setup, as well as an introduction into network analysis using graph theory. Then the final data processing flow will be presented in section 3.7 (p. 30), and applied approaches will be described. Remarks about the process of choosing the proper algorithm for the given data sets will be addressed. Finally, the development of spontaneous network activity over different maturation stages as well as the influence of different bio-polymers and polymer chain lengths will be compared and discussed.

Spontaneous network activity was recorded at three different stages of development: DIV8-9 (early), DIV22-23 (intermediate) and DIV40 (advanced). Also different polymer chain length were evaluated according to the significant differences of earlier results using fibrinogen as biopolymer (see section 7.0.1, p. 52). Instead, this section will scope the evidence of collagen-based hybrid hydrogels. Additionally to the previously tested molecular weights (6662 g/mol, 8118 g/mol, 65000 g/mol), a further PVP with 11100 g/mol was included, due to its compelling characteristics showed in the study published by Al-Enezy-Ulbrich et al..[130]

The development of the proper composition of the Collagen-PVP-*co*-GMA$_3$*mol*% was established in collaboration with Miriam Al Enezy-Ulbrich and Nicole Terefenko of the DWI Aachen.

A table with all results are presented in section A.1(p. 90). Details about the calcium imaging experiment can be found in section 3.6.2 (p. 30).

8.1. Influence of different molecular weights of PVP on spontaneous network activity development

As introduced in section 5 (p.41), generalized transfer entropy was applied to networks with more than five spontaneously active neurons. It is known that neuronal activity occurs already at early developmental stages.[165] GTE was applied to networks consisting of on average 34 to 122 active cells in early networks. The polymer chain length of 8118 g/mol provided an outstanding number of active neurons compared to the others (see fig. 8.1), getting close to numbers observed in organotypic cultures of 310 ± 127 cells.[166] Also the highest molecular weight showed an increased number of functional neurons, although it has to be mentioned, that this polymer chain length suffered from a bad reproducibility regarding its molecular weight during fabrication. Therefore, the results of this longest polymer chain length are shown, but viewed as not trustworthy. With time, the amount of spontaneously active cells decreased for all polymer chain lengths. A significant drop between early and advanced matured networks was observed for Collagen-PVP_{8118}-*co*-$GMA_{3mol\%}$, with an approximately 6.4-fold drop in spontaneously active neurons. As already described in section 7.0.2 (p. 56), neurons within Collagen-PVP_{11100}-*co*-$GMA_{3mol\%}$ died already after DIV22, whereby spontaneous activity in intermediate matured networks could be observed in just one of six cultures. Opposing results were obtained by Downes et al., who reported a relative constant number of active cells during development, whereas it should be noted that they measured 2D cell cultures.[167]

Another basic measure of network characteristics is the synchronous activity, here displayed in figure 8.2 as the frobenius norm of GTE (see section 2.5.2, p. 21). Also cross-correlation and phase synchronization estimates of connectivity were considered using the frobenius norm (for exemplary results see section A.2, p. 97), without any significant differences noticeable. According to Chiappalone et al., rodents show first synchronized spontaneous activity in 2D cell cultures at about two to three weeks recorded from micro-electrode arrays (MEAs).[168] It is known that early synchronization of spontaneous activity in a network triggers the functional maturation by influencing neurogenesis, synaptogenesis, myelination and many more.[165][169] This happens not only in the cortex but also in a variety of other regions of the brain, such as e.g. the hippocampus.[170][169]

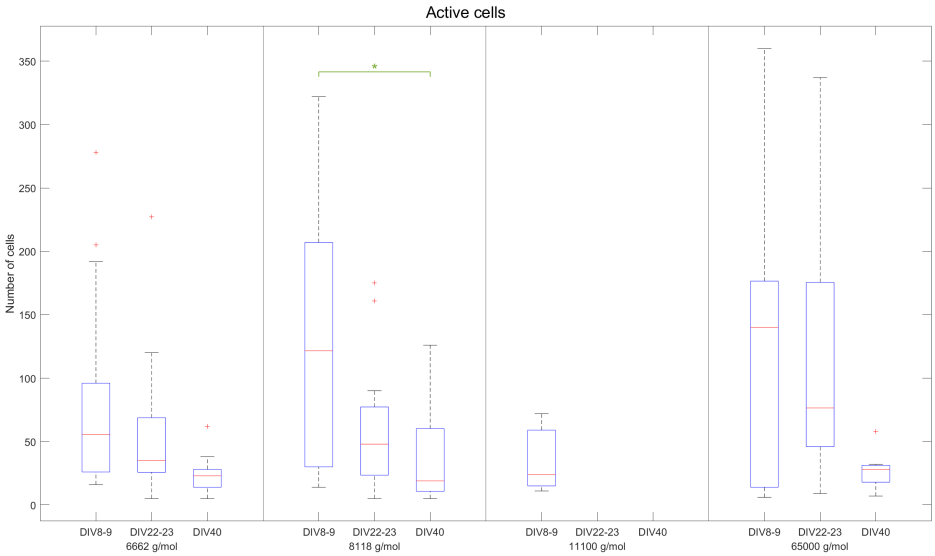

Figure 8.1.: Average number of spontaneously active cells observed in Collagen-PVP-*co*-GMA$_{3mol\%}$ hydrogels at different phases of maturation. Significant differences are depicted by stars (*** for p $\leqslant$ 0.001, ** for p $\leqslant$ 0.01 and * for p $\leqslant$ 0.05). Error bars denote the standard deviation.

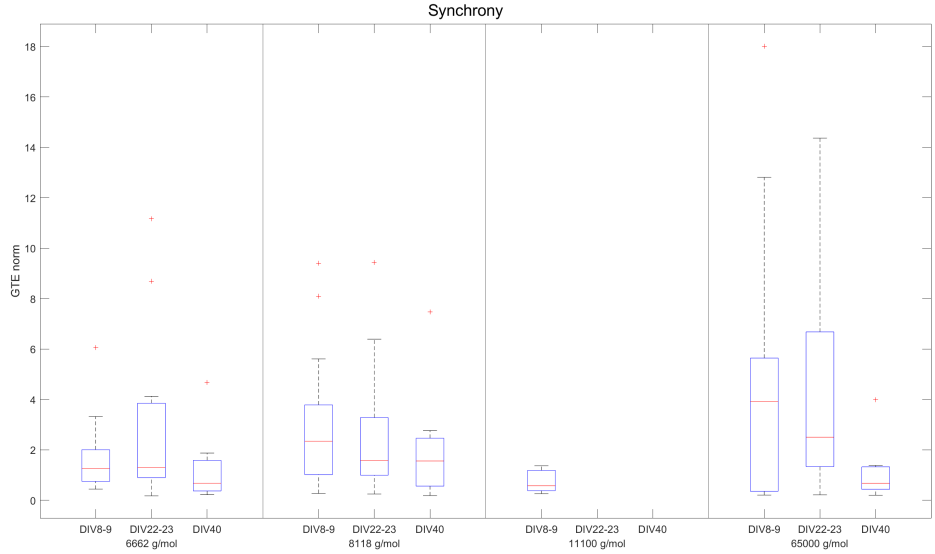

Figure 8.2.: Synchrony, depicted as the frobenius norm of GTE, of spontaneously active cells observed in Collagen-PVP-*co*-GMA$_{3mol\%}$ hydrogels at different phases of maturation. Significant differences are depicted by stars (*** for p $\leqslant$ 0.001, ** for p $\leqslant$ 0.01 and * for p $\leqslant$ 0.05). Error bars denote the standard deviation.

Synchrony was observed within this study already in early maturated networks of all PVP chain lengths. However, no significant changes could be observed over time, although a trend towards a decreasing synchrony over time of spontaneous active networks can be presumed, as the medians for Collagen-PVP_{8118}-*co*-$GMA_{3mol\%}$ slightly declined. Similar results were obtained by Enright et al., who studied the influence of astrocytes and oligodendrocytes onto the spontaneous network activity using multi-electrode arrays (MEAs).[16] Furthermore, it was reported that young cultures of about two weeks can show low synchronization due to an imbalanced ratio of exhibition and inhibition. However, literature also indicates a saturated state of synchrony after some time of maturation. Previous findings suggest an advanced level of maturation already at DIV8-9. In contrast, further network development may arise over time. Another cause can be the presence of a not yet functional network due to an excitatory-inhibitory imbalance. It has to be noted that GTE, as established by Stetter et al., was constructed to only detect inhibitory connectivity, indicating that preceding assumptions might be applicable. Due to the parallel visual inspection of recorded movies and raster plots, the assumption of a moderate to high level of synchronization in observed networks is well-founded.

In contrast to the synchrony, the mean firing rate showed different trends in development with increasing molecular weight. Instead, Collagen-PVP_{8118}-*co*-$GMA_{3mol\%}$ promoted a significant increase in firing rate from early (0.1±0.03 Hz mean±SD) to advanced matured networks (0.19±0.09 Hz). Remaining molecular weights, showed deviating results, with a roughly constant firing rate over time. Merely networks grown Collagen-PVP_{6662}-*co*-$GMA_{3mol\%}$ revealed a drop in the mean firing rate during the intermediate matured network stage. Low values at early maturation can be explained by unorganized firing patterns and a low synaptic density.[168]Literature shows similar mean firing rates of two weeks old cultures in the range of 7.1 events/min, increasing to 12.9 events/min at three weeks old 3D in vitro cultures[171], comparable to Collagen-PVP_{8118}-*co*-$GMA_{3mol\%}$. Also in organotypic cultures mean firing rates of about 0.79 ± 0.65 Hz could be observed.[166] Other studies report increases even higher than 0.5 Hz between DIV 20 - 30.[16, 172] It has to be noted that the presented results were computed from recordings of one minute duration (see section3.6.2, p. 30). A critical view on the influence of recording time on estimations of functional characteristics is described later in section 8.2, p.70. The limited recording time is most probably the major reason of inconsistencies in firing rates observed.

In order to expand on the network developmental characteristics, previously introduced network measures from graph theory can be used to estimate functional connectivity (see section 2.5.2, p.21). As depicted in figure 8.4, the number of links connected to a node decreased over time for all tested polymers. Especially Collagen-PVP_{8118}-*co*-$GMA_{3mol\%}$ denoted a significant drop from early to advanced matured networks. By contrast the strength, a weighted variant of the degree, implied a consistent progress. This behavior can be explained either by a poor functional differentiation [167], or contrary by synaptic pruning as a result of development. In order to study the underlying spontaneous network activity in more depth regarding network development, further estimations have to be made, as described in the following.

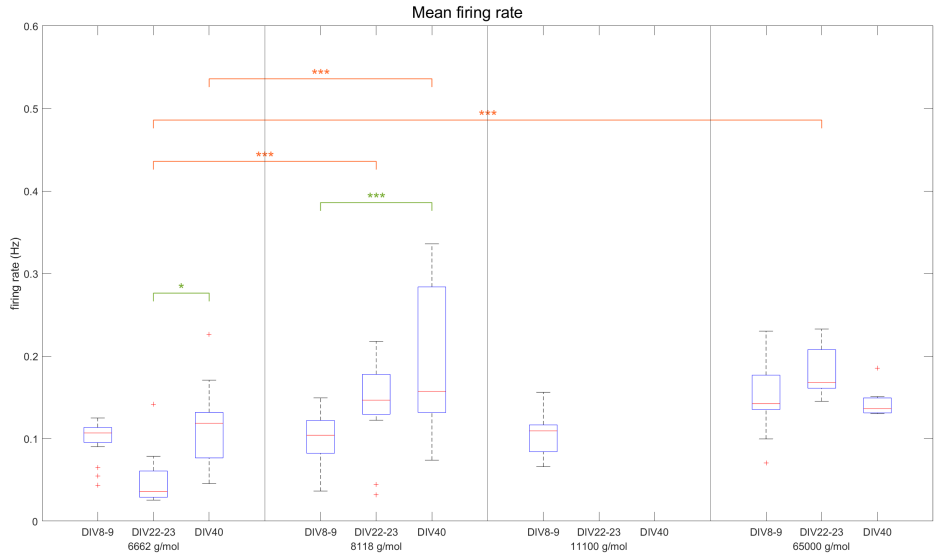

Figure 8.3.: Mean firing rate of spontaneously active cells observed in Collagen-PVP-*co*-GMA$_{3mol\%}$ hydrogels at different points of maturation. Significant differences are depicted by stars (*** for p $\leqslant$ 0.001, ** for p $\leqslant$ 0.01 and * for p $\leqslant$ 0.05). Error bars denote the standard deviation.

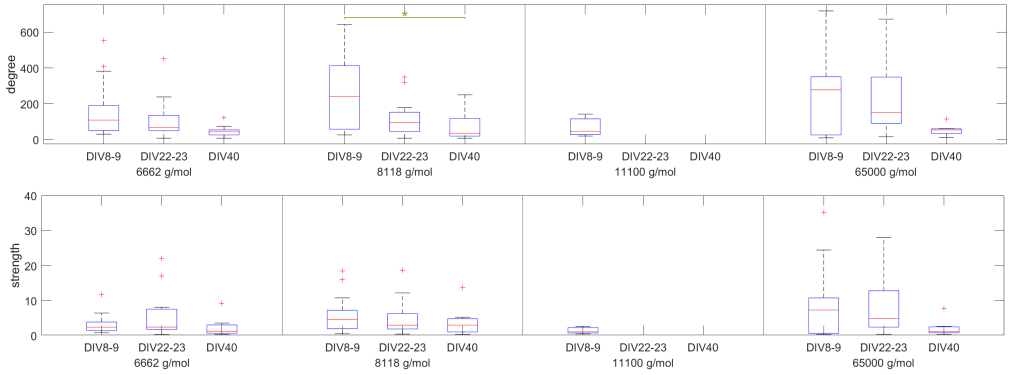

Figure 8.4.: Development of node degree and strength of spontaneously active networks in Collagen-PVP-*co*-GMA$_{3mol\%}$ hydrogels at different points of maturation. Significant differences are depicted by stars (*** for p $\leqslant$ 0.001, ** for p $\leqslant$ 0.01 and * for p $\leqslant$ 0.05). Error bars denote the standard deviation.

Healthy and physiological functioning networks are characterized by a balance of integration and segregation, which is known to establish during development.[105] In order to characterize the influence of different molecular weights on the development of cultured networks, these two measures were considered in more detail. Short average path lengths are known to be linked to efficient information flow [173], completely agreeing with the results presented. Figure 8.5 depicts three measures of integration (see section 2.5.2, p.21). For all tested polymers, the average characteristic path length decreased with maturation of the network. Lower molecular weights (6662 g/mol and 8118 g/mol) denoted significant drops between early and advanced matured networks, whereas no significant differences between the tested polymers could be observed. As expected, the local and global efficiency accordingly showed a significant increase with age.

Strong differences could be observed for measures of segregation between different molecular weights tested (see fig. 8.6). While transitivity implied an increasing trend with a significant change from early towards advanced networks for small molecular weights, the modularity seemed to stay constant over time, while increasing interquartile ranges were noticeable for 8118 g/mol polymers. Similar to Dingle et al. [171] and Shimono et al.[166], two to three communities, or modules, could be observed during the whole culture time, indicating a relatively weak community structure.[171] These results are indicative for the ability of fast information processing, as high clustering coefficients are known to support integration and resilience. [174, 175] In this study, transitivity was chosen as a variant of the clustering coefficient (see section 3.7.2, p.32).

In contrast to the transitivity, the average number of cells participating in a community decreased similar to the amount of spontaneously active cells (see p.75). Significantly higher numbers could be observed in early matured networks of small and moderate polymer chain length, compared to high molecular weights. The specialization of a network is thought to be highly influenced by the underlying community structure. With an increasing modularity, a higher level of segregation is associated, due to a strong inter-modular connectivity. This implies a weak functional level of the networks observed.

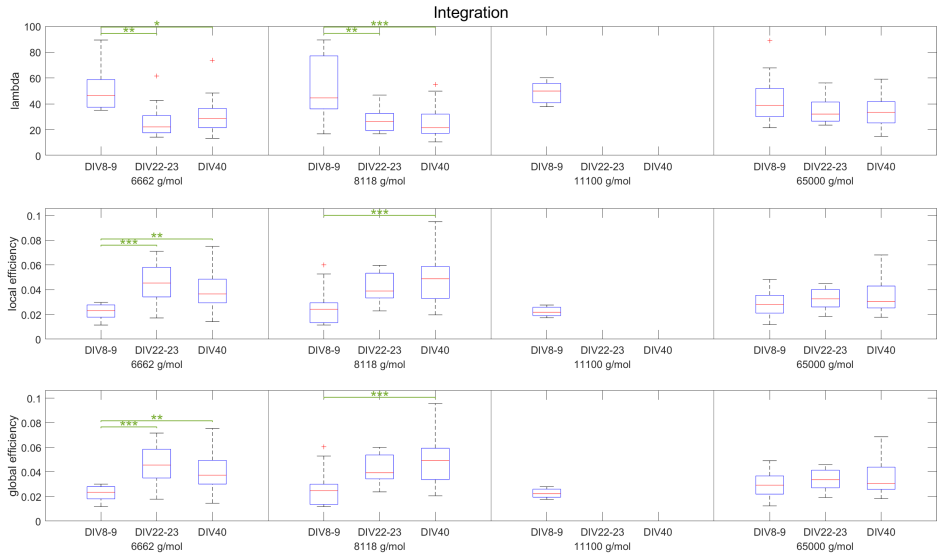

Figure 8.5.: Development of different measures of integration derived from spontaneously active networks in Collagen-PVP-*co*-GMA$_{3mol\%}$ hydrogels. Significant differences are depicted by stars (*** for p $\leqslant$ 0.001, ** for p $\leqslant$ 0.01 and * for p $\leqslant$ 0.05). Error bars denote the standard deviation.

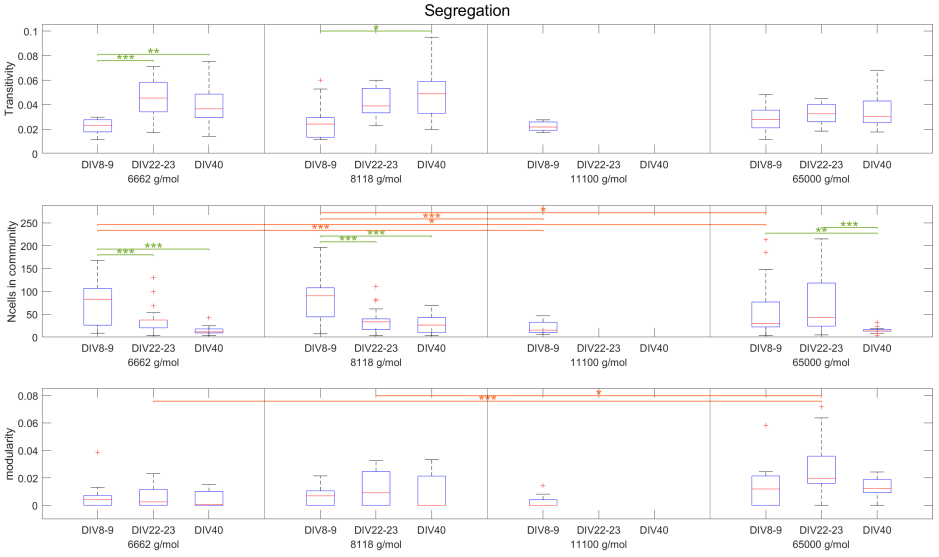

Figure 8.6.: Development of different measures of segregation derived from spontaneously active networks in Collagen-PVP-*co*-GMA$_{3mol\%}$ hydrogels. Significant differences are depicted by stars (*** for p $\leqslant$ 0.001, ** for p $\leqslant$ 0.01 and * for p $\leqslant$ 0.05). Error bars denote the standard deviation.

As previously described, modularity is driven by special nodes (see section 2.5.2, p.21). The importance of a node in a network can be described by its measure of centrality. Figure 8.7 shows the most commonly used network measures to infer centrality. Betweenness centrality, also a measure of information flow, stayed constant for all tested polymers with network development. Similar behavior could be noticed for the within-module z-score, whereas the participation coefficient may allow to imply a slight decreasing propensity.

Further distinctions between important nodes can be made by the classification into hub cells and further into connector and provincial hubs. The explicit classification used, is explained in section3.7.2, p.32, using previously described network measures. It is noticeable that the proportion between nodes being defined as hubs and non-hubs was, over time and polymers, roughly 1:1. The same applies for connector and provincial hubs. This implies a balance of within and inter-modular communication. Nevertheless, an overall decreasing trend could be observed, while Collagen-PVP$_{8118}$-*co*-GMA$_{3mol\%}$ was apparent regarding the amount of nodes being detected at DIV8-9.

Hub cells had been reported to be central actuators in information exchange, although their explicit role in shaping synchronous network behavior is still being investigated. Sun and coworkers described the synergy of hub cells and core activity patterns in dissociated neuronal cell cultures.[176] They found, that these core patterns are mainly driven by hub neurons, implicating the crucial role of hubs in spontaneous activity dynamics of developing networks. Opposing to observed results, in this study, Sun et al. reported an increase of identified hub cells during development. On the other hand, Dingle et al. was not able to detect any hub cells in untreated cultures, explained by unspecialized networks in combination with reported low modularity.[171]

Reasons for diverging results in detected hub cells can be versatile. To mention some major obstacles, focusing attention onto the chosen estimator of connectivity as well as the particular definition of hub cells is necessary. Besides, also experimental conditions may influence confound results, as it is e.g. known that cell density plays a major role in network maturation.

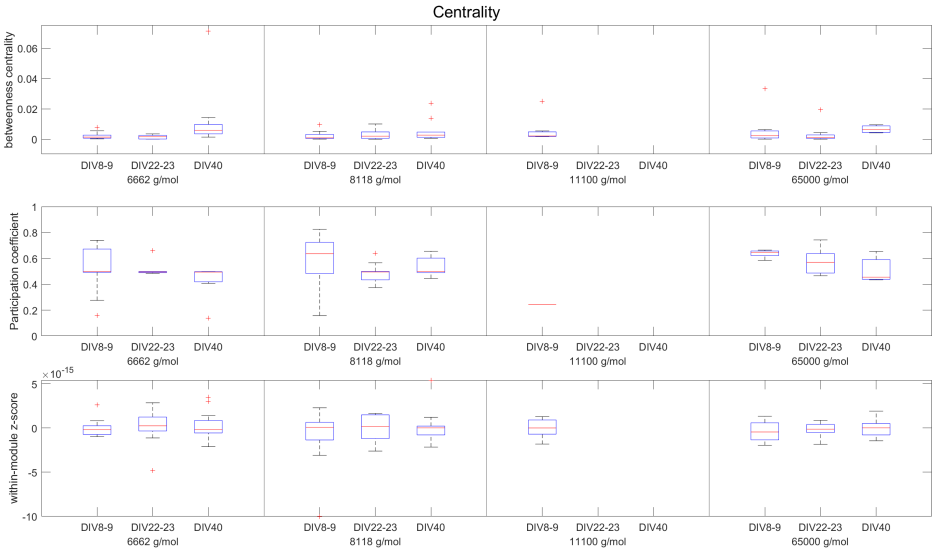

Figure 8.7.: Development of different measures of node centrality derived from spontaneously active networks in Collagen-PVP-*co*-GMA$_{3mol\%}$ hydrogels. Significant differences are depicted by stars (*** for $p \leqslant 0.001$, ** for $p \leqslant 0.01$ and * for $p \leqslant 0.05$). Error bars denote the standard deviation.

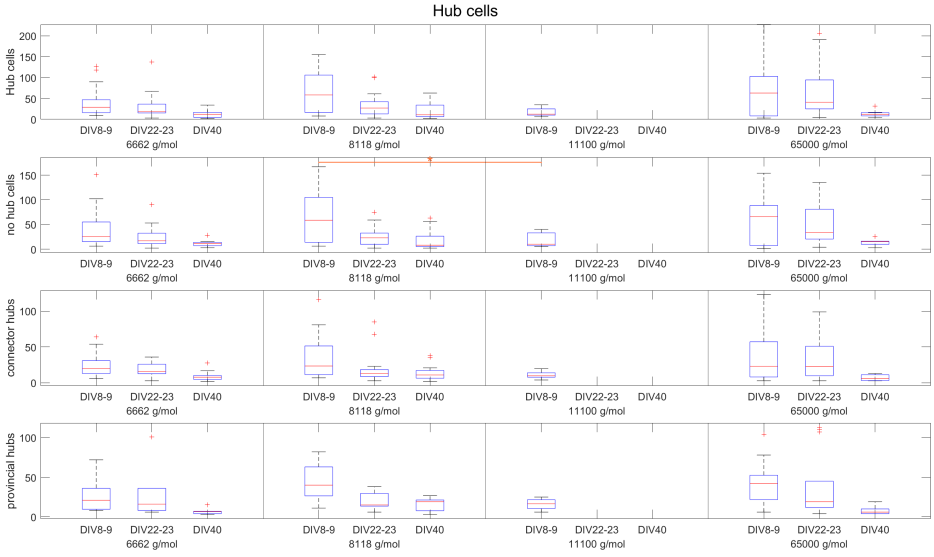

Figure 8.8.: Emergence of of hub cells in spontaneously active networks cultured in Collagen-PVP-*co*-GMA$_{3mol\%}$ hydrogels at different phases of maturation. Significant differences are depicted by stars (*** for $p \leqslant 0.001$, ** for $p \leqslant 0.01$ and * for $p \leqslant 0.05$). Error bars denote the standard deviation.

Another measure of network development is the small-worldness, as described in section 2.5.2, p.21. Small-world networks are also known to be influenced by the presence of hub nodes. Increasing amount of hub nodes had been reported to be correlated with small-world behavior, contrary to observations of the presented study.[167]

Figure 8.9 depicts the change of the small world propensity (SWP) over time for different polymers. It becomes apparent, that gels with smaller polymer chain length encouraged an slight increase in SWP, while higher molecular weights imply a decrease or roughly steady trend. Though no statistical significant differences could be observed. Nevertheless, these trends confirm previous findings regarding integration and segregation, as well as being in agreement with prevailing literature.

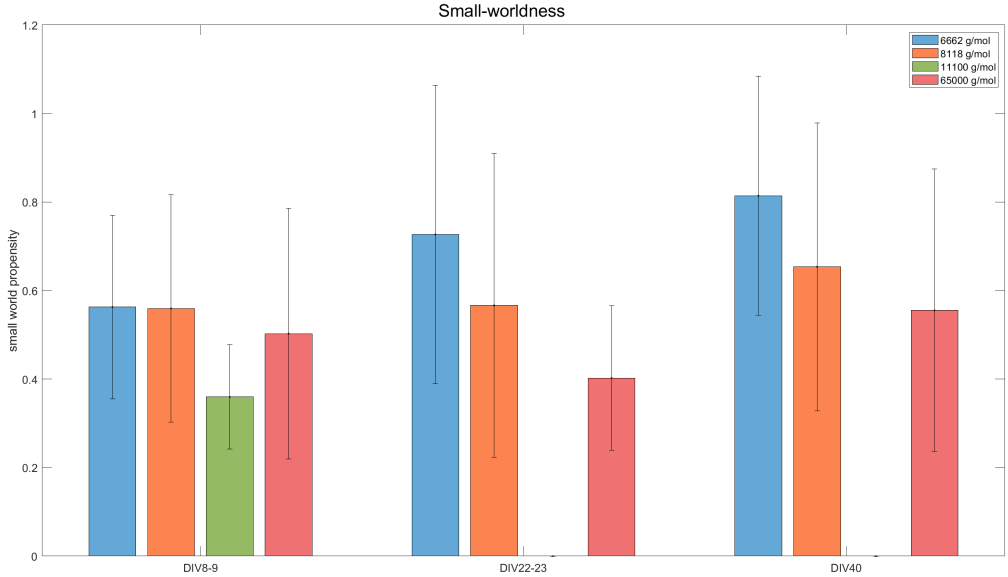

Figure 8.9.: Small-worldness of spontaneously active networks cultured in Collagen-PVP-*co*-GMA$_{3mol\%}$ hydrogels at different phases of maturation. Significant differences are depicted by stars (*** for $p \leqslant 0.001$, ** for $p \leqslant 0.01$ and * for $p \leqslant 0.05$). Error bars denote the standard deviation.

Besides the ability of a network to be in a balanced state of integration and segregation, a network can be characterized by the ability of resilience. The measure of choice in this study was the assortativity (see section 2.5.2, p.21). Biological networks are thought to generally show negative assortativity[177], implied as dissortativity, as also showed by experimental results of Wrosch et al..[100]

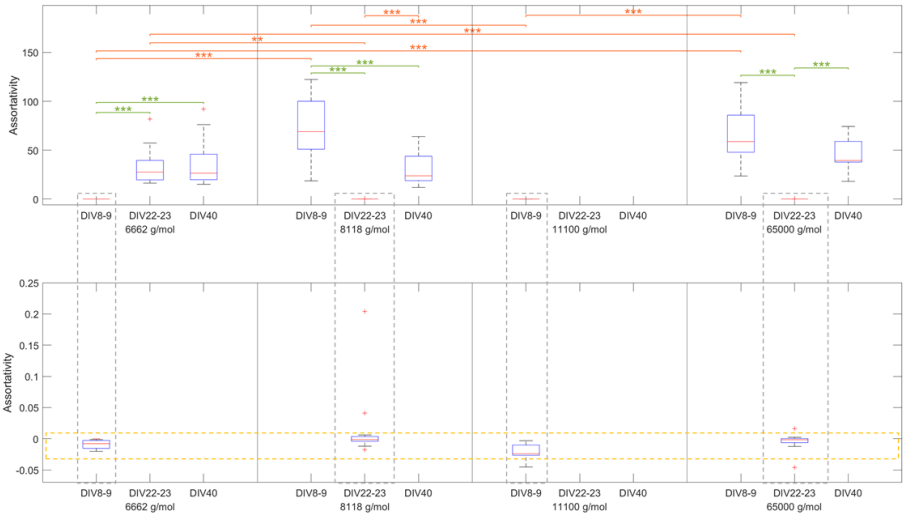

Figure 8.10.: Assortativity as measure of resilience in spontaneously active networks cultured in Collagen-PVP-*co*-GMA$_{3mol\%}$ hydrogels at different phases of maturation. Significant differences are depicted by stars (*** for p $\leqslant$ 0.001, ** for p $\leqslant$ 0.01 and * for p $\leqslant$ 0.05). Error bars denote the standard deviation.

Within this study, interesting observations of assortative behavior during developing networks in vitro could be reported. As depicted in figure 8.10 it could be differentiated between two behaviors. Networks cultured in Collagen-PVP$_{6662}$-*co*-GMA$_{3mol\%}$ showed in early matured stage a dissortative behavior. This changed significantly at DIV22-23, by a fold change of 3.7, and then equilibrate until DIV40. Also Collagen-PVP$_{11100}$-*co*-GMA$_{3mol\%}$ showed dissortativity in early matured networks. On the other hand, networks within Collagen-PVP$_{8118}$-*co*-GMA$_{3mol\%}$ supported a significantly higher assortativity in early maturity and then extremely droped to a scope close to zero, with a 4.5 fold change at DIV22-23. Subsequently, dissortativity changed to assortativity again until DIV40, although being $\sim$ 2.3 times lower than at DIV8-9. Bezel et al. reported dissortative networks to gain an important role in network communication regarding information transmission from a community towards other modules. Instead, assortative communities are reflective for segregation.[178] If following this hypothesis, networks growing in Collagen-PVP$_{6662}$-*co*-GMA$_{3mol\%}$ showed in early stages a dominantly integrative behavior changing to segregation. On the other hand, networks cultured in Collagen-PVP$_{8118}$-*co*-GMA$_{3mol\%}$ showed a strong potential of modularity at early maturation, followed by a significant change in network

behavior towards preferential information transmission, to then remodel into a new community structure. This behavior implies a change of in- and out-strength, which cannot be observed in common with previously described behavior (see appendix A.3, p. 99). The cause of this phenomenon might be the short recording time of one minute, discussed in the following section 8.2 on p.70.

8.1.0.1. Conclusions

This section scoped the influence of different polymer chain length in Collagen-PVP-*co*-$GMA_{3mol\%}$ on the development of spontaneous network activity. Thereupon, Collagen-PVP_{8118}-*co*-$GMA_{3mol\%}$ can be evaluated as being the most favorable culture system of primary neuronal cells compared to other molecular weights tested. Collagen-PVP_{8118}-*co*-$GMA_{3mol\%}$ outstandingly supports the physiological network development in absence of any external stimulation of the culture. Intrinsically, networks with a balanced integration and segregation, consisting of diverse hub cells, as well as an emerging resilient core, evolve over 40 days of culture.

8.2. Importance of recording times limited by setup possibilities

This section will scope the influence of recording times onto the presented results. It has to be mentioned that the maximum recording time possible was limited due to the setup. A maximum recording time of 5 minutes was possible (here denoted as long recording time), as the software started to freeze for 10 to 15 minutes after each recording, which made it impossible to scale the recordings. With increasing recording times the software would crash, also with reducing the window size of the region of interest (ROI) and a reasonable frame rate. Therefore, recording times of 1 minutes and 5 minutes were chosen to be the most sufficient settings. In the following, only graphs with statistical significant differences will be shown. Remaining graphs can be found in appendix A.5 (p. 103).

Significant differences could be observed for the mean firing rate (see fig. 8.11). While in short recording times the firing rate slightly increased, long recordings showed a more constant behavior over time with significantly lower median values. Figure 8.12 emphasizes the importance of recording times regarding dynamical patterns being visible. Dynamical activity patterns or core patterns were not possible to be visualized by short recording times. Even a recording time of 5 minutes was not sufficient to capture repetitive patterns, making results highly variable regarding the onset of the experiment. Literature shows a recording time of about 20 minutes up to 1.5 hours for *in vitro* and *in vivo* calcium imaging recordings, which was not possible with the given setup. However, a high number ob trials and recordings per gel made it possible to get a first glance about the underlying network behavior, as visible if considering other network measures evaluated.

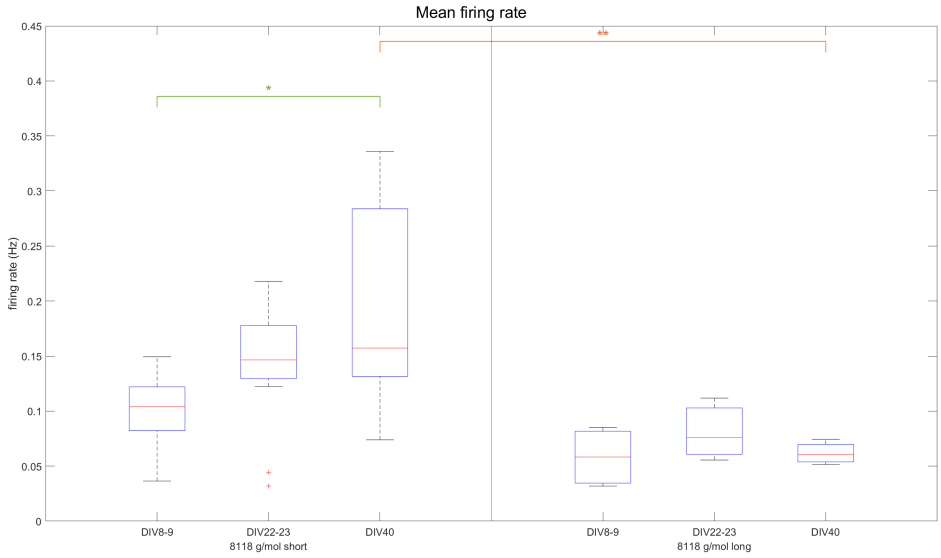

Figure 8.11.: Difference of the mean firing rate of spontaneously active cells cultured in Collagen-PVP-*co*-GMA$_{3mol\%}$ hydrogels, derived from different recording times. Significant differences are depicted by stars (*** for p $\leqslant$ 0.001, ** for p $\leqslant$ 0.01 and * for p $\leqslant$ 0.05). Error bars denote the standard deviation.

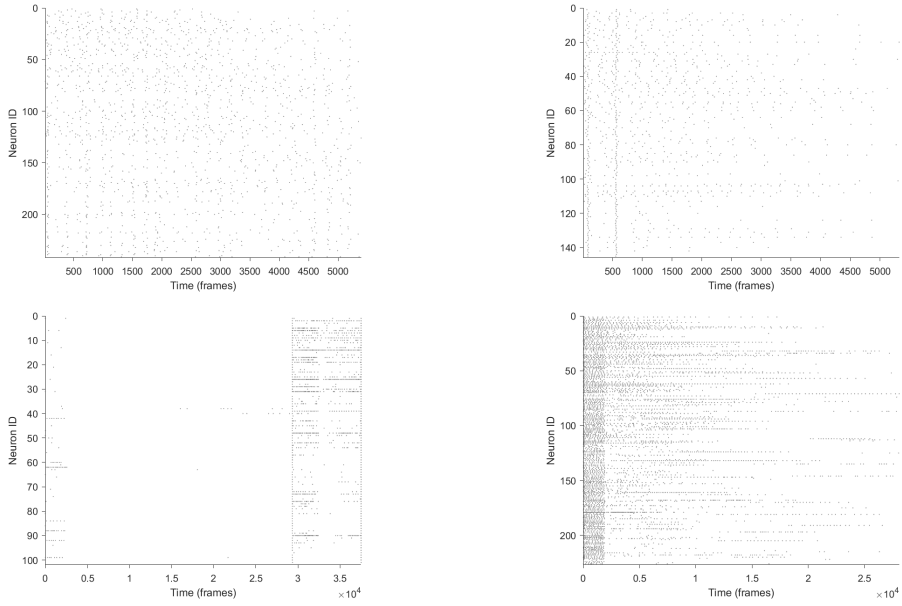

Figure 8.12.: Exemplary raster plots of spontaneous active networks cultured in Collagen-PVP-*co*-GMA$_3$*mol*% hydrogels. (pper row: short recording times, second row: long recording times.)

While no significant changes could be observed in the average amount of active cells, synchrony, degree and strength, as well as segregation, integration reveal distinct behaviors (see fig. 8.13). Instead of a clear reduction of the average characteristic path length, a drop at DIV22-23 could be observed. It has to be taken into account, that the number of trials at DIV22-23 for long recordings was limited to three gels, due to contamination issues, which might enhance the decreasing behavior at that point. Accordingly, the efficiency was increasing with decreasing lambda.

In the case of resilience, a change in assortativity towards observed behaviors of short molecular weight gels could be seen (see p.69). Instead of a drop at intermediate maturity stage, networks showed dissortativity already at early time points for long recordings, with an assortative trend with maturation (see fig. 8.14). Assortativity describes the correlation between the strength of all nodes connected to a sharing link. By having a look at the degree, of both short and long recordings, it is getting clear that the medians of shorter recording times revealed medians shifted towards zero, while medians of longer ones seem to be steady. It could be hypothesized that in case of short recordings, time windows of high activity had been captured, leading to a higher degree estimation. It is more likely that the real behavior of the underlying network resembles results obtained by long recordings. During early maturation, less connectivity was present, leading to a lower degree and a more dissortative characteristic. With maturation, connectivity was established and assortativity rised due to increasing segregation. During network specialization, functional connectivity was optimized, indicated by a significant leap of assortativity.

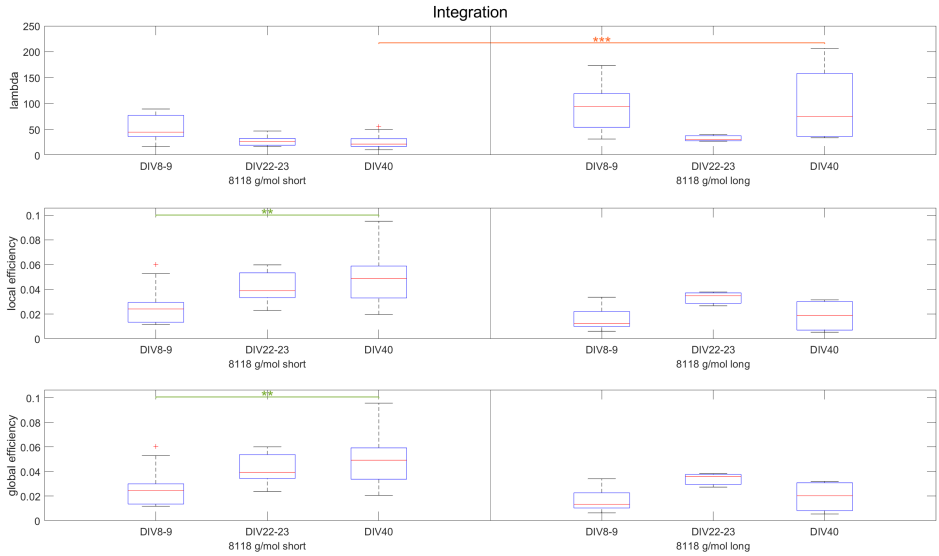

Figure 8.13.: Comparison of the development of different measures of integration from spontaneously active networks cultured in Collagen-PVP-*co*-$GMA_{3mol\%}$ hydrogels, derived from different recording times. Significant differences are depicted by stars (*** for $p \leqslant 0.001$, ** for $p \leqslant 0.01$ and * for $p \leqslant 0.05$). Error bars denote the standard deviation.

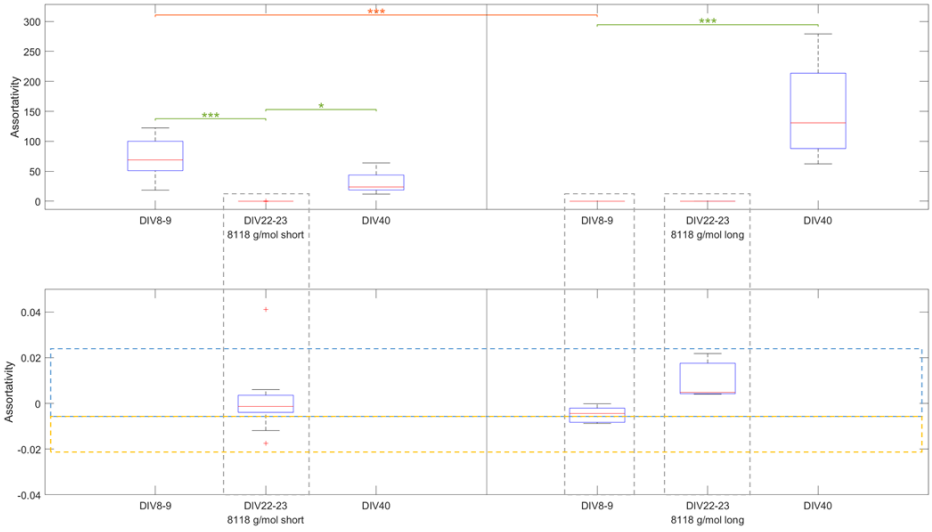

Figure 8.14.: Comparison of assortativity as measure of resilience in spontaneously active networks cultured in Collagen-PVP-*co*-$GMA_{3mol\%}$ hydrogels, derived from different recording times. Significant differences are depicted by stars (*** for $p \leqslant 0.001$, ** for $p \leqslant 0.01$ and * for $p \leqslant 0.05$). Error bars denote the standard deviation.

8.2.1. Conclusion

This section addressed the importance of recording times in functional connectivity estimation. The comparison of short (1 min) and long (5 min) recordings showed the significance of the recording time of choice in respect to the question of interest. An increase from one to five minutes did not affect the results significantly for most of the network measures. Drawback of the long recordings are the limited number of trials and inter-trial measurements due to setup limitations.

Therefore and regarding the observed influences of longer observation times, in the following only the short times will be evaluated. This will accomplish the needs to make a point about the supportive characteristics of the developed hybrid hydrogel.

In further studies, it will be necessary to increase the observation times drastically to at least 30 min, for more detailed and profound evaluation of issue-specific leading questions of interest.

8.3. PVP-*co*-GMA$_{3mol\%}$ has a major influence on network development compared to simple Collagen gels

This section will scope the comparison and advances of Collagen-PVP$_{8118}$-*co*-GMA$_{3mol\%}$, according to results described in section 8.1 on p.60, over simple collagen hydrogels.

The main and most compelling advantage of using collagen-PVP$_{8118}$-*co*-GMA$_{3mol\%}$ over simple collagen is the ability for long-term cultures, since networks cultured in collagen die after DIV22-23 (see section 6.2, p.48). However, there was no significant difference between the number of average active cells visible, emphasizing previous results of good biocompatibility of PVP-*co*-GMA$_{3mol\%}$ (see section 7, p.51). Same applies for further networks measures, wherefore this section will concentrate on main developmental indicators as the balance of integration and segregation, presence of hub cells and the ability for resilience. Remaining network measures, as evaluated previously, can be found in appendix A.4 on p.100 and do not show statistical significant differences in behavior.

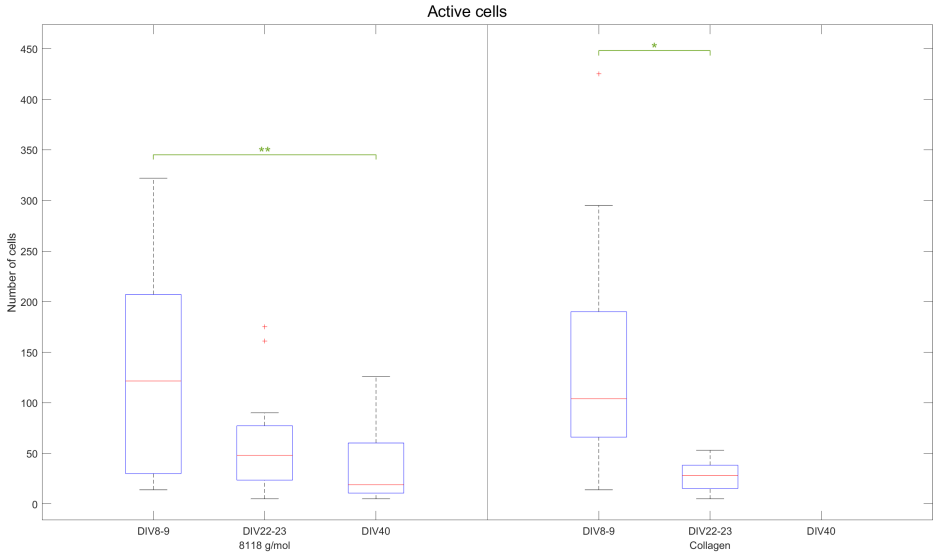

Figure 8.15.: Comparison of the average spontaneous active cells cultured in Collagen-PVP-*co*-GMA$_{3}$*mol*% and collagen hydrogels. Significant differences are depicted by stars (*** for $p \leqslant 0.001$, ** for $p \leqslant 0.01$ and * for $p \leqslant 0.05$). Error bars denote the standard deviation.

As described previously (section 2.5.2, p.21 and section 8.1, p.60), the balance of integration and segregation is an important characteristic of a healthy functioning network in the brain. Figure 8.16 and 8.17 depict the well balanced behavior of networks cultured in Collagen-PVP_{8118}-*co*-$GMA_{3mol\%}$ and collagen. While the ability of fast processing decreased, indicated by a decrease of the characteristic path length and an increase of efficiency, the ability of specialized processing was increasing, implied by an ascending transitivity. A weaker community structure could be implied for networks growing in simple collagen, since the median values were showing a clear inferior range. This could be confirmed by considering the number of communities in detail. Collagen exhibited, at DIV8-9, 2 ± 0.33 communities (mean $\pm$ SD), dropping to 1 ± 0.27 modules at DIV22-23. PVP-*co*-$GMA_{3mol\%}$ hydrogels promoted a solid community structure of 2 ± 0.48 for early and intermediate maturity staged, only ascending to 1 ± 0.51 modules at an advanced maturity.

As the community structure of a network is thought to essentially influence the networks' specialization, it can be hypothesized, that networks growing in Collagen-PVP_{8118}-*co*-$GMA_{3mol\%}$ hydrogels support advanced specialization compared to simple collagen gels. Emphasized by a greater variance of modularity and an overall increase of segregation and decreasing trend of integration. A further confirmation of this hypothesis is the similarity of results in comparison with organotypic cultures of Shimono et al., who reported on average two separate modules developing into large integrated communities.[166]

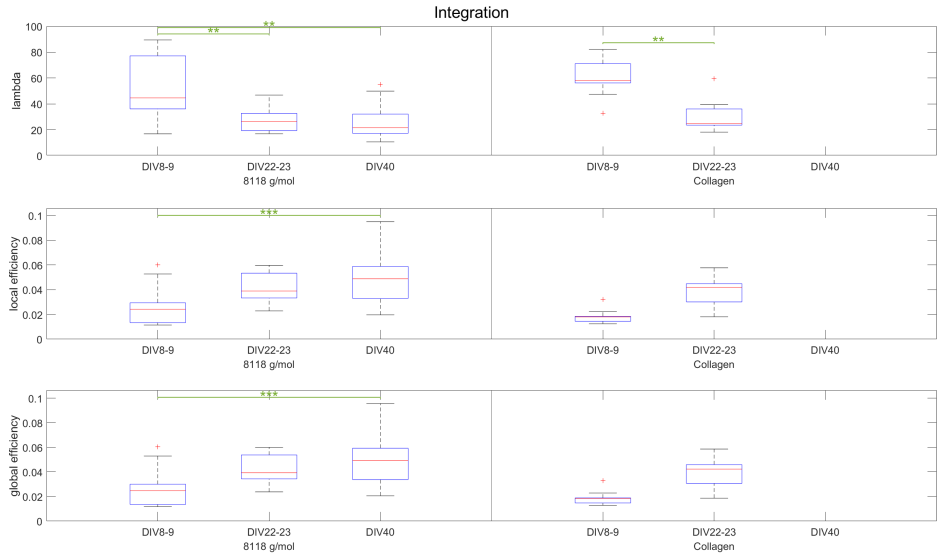

Figure 8.16.: Comparison of the ability for integration of spontaneous active cells cultured in Collagen-PVP-*co*-GMA$_3$*mol*% and collagen hydrogels. Significant differences are depicted by stars (*** for p $\leqslant$ 0.001, ** for p $\leqslant$ 0.01 and * for p $\leqslant$ 0.05). Error bars denote the standard deviation.

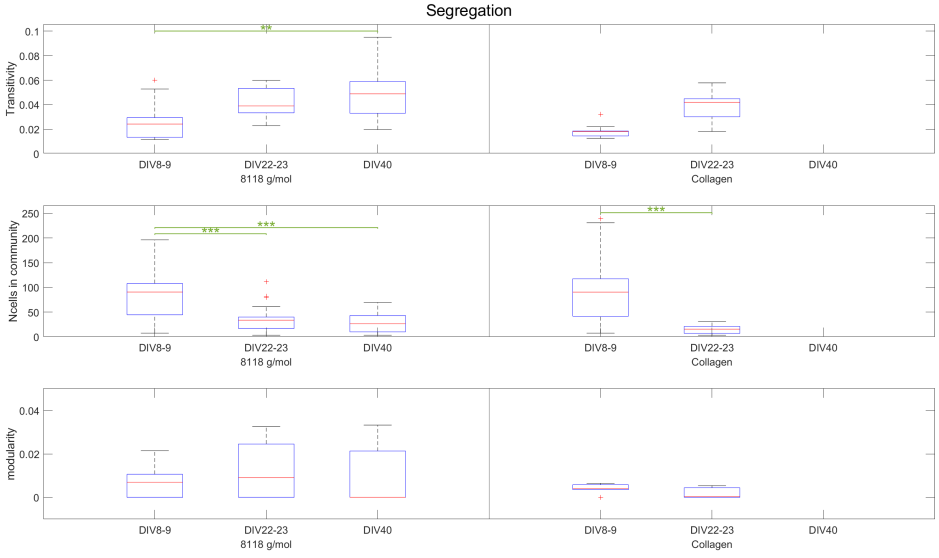

Figure 8.17.: Comparison of the ability for segregation of spontaneous active cells cultured in Collagen-PVP-*co*-GMA$_3$*mol*% and collagen hydrogels. Significant differences are depicted by stars (*** for p $\leqslant$ 0.001, ** for p $\leqslant$ 0.01 and * for p $\leqslant$ 0.05). Error bars denote the standard deviation.

The ability of network resilience showed, as expected, two different behaviors (see fig. 8.18). As discussed in section 8.2 (p.70) the reported progress of assortativity of short recording times does most probably not reflect the real network behavior. In light of the fact that a comparison between two different recording times would eventuate in misleading results, no profound comparison can be done at this point. A detailed comparison of long recording times of Collagen-PVP$_{8118}$-*co*-GMA$_{3mol\%}$ and simple collagen gels is in preparation for publication and to be submitted.

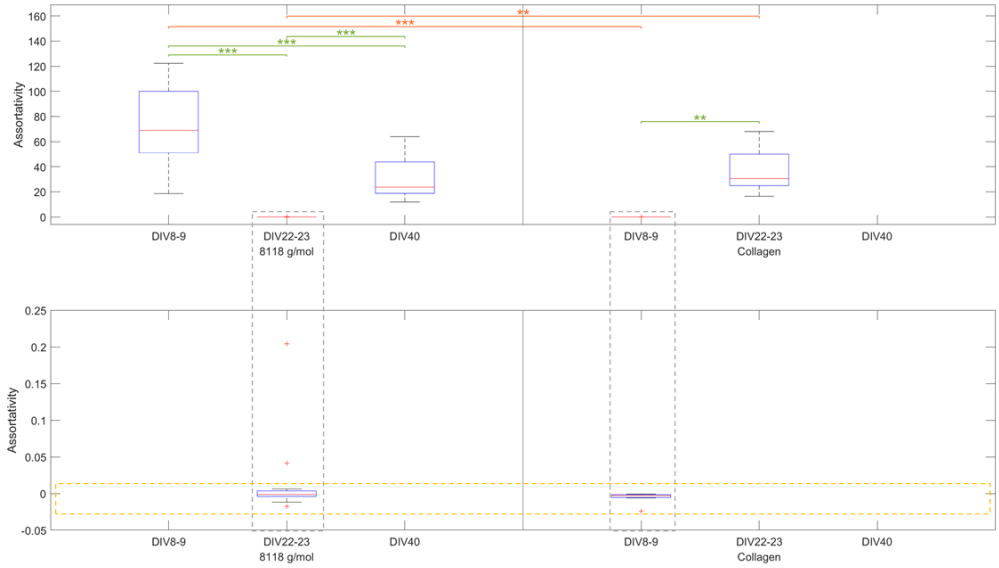

Figure 8.18.: Comparison of the ability for resilience of spontaneous active cells cultured in Collagen-PVP-*co*-GMA$_3$*mol*% and collagen hydrogels. Significant differences are depicted by stars (*** for p $\leqslant$ 0.001, ** for p $\leqslant$ 0.01 and * for p $\leqslant$ 0.05). Error bars denote the standard deviation.

8.3.1. Conclusion

This section compared the autologous dynamic network development between a natural hydrogel (collagen) and the established biohybrid hydrogel (Collagen-PVP-*co*-GMA$_3$*mol*%).The results obtained, clearly show the advantageous effect of PVP-*co*-GMA$_{3mol\%}$ in collagen hydrogels. The addition of the polymer allow, the long-term cultivation of highly spontaneous active neuronal networks. These networks owe a stronger community structure and enhanced resilient core in comparison with cultures growing in a simple collagen gel.

9. Conclusion and scientific relevance

Objective of this project was the establishment of a modular system for the 3D cultivation of primary neuronal cells, with the desirable tuneability in mechanical and chemical properties. Biohybrid hydrogels present an optimal system to reach desired needs for brain-like tissue, as naturally mechanical weak biopolymers can be tuned by synthetic polymers.[18] In cooperation with Miriam Al-Enezy Ulbrich (DWI Aachen, AG Pich) it was possible to create the novel Collagen-PVP-*co*-GMA$_3$*mol*% biohybrid hydrogel, that promotes physiological development of neuronal cells, both on the morphological and functional level. By comparatively evaluating the respective simple biopolymer hydrogels, it was possible to spotlight the advances of the PVP addition.

Initially, Fibrin-PVP-*co*-GMA$_3$*mol*% had been in focus for a suitable candidate as culture environment. It could be shown that neuronal cells dislike given conditions, observed by various factors. Cell viability is negatively influenced, declining with the addition of the synthetic polymer, although a great variety of porosity is given. Moreover cells escape from low molecular weight Fibrin-PVP-*co*-GMA$_3$*mol*% gels, as also for simple fibrin. Whereas long polymer chain length promote the establishment of a cell free zone at the edges of the gel and non-physiological stellar-like appearance of entrapped cells. Moreover neurons and astrocytes tend to spatially separate withing Fibrin-PVP-*co*-GMA$_3$*mol*% gels.

These phenomena could be abolished by the use of collagen instead of fibrin. Since fibrin is not a natural component of the CNS's ECM, collagen fade into focus, as it is (although rarely) present in the ECM. Most conclusive its high biocompatibility, well known polymerization and relatively straight forward coupling to PVP, as well as plenty applications in the field of neuroscience.[179, 180, 181] Collagen-PVP-*co*-GMA$_3$*mol*% showed outstanding results compared to fibrin-based biohybrid gels. Most important advantage is the significantly increased viability of cultured cells (about 75% DIV40 in hybrid hydrogels, about 50% at DIV40 in simple collagen gels). Also the addition of PVP to collagen revealed great advantages, as by addition long-term cultivation become possible. Besides, while adding PVP the necessity of using tranexamic acid fades, as results imply the prevention of gel degradation (at least for the monitored culture period of 40 days). Also no gel contraction could be observed as reported in some literature.[182] These findings suggest a mechanical improvement of the hydrogel by addition of PVP, which has to be proven by further rheological analysis.

However, different influences of molecular weights in Collagen-PVP-*co*-GMA$_3$*mol*% could be observed compared to Fibrin-PVP-*co*-GMA$_3$*mol*%. Excepting high molecular weights (11100g/-mol), Collagen-PVP-*co*-GMA$_3$*mol*% promotes fast neurite outgrowth, showing complex network formation already at DIV8-9 similar to organotypic cultures.[164] It was shown that networks could be maintained for at least 40 days in culture, using low molecular weights (6662 g/mol,

8118 g/mol). Networks cultured in gels with long polymer chain length died after DIV22, while showing already diminished activity at that point.

It could be shown that Collagen-PVP$_{8118}$-*co*-GMA$_{3mol\%}$ hydrogels promote the physiological development of spontaneous network activity. Whereby an increasing polymer chain length negatively influences the network morphology and functionality. The functional network development and specialization was evaluated by characteristic measures described in section 3.7.2 (p.32). These network measures can be computed from connectivity estimates (see section 2.5). In this project GTE was the algorithm of choice (see section 5, p. 41). As already mentioned earlier, the direct comparison of results derived from GTE with literature data is not possible, due to too many inconsistent variables depending on the way of implementation (see section 5, p. 41). However, it seems fair enough to compare biases along different estimates and computation methods, in order to evaluate the given results.

Cortical network development can be graded into three phases: (1) over-connectivity, (2) synaptic pruning and (3) reduction of connectivity.[183] Main actuator of this maturation is known to be early synchronous network activity, as also observed in Collagen-PVP$_{8118}$-*co*-GMA$_{3mol\%}$ hydrogels.[165, 169, 184] This early synchronization is thought to be a crucial step in cortical development, observed similarly in rodents and humans [185], suggesting the importance of clinical relevance of the presented culture system. Also the mean firing rates of spontaneously active networks in Collagen-PVP$_{8118}$-*co*-GMA$_{3mol\%}$ show similar magnitudes as reported in literature.[166, 168, 171] Further an average number of active cells close to observed ranges in organotypic cultures could be shown, mainly due to the high cell concentration used (see 3.1.2, p.26), being close to physiological density of e.g. the neocortex comprising about 20 000 cells/mm^3. Emphasizing the meaningful advantage of 3D cultures over simple 2D systems.[167]

Collagen-PVP$_{8118}$-*co*-GMA$_{3mol\%}$ hydrogels appear to support the development of networks with balanced integration and segregation. This balance is of main importance for healthy functioning networks, revealing the ability for fast and specialized information processing at the same time.[105] These findings could be confirmed by the small-world propensity, with an increasing course during maturation. Small-worldness is known to be correlated with increased presence of hub cells. Converse observations could be seen for the given hybrid hydrogel. Special hub cells, as connector and provincial hubs, support the network in efficient information processing. It could be observed that Collagen-PVP$_{8118}$-*co*-GMA$_{3mol\%}$ promotes the establishment of an equilibrated ratio of connector and provincial hubs throughout the whole culture time, although decreasing with maturation, being contra indicative for the state of network development indicated previously. However, it has to be noted that the overall amount of active cells is decreasing within the monitored culture period. Diverse observations can be also found in literature. Dingle et al. could not detect any hub cells in primary cortical mouse cells cultured Silk fibroin scaffolds. They coated the scaffold surface with PDL and laminin for proper cell adhesion, which is not necessary using Collagen-PVP$_{8118}$-*co*-GMA$_{3mol\%}$. Moreover they used a cell density of about 1.2—1.3 x 10^6 cells/mm^3, whereas in this project a comparably sparse amount of about 8 500 cells/mm^3 had been used. The high amount used by Dingle et al. would imply a faster maturation of network, though they reported opposite results. In comparison, Collagen-

PVP_{8118}-*co*-$GMA_{3mol\%}$ seems to support sophisticated maturation on the basis of underlying observations.

Besides, modularity is one of the amplified characteristics, facilitating network specialization, associated with increased segregation. A similar number of communities (2-3) could be observed as reported in Literature [166, 171], with a constant modularity over the whole culture period, indicating a weak community structure in combination with a decreasing transitivity. Instead, a strong increase in the ability of resilience can be observed in developing networks cultured in Collagen-PVP_{8118}-*co*-$GMA_{3mol\%}$. Beginning with a dissortative behavior the network further matures, gaining strong assortative properties in advanced matured networks (DIV40). Betzel et al. states that dissortativity is essential for inter-modular communication, while assortativity is indicative for increased segregation.[178] This would mean that the studied networks undergo a known physiological development from integrated to balanced segregative complex functional networks, similarly to the human brain development.

Although the cultured networks matured in the absence of external stimuli and had been dissociated from E18 cortex, they had been able to intrinsically undergo a physiological development de novo, enabled through the supportive properties of Collagen-PVP_{8118}-*co*-$GMA_{3mol\%}$.[97, 171, 165] Recordings at even earlier maturation stages might be revealing about the de facto functional condition of networks observed at DIV8-9 and older.

Comprising, this work lay the foundation for further profound studies of fundamental and clinical relevant research, using Collagen-PVP_{8118}-*co*-$GMA_{3mol\%}$. For instance the study of early cortical development or the influence of external stimuli on the network maturation ,as well as clinical relevant research as e.g. the modeling of neurodegenerative diseases or considering the system as hydrogel coatings for the prevention of chronic implant inflammation, is facilitated. The following section will scope some opportunities for future applications, some of which had been already initiated.

10. Applications and future perspectives

The developed Collagen-PVP$_{8118}$-*co*-GMA$_{3mol\%}$ biohybrid hydrogel represents a valuable tool for 3D cell cultivation of higher biological relevance. The physiological development of neuronal networks grown from primary rat cortical cells, could be observed. The chemical, as well as, mechanical tuneability allows for various applications. This chapter will give an overview of powerful future research. For certain applications the fundamental experiments were already conducted.

10.1. Disease modeling and basic research

In the scope of the presented project it would be interesting to gather further recordings of spontaneous network dynamics in extended recording times of at least 30 minutes. This would allow a profound study of oscillatory behavior or distinct patterns. In order to better understand the emergence and establishment of hub cells it would be interesting to monitor same regions of the hydrogels at different stages of network maturation. This would reveal the behavior of specific cells which might change change its task within a community or the whole network.

Furthermore Collagen-PVP$_{8118}$-*co*-GMA$_{3mol\%}$ allows the specific modification by biofunctionalization of the gel. Influences of distinct adhesion ligands could be analyzed or diseases as e.g. Alzheimer could be reconstructed.

The next level of complexity to the presented culture system could be reached by mimicking the structural organization of cortical brain regions, as attempted by Tang-Schomer et al. (see fig. 10.1).

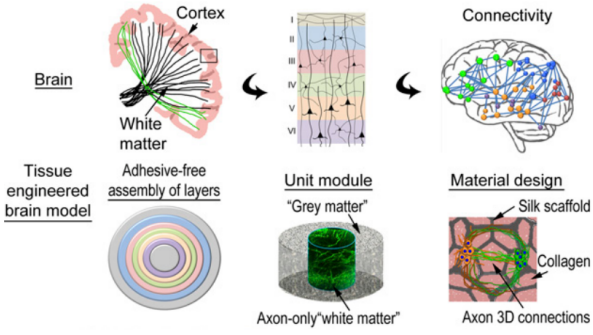

Figure 10.1.: Schematic showing a cortical mimic by means of hydrogel supported 3D cultivation. Figure adapted from [186]

10.2. Interfacing with electrodes

10.2.1. Hydrogels as electrode coatings

Due to the hydrophobic nature of most chronic implants, the foreign body response (FBR) is initiated, causing the deposition of inflammatory plasma proteins onto the surface of the device.[187, 188] Besides the damage of the electronic device, the encapsulation by a fibrotic layer lead to a loss of sensitivity, by physically separating it from the tissue of interest.[187, 188, 189] The addition of a conductive layer with a cell-entrapped hydrogel, several issues can be addressed within one device (fig. 10.2). So called biohybrid implants not only offer a softer sensation of the electronic device, while impairing FBR, but also improve the interaction with host tissue, enabling a better electronic coupling.[190]

Due to the compelling properties of Collagen-PVP_{8118}-*co*-$GMA_{3mol\%}$, it would be particularly suitable for such applications. The low stiffness and favorable environment for complex network development may allow an advanced tissue electrode interface. However the conductive properties of Collagen-PVP_{8118}-*co*-$GMA_{3mol\%}$ need to be tested initially (this is part of a current master thesis by Joscha Graeve (B.Sc.), RWTH Aachen).

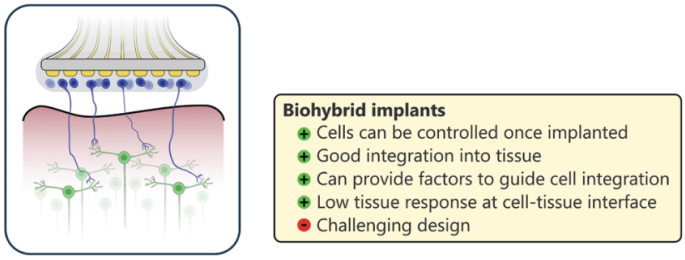

Figure 10.2.: Schematic of a biohybrid Implant and it's advantages and disadvantages. Figure adapted from [190].

10.2.2. Different types of electrodes

For further functional connectivity exploration Collagen-PVP_{8118}-*co*-$GMA_{3mol\%}$ hydrogels may be interfaced with electronics in vitro. Recently two different electrode devices had been established at our institute (ICS-8, Forschungszentrum Jülich). Both approaches possess great capability for functional evaluation of 3D cultures, as described in the following.

The **Nano Neuro Net**, investigated by Kireev et al., is characterized by it's flexible mesh design, allowing the penetration of cells (see fig. 10.3). Within the presented project an customized design of these N^3-MEA probes was conceptualized (see fig. 10.4). Implementing the probe horizontally into a culture dish, enables the entrapment of the device in a hydrogel system. By using a tiered polymerization process (see fig. 10.4, schematic on the right), the electrode can be placed in the center of the hydrogel, allowing an integrated development of a functional network with an electronic device. In order to meet a cell culture suitable device, a small DIP connector was designed by another doctoral researcher, K. Srikantharajah. However this approach requires a mechanically strong and stable hydrogel. Pilot tests had been successfully performed using

Fibrin-PVP_{8118}-*co*-$GMA_{3mol\%}$, due to it's substantial mechanical properties. Further modifications of Collagen-PVP_{8118}-*co*-$GMA_{3mol\%}$, in means of further optimized polymer-biopolymer ratio and probably introduction by a supportive pillar structure, will lead to equivalent results.

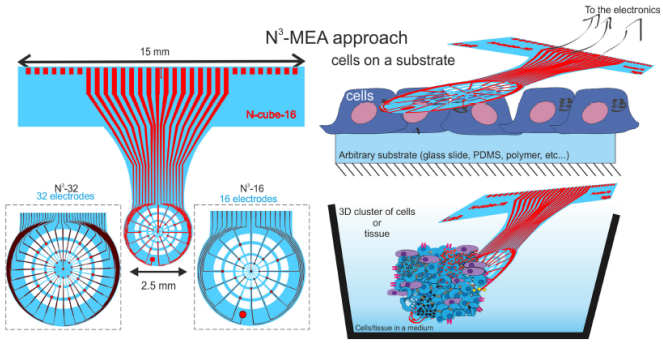

Figure 10.3.: Schematic of the 'Nano Neuro Net' probe and examples of applications. Figure adapted from [191]

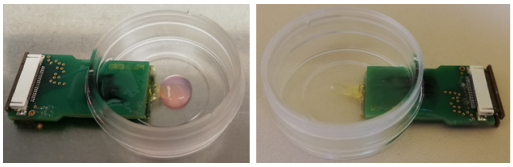

Figure 10.4.: Cultivation device with integrated Nano Neuro Net, suitable for the long-term cultivation of 3D hydrogel-based cell cultures.

A similar approach has recently been published by McDonald et al., who successfully interfaced a mesh electrode with neuronal organoids (see fig. 10.5), addressing the growing need of explorative devices of long-term cultivation.

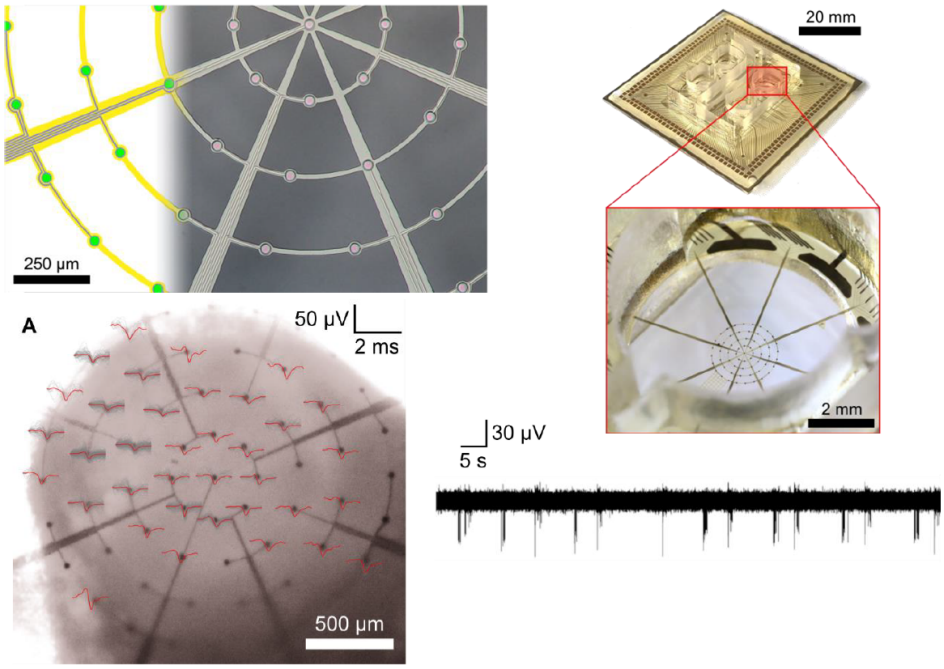

Figure 10.5.: Schematic of a mesh micro-electrode array, interfaced with a cortical organoid, developed at the NMI. Figure adapted from [192]

A further promising electrode device had been investigated by K. Srikantharajah, a doctoral researcher of our institute. She developed **michigan style Parylene-C based microelectrodes** with a high potential for 3D interfacing of tissue-mimicks in vitro. In a pilot test cells in Fibrin-PVP_{8118}-*co*-$GMA_{3mol\%}$ gels had been cultured by the support of pillar structures (fabricated by S. Zips, TU Munich). These pillar structures were meant to increase the height of the hydrogels to meet the active shank length and provide a defined surface. Electrophysiological spiking activity could be recorded from neuronal networks at DIV 22, as shown exemplary in figure 10.6.

The great potential of this device lies in the possibility to reproduce a recently published work by Soscia et al., shown in figure 10.7. They introduced a '3DMEA' device, that enables the simultaneous recording of electrodes of different spatial distribution. Moreover they showed the successful cultivation of Human induced pluripotent stem cell (hiPSC)-derived neurons and astrocytes for 45 days in culture, allowing profound study of the functional development of 3D cultured tissue mimicks. [193]

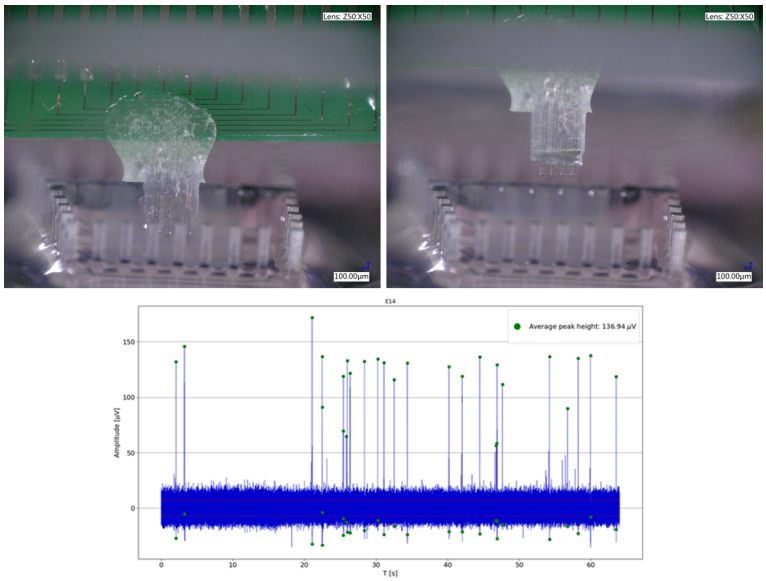

Figure 10.6.: Depiction of the insertion of flexible shank electrodes into a 3D hydrogel-based cultivation and an exemplary electrophysiological recording.

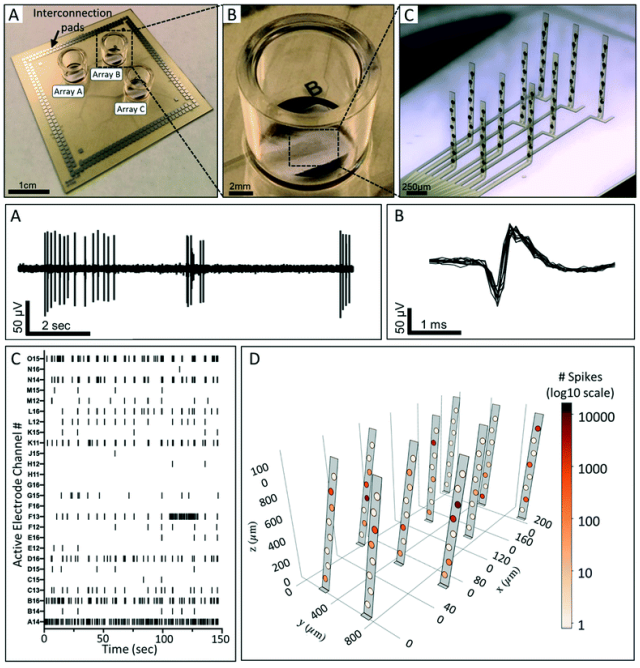

Figure 10.7.: Depiction of a flexible 3-dimensional micro-electrode array developed by Soscia et al., for the use of *in vitro* brain models. Figure adapted from [193]

A. Supplemental figures and tables

A.1. Data table

		C-PVP 6662 g/mol DIV		
		8	**22**	**40**
	Active cells	55.5 ± 56.7778	35 ± 42.0165	23 ± 10.5917
	Firing rate (HZ)	0.1069 ± 0.0168	0.0359 ± 0.0247	0.1185 ± 0.0348
	Syncrhonity (GTE norm)	1.2612 ± 0.8814	1.2981 ± 2.6502	0.67571 ± 0.8375
centrality	**Betweenness centrality (bc)**	0.0022179 ± 0.0016	0.001512 ± 0.0012	0.013301 ± 0.0131
centrality	**Participation coefficient (Pcoeff)**	0.49892 ± 0.1202	0.49523 ± 0.0463	0.49445 ± 0.0799
centrality	**Within-module z-score (Z)**	-1.7968E-16 ± 6.1354E-16	2.5905E-16 ± 1.2642E-15	-1.6653E-16 ± 1.1440E-15
Degree	**Degree**	109 ± 113.5556	68 ± 84.0331	44 ± 21.1834
Degree	**In-degree**	54.5 ± 56.7778	34 ± 42.0165	22 ± 10.5917
Degree	**Out-degree**	54.5 ± 56.7779	34 ± 42.0165	22 ± 10.5917
Node strength	**Strength**	2.4057 ± 1.7220	2.4388 ± 5.2273	1.2707 ± 1.6476
Node strength	**In-strength**	1.2029 ± 0.8610	1.2194 ± 2.6137	0.63534 ± 0.8238
Node strength	**Out-strength**	1.2029 ± 0.8611	1.2194 ± 2.6138	0.63534 ± 0.8239
Hubs	**Hub cells**	29 ± 26.6667	18 ± 24.3802	12 ± 6.5089
Hubs	**No hubs cells**	25.5 ± 30.5185	17 ± 17.7521	11 ± 4.1065
Hubs	**Connector Hubs**	20 ± 11.9630	16 ± 7.4545	8 ± 4.4734
Hubs	**Peripheral Hubs**	21 ± 17.2727	16 ± 25.3333	6.5 ± 2.6667
Integration	**Lambda**	46.4794 ± 14.7044	22.2634 ± 9.9819	28.8657 ± 11.3526
Integration	**Local efficiency**	0.023105 ± 0.0051	0.045394 ± 0.0135	0.036628 ± 0.0131
Integration	**Global Efficiency**	0.023477 ± 0.0052	0.045614 ± 0.0134	0.037399 ± 0.0131
Segregation	**Transitivity**	0.023105 ± 0.0051	0.045394 ± 0.0135	0.036628 ± 0.0131
Segregation	**Number of cells in a community**	82.9118 ± 50.0368	37.5789 ± 14.4140	11.9 ± 5.8451
Segregation	**Modularity**	0.0043186 ± 0.0055	0.0025818 ± 0.0067	0.00074889 ± 0.0055
Segregation	**Number of communities**	2 ± 0.5617	2 ± 0.5785	2 ± 0.4970
	SWP	0.5627 ± 0.1672	0.7269 ± 0.2996	0.8142 ± 0.2129
	Assortativity	-0.0088 ± 0.0049	33.5742 ± 14.677	37.3778 ± 18.667

		C-PVP 8118 g/mol DIV		
		8	**22**	**40**
	Active cells	122 ± 88	48 ± 39	19 ± 29
	Firing rate (HZ)	0.1003 ± 0.0262	0.1427 ± 0.0409	0.1894 ± 0.0755
	Syncrhonity (GTE norm)	2.3414 ± 1.8657	1.579 ± 1.9137	1.5589 ± 1.1417
centrality	**Betweenness centrality (bc)**	0.0020529 ± 0.0019	0.0031268 ± 0.0025	0.0055686 ± 0.0053
	Participation coefficient (Pcoeff)	0.63633 ± 0.1405	0.49525 ± 0.0531	0.4982 ± 0.0657
	Within-module z-score (Z)	7.78E-17 ± 1.6837E-15	1.7642E-16 ± 1.2392E-15	1.7530E-17 ± 9.5826E-16
Degree	**Degree**	241 ± 176.1	94 ± 77.9882	36 ± 58.6574
	In-degree	120.5 ± 88.05	47 ± 38.9941	18 ± 29.3287
	Out-degree	120.5 ± 88.06	48 ± 38.9941	19 ± 29.3287
Node strength	**Strength**	4.562 ± 3.62	2.9754 ± 3.7344	2.9843 ± 2.1572
	In-strength	2.281 ± 1.8104	1.4877 ± 1.8672	1.4921 ± 1.0786
	Out-strength	2.281 ± 1.8105	1.4877 ± 1.8673	1.4921 ± 1.0787
Hubs	**Hub cells**	58.5 ± 43.25	27 ± 24.2249	11 ± 15.0242
	No hubs cells	62.5 ± 44.8	26 ± 15.54	18.06 ± 14.31
	Connector Hubs	23.5 ± 22.5	13 ± 17.03	11 ± 7.47
	Peripheral Hubs	44.1 ± 17.47	20 ± 9.1	15.6 ± 7.06
Integration	**Lambda**	44.6305 ± 21.2470	26.5178 ± 7.4206	21.5621 ± 10.3999
	Local efficiency	0.024151 ± 0.0110	0.03895 ± 0.0097	0.048869 ± 0.0148
	Global Efficiency	0.024794 ± 0.0110	0.03942 ± 0.0096	0.049259 ± 0.0148
Segregation	**Transitivity**	0.024151 ± 0.0110	0.03895 ± 0.0097	0.048869 ± 0.0148
	Number of cells in a community	90.6111 ± 34.4589	33.5672 ± 16.7715	26.5 ± 18.002
	Modularity	0.0069116 ± 0.0052	0.009112 ± 0.0102	1.3164E-16 ± 0.0104
	Number of communities	2 ± 0.4550	2 ± 0.4260	1 ± 0.4844
	SWP	0.5595 ± 0.2157	0.5666 ± 0.314	0.6536 ± 0.3083
	Assortativity	71.6441 ± 27.1694	0.0161 ± 0.0328	31.1285 ± 13.6539

		C-PVP 8118 g/mol DIV		
		8	**22**	**40**
	Active cells	122 ± 88	48 ± 39	19 ± 29
	Firing rate (HZ)	0.1003 ± 0.0262	0.1427 ± 0.0409	0.1894 ± 0.0755
	Syncrhonity (GTE norm)	2.3414 ± 1.8657	1.579 ± 1.9137	1.5589 ± 1.1417
centrality	**Betweenness centrality (bc)**	0.0020529 ± 0.0019	0.0031268 ± 0.0025	0.0055686 ± 0.0053
	Participation coefficient (Pcoeff)	0.63633 ± 0.1405	0.49525 ± 0.0531	0.4982 ± 0.0657
	Within-module z-score (Z)	7.78E-17 ± 1.6837E-15	1.7642E-16 ± 1.2392E-15	1.7530E-17 ± 9.5826E-16
Degree	**Degree**	241 ± 176.1	94 ± 77.9882	36 ± 58.6574
	In-degree	120.5 ± 88.05	47 ± 38.9941	18 ± 29.3287
	Out-degree	120.5 ± 88.06	48 ± 38.9941	19 ± 29.3287
Node strength	**Strength**	4.562 ± 3.62	2.9754 ± 3.7344	2.9843 ± 2.1572
	In-strength	2.281 ± 1.8104	1.4877 ± 1.8672	1.4921 ± 1.0786
	Out-strength	2.281 ± 1.8105	1.4877 ± 1.8673	1.4921 ± 1.0787
Hubs	**Hub cells**	58.5 ± 43.25	27 ± 24.2249	11 ± 15.0242
	No hubs cells	62.5 ± 44.8	26 ± 15.54	18.06 ± 14.31
	Connector Hubs	23.5 ± 22.5	13 ± 17.03	11 ± 7.47
	Peripheral Hubs	44.1 ± 17.47	20 ± 9.1	15.6 ± 7.06
Integration	**Lambda**	44.6305 ± 21.2470	26.5178 ± 7.4206	21.5621 ± 10.3999
	Local efficiency	0.024151 ± 0.0110	0.03895 ± 0.0097	0.048869 ± 0.0148
	Global Efficiency	0.024794 ± 0.0110	0.03942 ± 0.0096	0.049259 ± 0.0148
Segregation	**Transitivity**	0.024151 ± 0.0110	0.03895 ± 0.0097	0.048869 ± 0.0148
	Number of cells in a community	90.6111 ± 34.4589	33.5672 ± 16.7715	26.5 ± 18.002
	Modularity	0.0069116 ± 0.0052	0.009112 ± 0.0102	1.3164E-16 ± 0.0104
	Number of communities	2 ± 0.4550	2 ± 0.4260	1 ± 0.4844
	SWP	0.5595 ± 0.2157	0.5666 ± 0.314	0.6536 ± 0.3083
	Assortativity	71.6441 ± 27.1694	0.0161 ± 0.0328	31.1285 ± 13.6539

		C-PVP 1100 g/mol DIV		
		8	**22**	**40**
	Active cells	24 ± 19.7		
	Firing rate (HZ)	0.1046 ± 0.0197		
	Syncrhonity (GTE norm)	0.5782 ± 0.3524		
centrality	**Betweenness centrality (bc)**	0.0056 ± 0.0048		
	Participation coefficient (Pcoeff)	0.2447 ± 0.2481		
	Within-module z-score (Z)	-2.2025E-17 ± 8.1095E-16		
Degree	**Degree**	65 ± 39.4		
	In-degree	32.5 ± 19.7		
	Out-degree	32.5 ± 19.7		
Node strength	**Strength**	1.3597 ± 0.6767		
	In-strength	0.6799 ± 0.3383		
	Out-strength	0.6799 ± 0.3383		
Hubs	**Hub cells**	12.5 ± 8.72		
	No hubs cells	10 ± 11.56		
	Connector Hubs	10 ± 3.38		
	Peripheral Hubs	16.5 ± 5.5		
Integration	**Lambda**	48.9701 ± 7.3597		
	Local efficiency	0.0221 ± 0.0033		
	Global Efficiency	0.0225 ± 0.0033		
Segregation	**Transitivity**	0.0221 ± 0.0033		
	Number of cells in a community	15.3125 ± 10.7945		
	Modularity	0.0030 ± 0.0036		
	Number of communities	1 ± 0.48		
	SWP	0.3595 ± 0.0847		
	Assortativity	-0.0204 ± 0.0097		

		C-PVP 65000 g/mol DIV		
		8	**22**	**40**
	Active cells	140 ± 95.2899	76.5 ± 86.9297	28 ± 10.3265
	Firing rate (HZ)	0.1423 ± 0.0285	0.1678 ± 0.0245	0.1362 ± 0.0137
	Syncrhonity (GTE norm)	3.9228 ± 3.8906	2.5015 ± 3.4063	0.675 ± 0.8542
centrality	**Betweenness centrality (bc)**	0.0024 ± 0.0051	0.001 ± 0.0026	0.0063 ± 0.0019
centrality	**Participation coefficient (Pcoeff)**	0.6462 ± 0.0202	0.5688 ± 0.0764	0.4547 ± 0.0785
centrality	**Within-module z-score (Z)**	-4.4126E-16 ± 8.5329E-16	-1.2907E-16 ± 5.2334E-16	2.2970E-17 ± 8.2468E-16
Degree	**Degree**	278 ± 190.5799	151 ± 173.8594	54 ± 20.6531
Degree	**In-degree**	139 ± 95.2899	75.5 ± 86.9297	27 ± 10.3265
Degree	**Out-degree**	139 ± 95.2899	75.5 ± 86.9297	27 ± 10.3265
Node strength	**Strength**	7.3147 ± 7.5026	4.8198 ± 6.6443	1.2482 ± 1.6797
Node strength	**In-strength**	3.6574 ± 3.7513	2.4099 ± 3.3222	0.6241 ± 0.8399
Node strength	**Out-strength**	3.6574 ± 3.7513	2.4099 ± 3.3222	0.6241 ± 0.8399
Hubs	**Hub cells**	63 ± 54.5917	41 ± 50.8984	12 ± 6.0816
Hubs	**No hubs cells**	66 ± 42	33.5 ± 36.0313	15 ± 5.0204
Hubs	**Connector Hubs**	23 ± 30.6036	22.5 ± 23.2188	6 ± 3.5102
Hubs	**Peripheral Hubs**	42 ± 20.9877	19 ± 30.1778	6 ± 4.2222
Integration	**Lambda**	38.9462 ± 15.1361	32.1422 ± 8.0640	33.4257 ± 10.6261
Integration	**Local efficiency**	0.0279 ± 0.0091	0.0326 ± 0.0067	0.0304 ± 0.0124
Integration	**Global Efficiency**	0.0293 ± 0.0093	0.0337 ± 0.0068	0.0307 ± 0.0124
Segregation	**Transitivity**	0.0279 ± 0.0091	0.0326 ± 0.0067	0.0304 ± 0.0124
Segregation	**Number of cells in a community**	29.875 ± 37.5670	42.8421 ± 44.3244	13.5556 ± 4.0513
Segregation	**Modularity**	0.0119 ± 0.0112	0.0198 ± 0.0162	0.0124 ± 0.0055
Segregation	**Number of communities**	2 ± 0.6154	2 ± 0.3281	2 ± 0.2857
	SWP	0.5026 ± 0.2248	0.4024 ± 0.1287	0.5553 ± 0.2541
	Assortativity	64.6098 ± 21.5641	-0.0042 ± 0.007	46.0138 ± 14.3019

		C-PVP 5min 8118 g/mol DIV		
		8	**22**	**40**
	Active cells	101 ± 53.52	17 ± 27.5556	68 ± 38.25
	Firing rate (HZ)	0.0582 ± 0.0197	0.0811 ± 0.0205	0.0618 ± 0.008
	Syncrhonity (GTE norm)	1.1076 ± 1.5284	0.616 ± 1.1151	1.6041 ± 1.5804
centrality	**Betweenness centrality (bc)**	0.0024 ± 0.0018	0.0229 ± 0.0123	0.0115 ± 0.0108
centrality	**Participation coefficient (Pcoeff)**	0.4624 ± 0.1153	0.4638 ± 0.0599	0.6048 ± 0.0610
centrality	**Within-module z-score (Z)**	2.8048E-16 ± 3.12130E-16	-3.8368E-16 ± 1.4260E-15	2.6716E-16 ± 1.2619E-15
Degree	**Degree**	200 ± 107.04	32 ± 55.1111	134 ± 76.5
Degree	**In-degree**	100 ± 53.52	16 ± 27.56	67 ± 38.25
Degree	**Out-degree**	100 ± 53.52	16 ± 27.56	67 ± 38.25
Node strength	**Strength**	1.9748 ± 2.95	1.1451 ± 2.19	3.0164 ± 3.06
Node strength	**In-strength**	0.9874 ± 1.47	0.5726 ± 1.1	1.5082 ± 1.53
Node strength	**Out-strength**	0.9874 ± 1.47	0.5726 ± 1.1	1.5082 ± 1.53
Hubs	**Hub cells**	59 ± 33.04	9 ± 18.89	36 ± 26.5
Hubs	**No hubs cells**	42 ± 20.48	9 ± 8.67	32 ± 13.75
Hubs	**Connector Hubs**	23 ± 17.12	4 ± 15.11	24.5 ± 19.25
Hubs	**Peripheral Hubs**	39.5 ± 25.75	5 ± 3.78	15 ± 4.67
Integration	**Lambda**	94.5907 ± 36.79	30.3063 ± 5.13	74.5586 ± 60.8
Integration	**Local efficiency**	0.0125 ± 0.0077	0.0349 ± 0.0043	0.0188 ± 0.0115
Integration	**Global Efficiency**	0.0133 ± 0.0077	0.0359 ± 0.0043	0.0204 ± 0.0113
Segregation	**Transitivity**	0.0125 ± 0.0077	0.0349 ± 0.0043	0.0188 ± 0.0115
Segregation	**Number of cells in a community**	62 ± 23.43	9.67 ± 13.56	32.09 ± 17.79
Segregation	**Modularity**	0.0115 ± 0.0055	0.0108 ± 0.0044	0.0248 ± 0.0127
Segregation	**Number of communities**	2 ± 0.32	2 ± 0	2 ± 0.375
	SWP	0.3141 ± 0.0271	0.7594 ± 0.311	0.5232 ± 0.1262
	Assortativity	-0.0048 ± 0.0029	0.0102 ± 0.0077	150.7398 ± 64.1763

		Collagen DIV		
		8	**22**	**40**
	Active cells	104 ± 52	28 ± 11.4286	
	Firing rate (HZ)	0.1127 ± 0.0088	0.1696 ± 0.0291	
	Syncrhonity (GTE norm)	2.4799 ± 1.206	1.1835 ± 0.6722	
centrality	**Betweenness centrality (bc)**	0.00082364 ± 0.0011	0.0031 ± 0.0058	
centrality	**Participation coefficient (Pcoeff)**	0.7191 ± 0.0873	0.4506 ± 0.1286	
centrality	**Within-module z-score (Z)**	-2.8908E-16 ± 1.0406E-15	-2.3685E-16 ± 1.1251E-15	
Degree	**Degree**	294.6 ± 187.52	54 ± 22.8571	
Degree	**In-degree**	147.3 ± 93.76	27 ± 11.4286	
Degree	**Out-degree**	147.3 ± 93.76	27 ± 11.4286	
Node strength	**Strength**	4.7758 ± 2.3223	2.2595 ± 1.3053	
Node strength	**In-strength**	2.0893 ± 1.1611	1.1436 ± 0.6527	
Node strength	**Out-strength**	2.3879 ± 1.1611	1.1298 ± 0.6527	
Hubs	**Hub cells**	71.3 ± 40.02	15.1429 ± 6.0816	
Hubs	**No hubs cells**	77 ± 53.8	12.8571 ± 6.9388	
Hubs	**Connector Hubs**	35.2 ± 18.68	9.7143 ± 5.6735	
Hubs	**Peripheral Hubs**	45.125 ± 24.1563	9.5 ± 3.5	
Integration	**Lambda**	61.0449 ± 11.2496	30.8992 ± 10.5825	
Integration	**Local efficiency**	0.0183 ± 0.0037	0.0389 ± 0.0094	
Integration	**Global Efficiency**	0.0187 ± 0.0038	0.0398 ± 0.0095	
Segregation	**Transitivity**	0.0183 ± 0.0037	0.0389 ± 0.0094	
Segregation	**Number of cells in a community**	93.8695 ± 48.4795	15.1576 ± 5.7542	
Segregation	**Modularity**	0.004 ± 0.0017	0.0021 ± 0.0022	
Segregation	**Number of communities**	2 ± 0.32	2 ± 0.4898	
	SWP	0.5428 ± 0.1425	0.6002 ± 0.3427	
	Assortativity	0.0051 ± 0.0041	36.5276 ± 14.6396	

A.2. Synchrony derived from different adjacency matrices

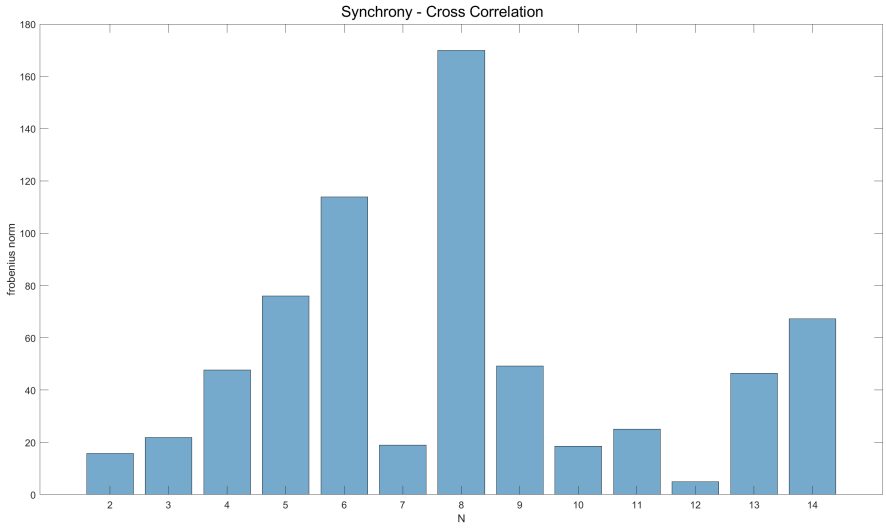

Figure A.1.: Exemplary synchrony computed using the frobenius norm of the Cross Correlation at DIV. (N:amount of samples)

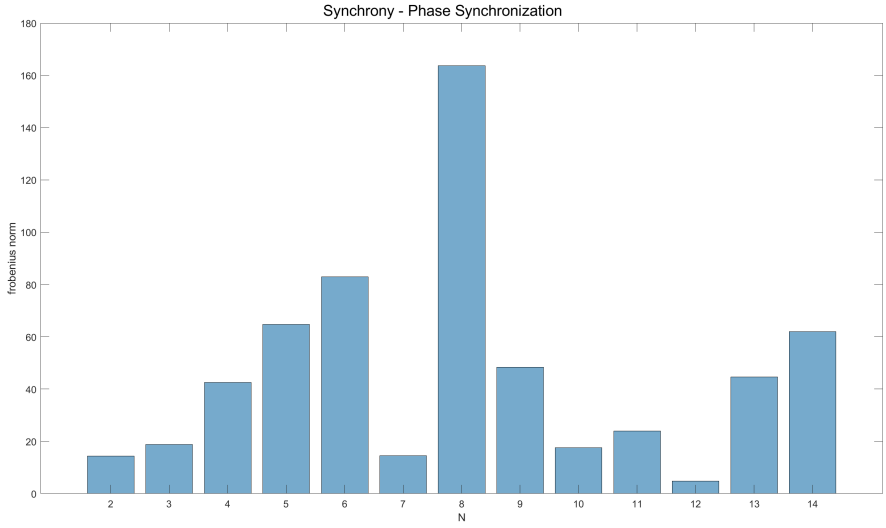

Figure A.2.: Exemplary synchrony computed using the frobenius norm of the Phase Synchronization.

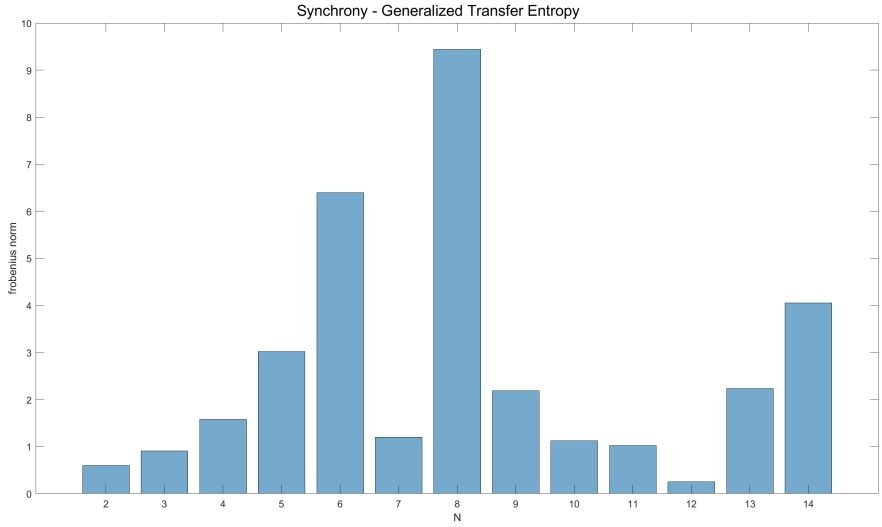

Figure A.3.: Exemplary synchrony computed using the frobenius norm of the Generalized transfer Enthropy.

A.3. Node strength and degree in biohybrid hydrogels with different PVP polymer chain lengths

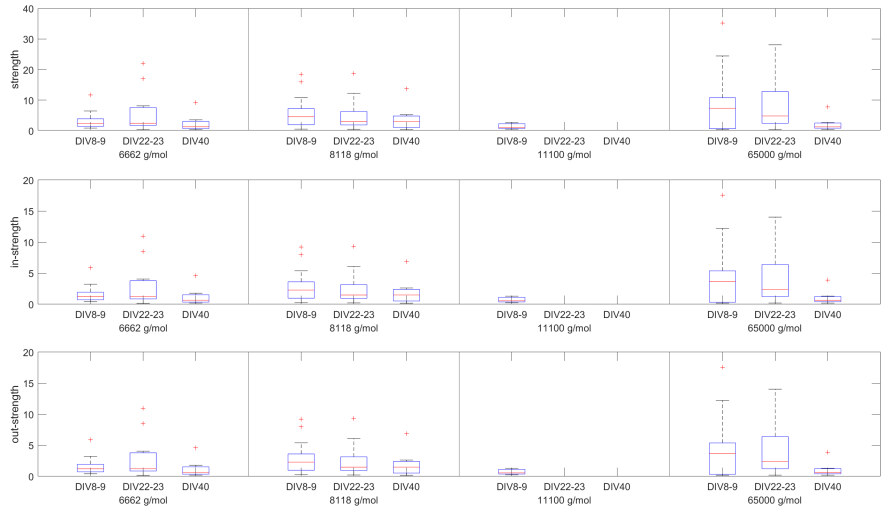

Figure A.4.: Development of node strength of spontaneously active networks in Collagen-PVP-*co*-$GMA_{3mol\%}$ hydrogels at different points of maturation. In- and out-strength show the same development. Significant differences are depicted by stars (*** for $p \leqslant 0.001$, ** for $p \leqslant 0.01$ and * for $p \leqslant 0.05$). Error bars denote the standard deviation.

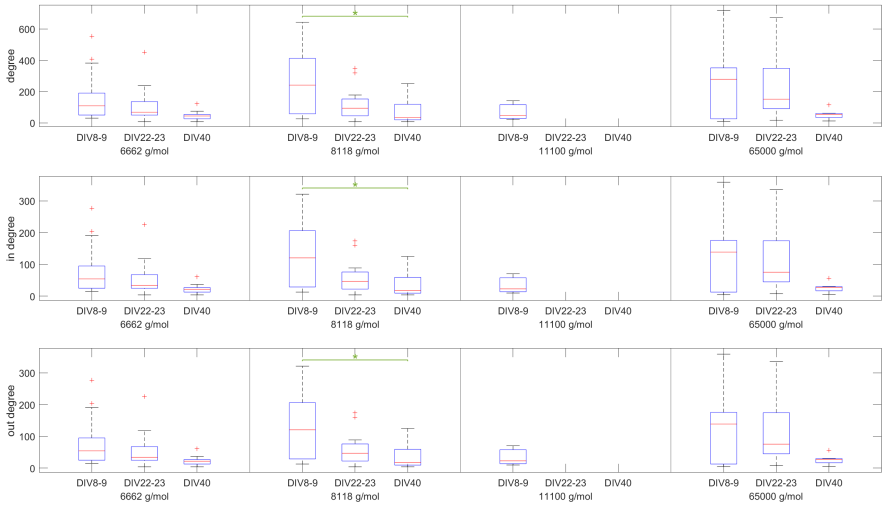

Figure A.5.: Development of node degree of spontaneously active networks in Collagen-PVP-*co*-$GMA_{3mol\%}$ hydrogels at different points of maturation. In- and out-degree show the same development. There are no significant differences. Error bars denote the standard deviation.

A.4. Biohybrid hydrogel vs. Collagen

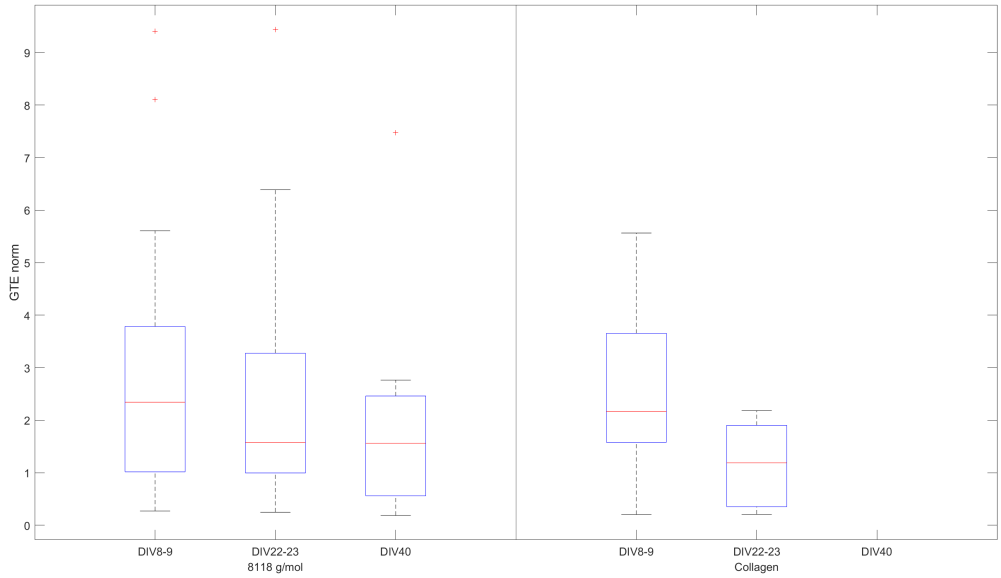

Figure A.6.: Synchrony, depicted as the frobenius norm of GTE, of spontaneously active cells observed in Collagen-PVP$_{8118g/mol}$-*co*-GMA$_{3mol\%}$ and Collagen hydrogels at different phases of maturation. There are no significant differences. Error bars denote the standard deviation.

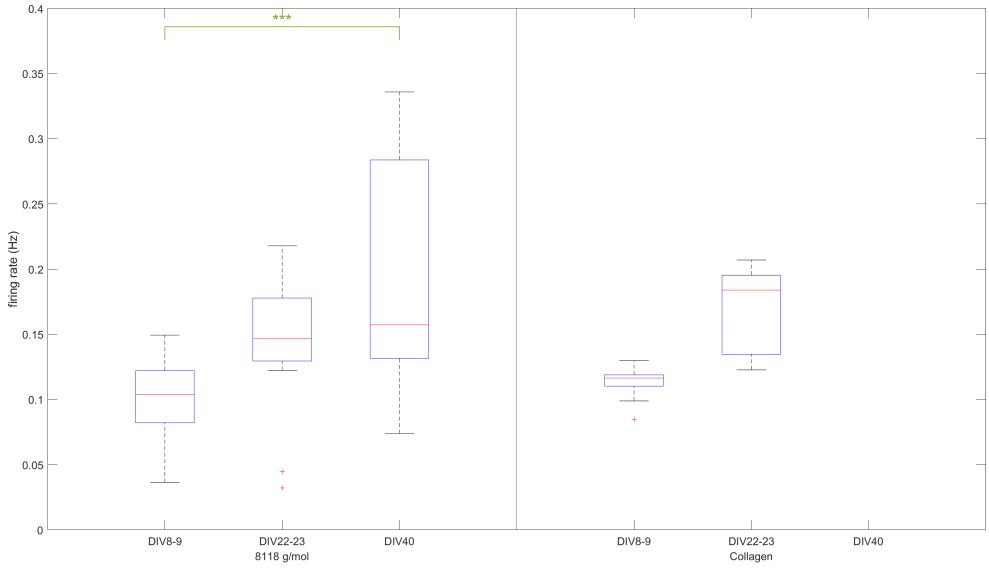

Figure A.7.: Mean firing rate of spontaneously active cells observed in Collagen-PVP$_{8118g/mol}$-*co*-GMA$_{3mol\%}$ and Collagen hydrogels at different points of maturation. Significant differences are depicted by stars (*** for $p \leqslant 0.001$, ** for $p \leqslant 0.01$ and * for $p \leqslant 0.05$). Error bars denote the standard deviation.

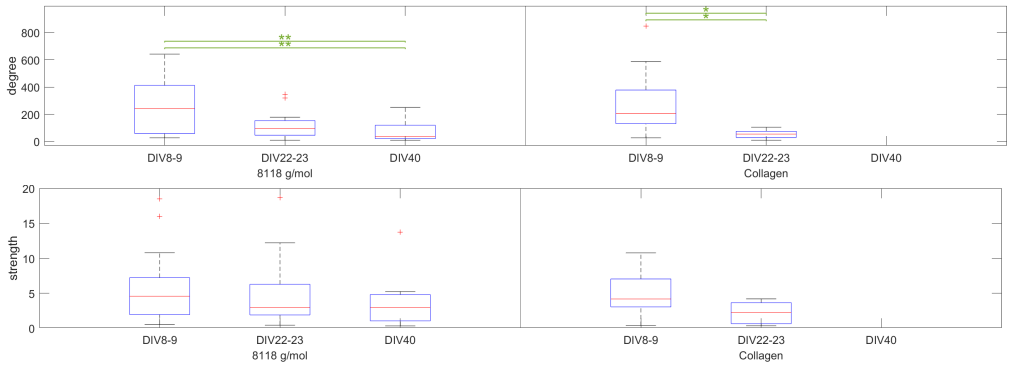

Figure A.8.: Development of node degree and strength of spontaneously active networks in Collagen-PVP$_{8118g/mol}$-*co*-GMA$_{3mol\%}$ and Collagen hydrogels at different points of maturation. Significant differences are depicted by stars (*** for p $\leqslant$ 0.001, ** for p $\leqslant$ 0.01 and * for p $\leqslant$ 0.05). Error bars denote the standard deviation.

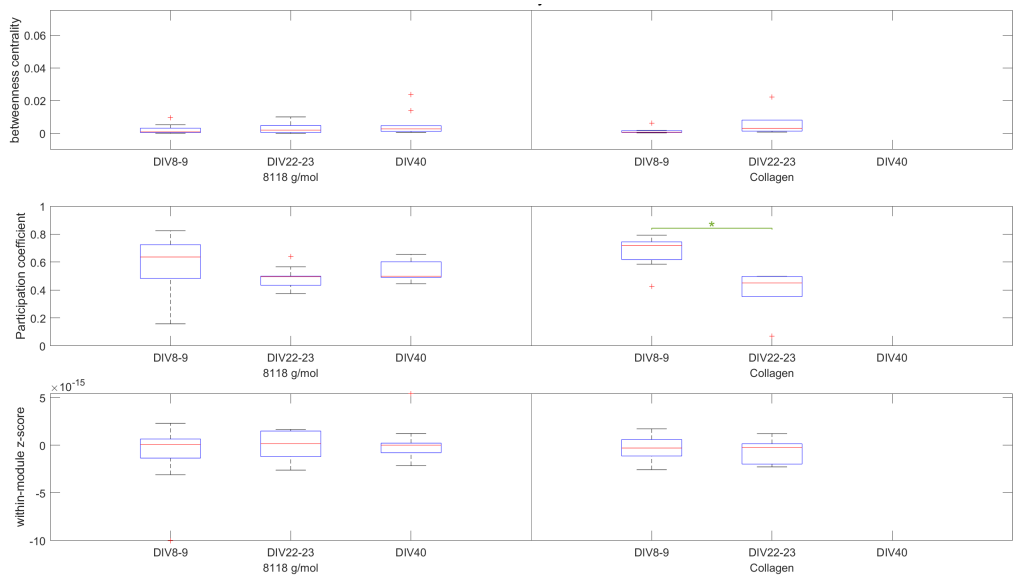

Figure A.9.: Development of different measures of node centrality derived from spontaneously active networks in Collagen-PVP$_{8118g/mol}$-*co*-GMA$_{3mol\%}$ and Collagen hydrogels. Significant differences are depicted by stars (*** for p $\leqslant$ 0.001, ** for p $\leqslant$ 0.01 and * for p $\leqslant$ 0.05). Error bars denote the standard deviation.

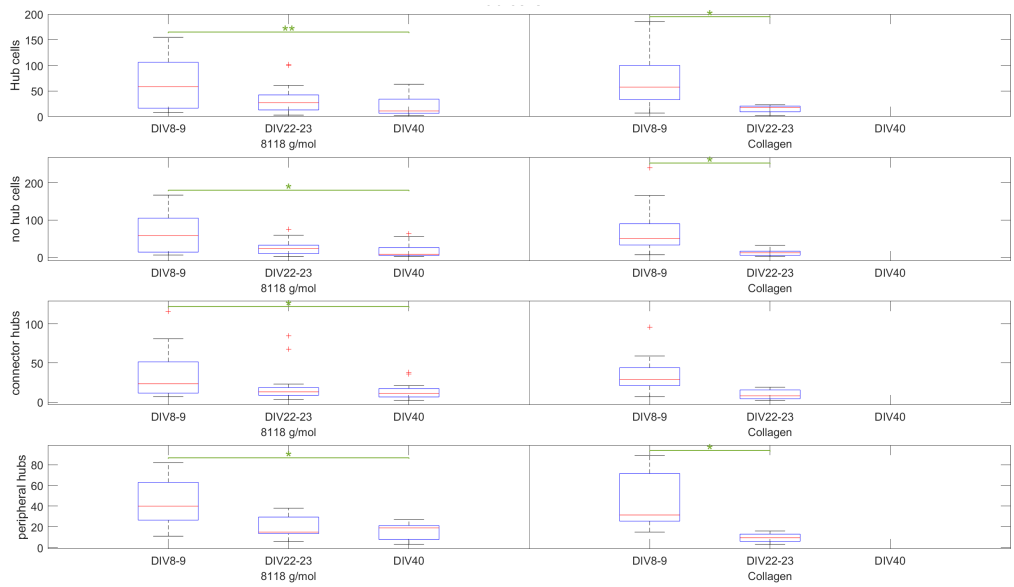

Figure A.10.: Emergence of of hub cells in spontaneously active networks cultured in Collagen-PVP$_{8118g/mol}$-*co*-GMA$_{3mol\%}$ and Collagen hydrogels at different phases of maturation. Significant differences are depicted by stars (*** for $p \leqslant 0.001$, ** for $p \leqslant 0.01$ and * for $p \leqslant 0.05$). Error bars denote the standard deviation.

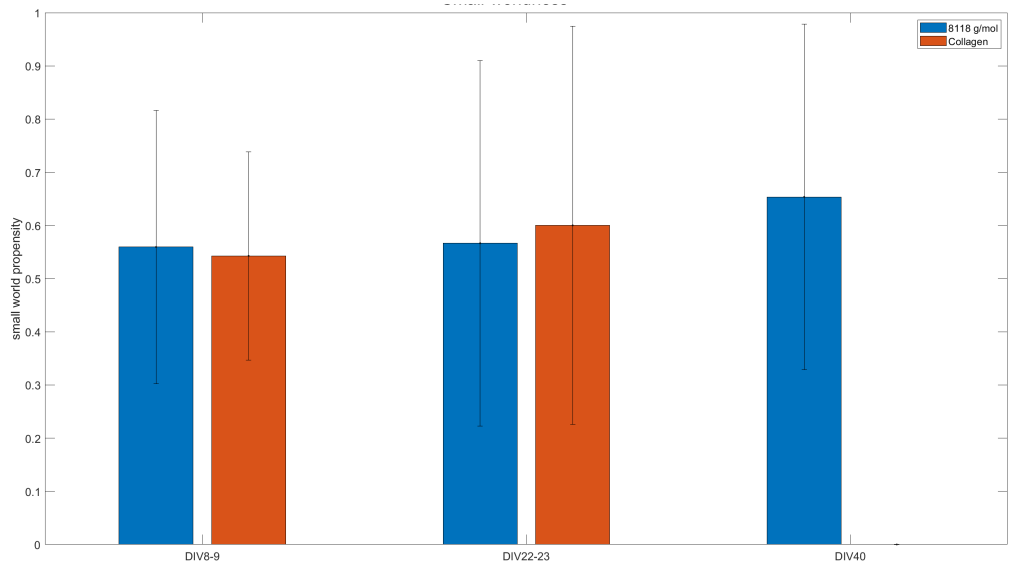

Figure A.11.: Small-worldness of spontaneously active networks cultured in Collagen-PVP$_{8118g/mol}$-*co*-GMA$_{3mol\%}$ and Collagen hydrogels at different phases of maturation. There are no significant differences for $p \leqslant 0.05$. Error bars denote the standard deviation.

A.5. Importance of recording times

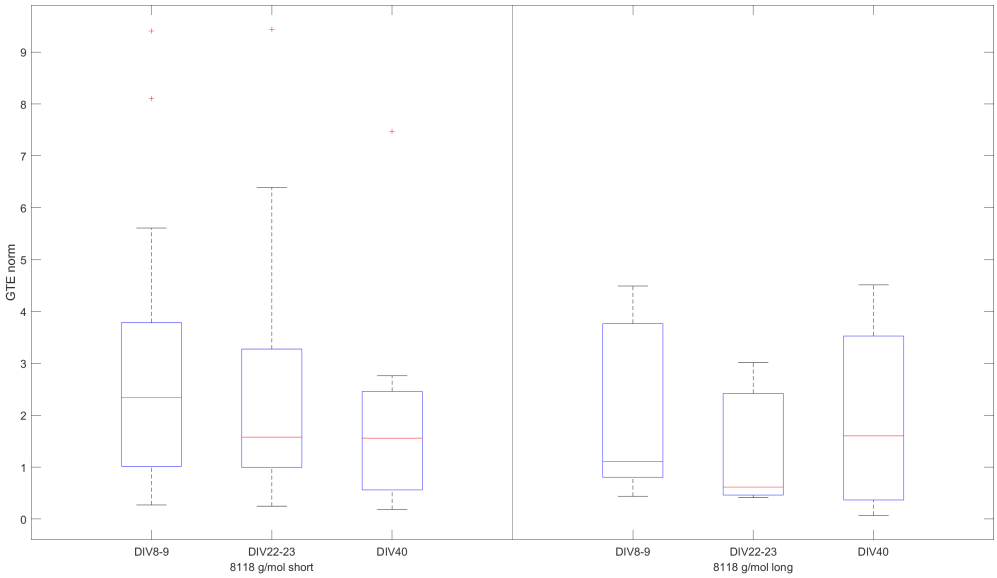

Figure A.12.: Synchrony, depicted as the frobenius norm of GTE, of spontaneously active cells observed in Collagen-PVP-*co*-GMA$_{3mol\%}$, derived from different recording times. There are no significant differences for $p \leqslant 0.05$. Error bars denote the standard deviation.

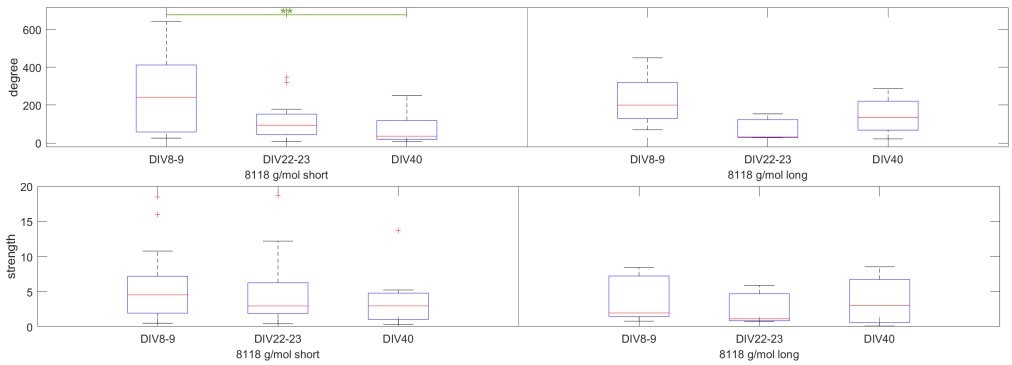

Figure A.13.: Development of node degree and strength of spontaneously active networks in Collagen-PVP-*co*-GMA$_{3mol\%}$, derived from different recording times. Significant differences are depicted by stars (*** for $p \leqslant 0.001$, ** for $p \leqslant 0.01$ and * for $p \leqslant 0.05$). Error bars denote the standard deviation.

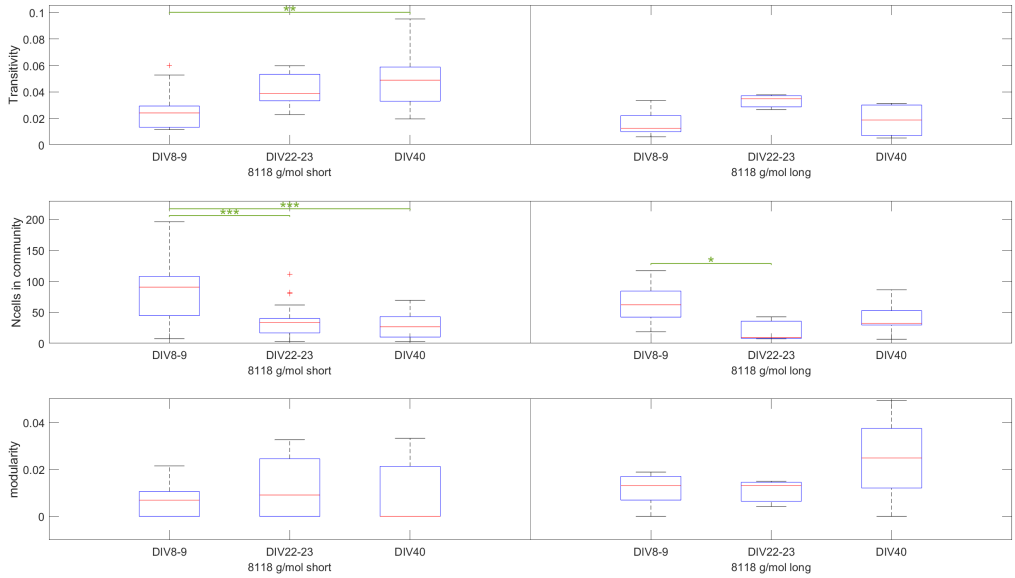

Figure A.14.: Development of different measures of segregation derived from spontaneously active networks in Collagen-PVP-*co*-GMA$_{3mol\%}$, of different recording times. Significant differences are depicted by stars (*** for $p \leqslant 0.001$, ** for $p \leqslant 0.01$ and * for $p \leqslant 0.05$). Error bars denote the standard deviation.

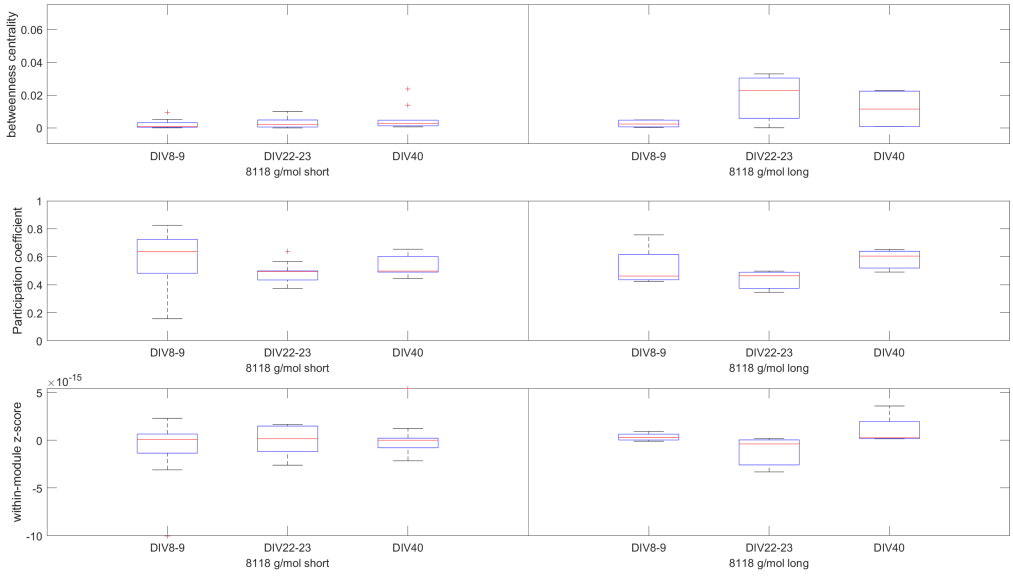

Figure A.15.: Development of different measures of centrality of spontaneously active networks in Collagen-PVP-*co*-GMA$_{3mol\%}$, derived from different recording times. There are no significant differences for $p \leqslant 0.05$. Error bars denote the standard deviation.

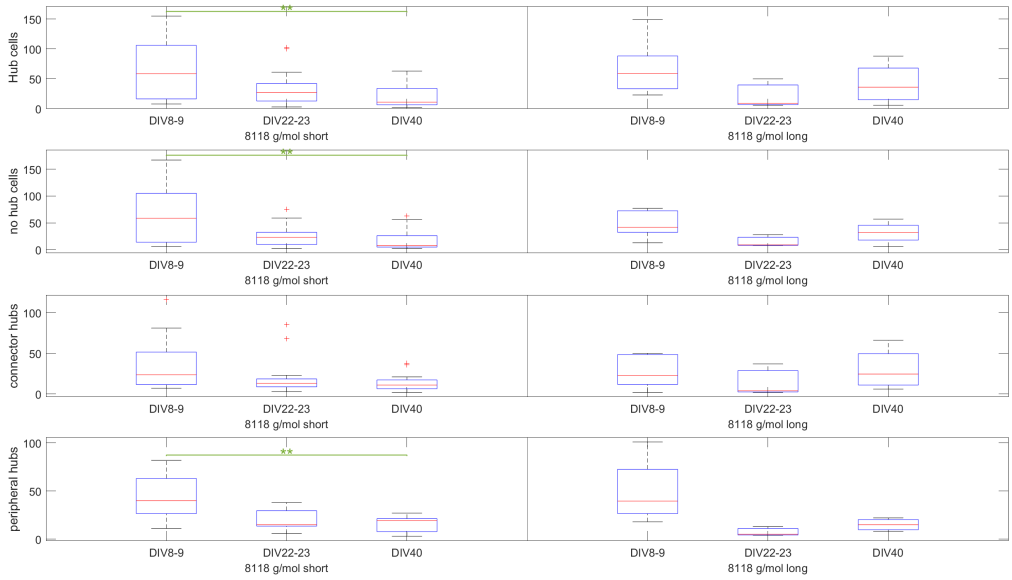

Figure A.16.: Emergence of of hub cells in spontaneously active networks cultured in Collagen-PVP-*co*-GMA$_{3mol\%}$, derived from different recording times. Significant differences are depicted by stars (*** for $p \leqslant 0.001$, ** for $p \leqslant 0.01$ and * for $p \leqslant 0.05$). Error bars denote the standard deviation.

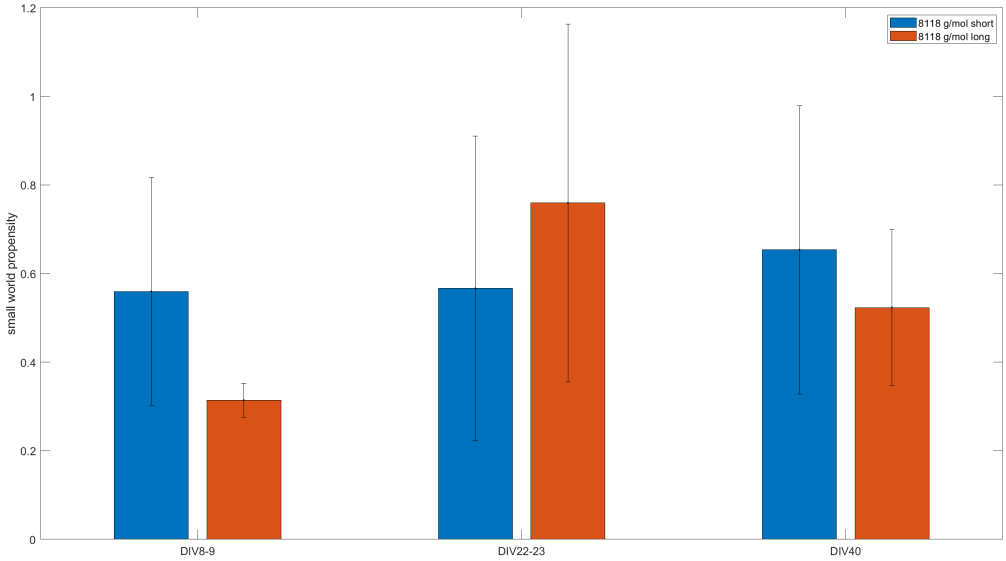

Figure A.17.: small-worldness of spontaneously active networks cultured in Collagen-PVP-*co*-GMA$_{3mol\%}$, derived from different recording times. There are no significant differences for $p \leqslant 0.05$. Error bars denote the standard deviation.

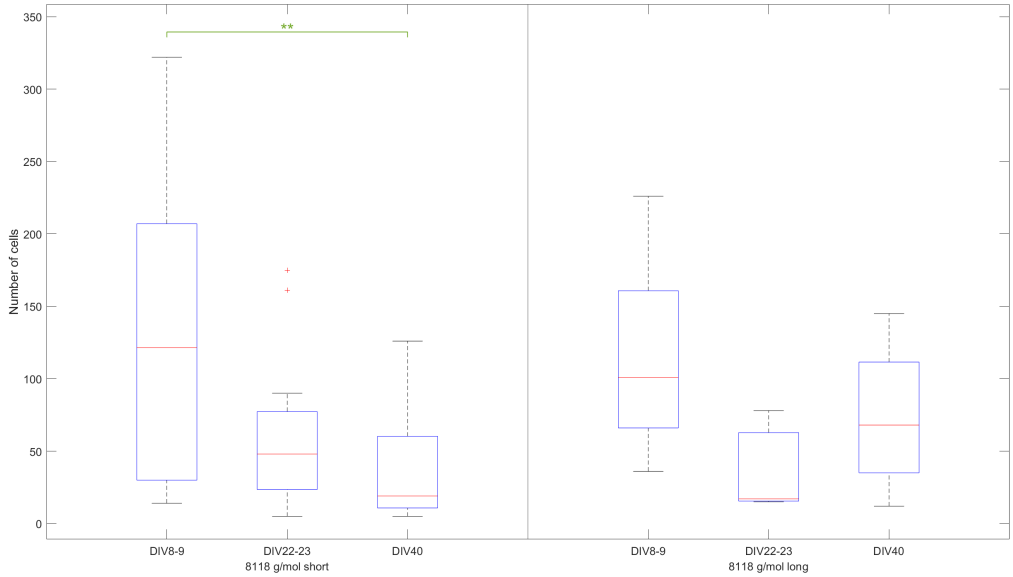

Figure A.18.: Average number of spontaneously active cells observed in spontaneously active networks cultured in Collagen-PVP-*co*-$GMA_{3mol\%}$, derived from different recording times. Significant differences are depicted by stars (*** for $p \leqslant 0.001$, ** for $p \leqslant 0.01$ and * for $p \leqslant 0.05$). Error bars denote the standard deviation.

Bibliography

[1] SeekPNG. Brain Human Anatomy - Brain Clip Art.

[2] Yurii Zasimov. Brain Logo Silhouette Top ViewBrain Logo silhouette top view design vector template. Brainstorm think idea Logotype concept icon.

[3] Rachel Tompa. 5 unsolved mysteries about the brain, 2019.

[4] Alzheimer Forschung Initiative e.V. Die Alzheimer-Krankheit: Morbus Alzheimer einfach erklärt, 2021.

[5] Jerry Silver, Martin E. Schwab, and Phillip G. Popovich. Central nervous system regenerative failure: Role of oligodendrocytes, astrocytes, and microglia. *Cold Spring Harbor Perspectives in Biology*, 7(3), 2015.

[6] Pallavi Madhusudanan, Gayathri Raju, and Sahadev Shankarappa. Hydrogel systems and their role in neural tissue engineering. *Journal of The Royal Society Interface*, 17(162):20190505, jan 2020.

[7] Lifu Sheng, Iryna Leshchyns'Ka, and Vladimir Sytnyk. Cell adhesion and intracellular calcium signaling in neurons, dec 2013.

[8] R. Douglas Fields. Cell Adhesion Molecules: Implications for Neurological Disease. *The Neuroscientist*, 4(1):4–8, jan 1998.

[9] Alexander Dityatev and Melitta Schachner. Extracellular matrix molecules and synaptic plasticity. *Nature Reviews Neuroscience*, 4(6):456–468, 2003.

[10] Alexander Dityatev, Melitta Schachner, and Peter Sonderegger. The dual role of the extracellular matrix in synaptic plasticity and homeostasis, nov 2010.

[11] Christine M. Gall and Gary Lynch. Integrins, synaptic plasticity and epileptogenesis, 2004.

[12] Joachim Herz and Ying Chen. Reelin, lipoprotein receptors and synaptic plasticity, nov 2006.

[13] Christine M. Gall and Gary Lynch. Integrins, synaptic plasticity and epileptogenesis, 2004.

[14] Xin Wu and Doodipala Samba Reddy. Integrins as receptor targets for neurological disorders, apr 2012.

[15] Christine Grienberger and Arthur Konnerth. Imaging Calcium in Neurons. *Neuron*, 73(5):862–885, 2012.

[16] Heather A. Enright, Doris Lam, Aimy Sebastian, Ana Paula Sales, Jose Cadena, Nicholas R. Hum, Joanne J. Osburn, Sandra K.G. Peters, Bryan Petkus, David A. Soscia, Kristen S. Kulp, Gabriela G. Loots, Elizabeth K. Wheeler, and Nicholas O. Fischer. Functional and transcriptional characterization of complex neuronal co-cultures. *Scientific Reports*, 10(1):1–14, dec 2020.

[17] Mehdi Jorfi, Carla D'Avanzo, Doo Yeon Kim, and Daniel Irimia. Three-Dimensional Models of the Human Brain Development and Diseases. *Advanced Healthcare Materials*, 7(1), jan 2018.

[18] Christopher D. Spicer. Hydrogel scaffolds for tissue engineering: The importance of polymer choice. *Polymer Chemistry*, 11(2):184–219, 2020.

[19] Nobuaki Maeda. Proteoglycans and neuronal migration in the cerebral cortex during development and disease. *Frontiers in Neuroscience*, 9(MAR):98, mar 2015.

[20] E. R. Burnside and E. J. Bradbury. Review: Manipulating the extracellular matrix and its role in brain and spinal cord plasticity and repair. *Neuropathology and Applied Neurobiology*, 40(1):26–59, feb 2014.

[21] Yiming Lei, Hongbin Han, Fan Yuan, Aqeel Javeed, and Yong Zhao. The brain interstitial system: Anatomy, modeling, in vivo measurement, and applications, oct 2017.

[22] Disha Sood, Karolina Chwalek, Emily Stuntz, Dimitra Pouli, Chuang Du, Min Tang-Schomer, Irene Georgakoudi, Lauren D. Black, and David L. Kaplan. Fetal Brain Extracellular Matrix Boosts Neuronal Network Formation in 3D Bioengineered Model of Cortical Brain Tissue. *ACS Biomaterials Science and Engineering*, 2(1):131–140, jan 2016.

[23] Lorraine W Lau, Rowena Cua, Michael B Keough, Sarah Haylock-Jacobs, and V. Wee Yong. Pathophysiology of the brain extracellular matrix: a new target for remyelination. *Nature Reviews Neuroscience*, 14(10):722–729, oct 2013.

[24] Gerlinde Köppe, Gert Brückner, Kurt Brauer, Wolfgang Härtig, and Volker Bigl. Developmental patterns of proteoglycan-containing extracellular matrix in perineuronal nets and neuropil of the postnatal rat brain. *Cell and Tissue Research*, 288(1):33–41, mar 1997.

[25] Daniela Carulli, Kate E. Rhodes, and James W. Fawcett. Upregulation of aggrecan, link protein 1, and hyaluronan synthases during formation of perineuronal nets in the rat cerebellum. *The Journal of Comparative Neurology*, 501(1):83–94, mar 2007.

[26] Jessica C. F. Kwok, Daniela Carulli, and James W. Fawcett. In vitro modeling of perineuronal nets: hyaluronan synthase and link protein are necessary for their formation and integrity. *Journal of Neurochemistry*, 114(5):no–no, jul 2010.

[27] Jessica C.F. Kwok, Gunnar Dick, Difei Wang, and James W. Fawcett. Extracellular matrix and perineuronal nets in CNS repair. *Developmental Neurobiology*, 71(11):1073–1089, nov 2011.

[28] Kurt Brauer, Wolfgang Ha¨rtig, Volker Bigl, and Gert Bru¨ckner. Distribution of parvalbumin-containing neurons and lectin-binding perineuronal nets in the rat basal forebrain. *Brain Research*, 631(1):167–170, dec 1993.

[29] Eva Sabine Wintergerst, Andreas Faissner, and Marco R. Celio. The proteoglycan DSD-1-PG occurs in perineuronal nets around parvalbumin-immunoreactive interneurons of the rat cerebral cortex. *International Journal of Developmental Neuroscience*, 14(3):249–255, 1996.

[30] Neil P. Morris and Zaineb Henderson. Perineuronal nets ensheath fast spiking, parvalbumin-immunoreactive neurons in the medial septum/diagonal band complex. *European Journal of Neuroscience*, 12(3):828–838, mar 2000.

[31] Sabrina Reimers, Maike Hartlage-Rübsamen, Gert Brückner, and Steffen Roßner. Formation of perineuronal nets in organotypic mouse brain slice cultures is independent of neuronal glutamatergic activity. *European Journal of Neuroscience*, 25(9):2640–2648, jun 2007.

[32] Eric R. Kandel, James H. Schwartz, Thomas M. Jessell, Steven A. Siegelbaum, and A. J. Hudspeth. *Principles of neural science*. McGraw-Hill New York, 4th editio edition, 2000.

[33] MolecularDevices. What is an action potential?

[34] Alberto E Pereda and Dominick P Purpura. Electrical synapses and their functional interactions with chemical synapses. *Nature Publishing Group*, 15, 2014.

[35] Caleb Jensen and Yong Teng. Is It Time to Start Transitioning From 2D to 3D Cell Culture?, mar 2020.

[36] Mina J. Bissell, H. Glenn Hall, and Gordon Parry. How does the extracellular matrix direct gene expression? *Journal of Theoretical Biology*, 99(1):31–68, nov 1982.

[37] Robert Langer and Joseph P. Vacanti. Tissue engineering. *Science*, 260(5110):920–926, may 1993.

[38] Michael J. Kratochvil, Alexis J. Seymour, Thomas L. Li, Sergiu P. Paşca, Calvin J. Kuo, and Sarah C. Heilshorn. Engineered materials for organoid systems, sep 2019.

[39] Paul D. Drumheller and Jeffrey A. Hubbell. Densely crosslinked polymer networks of poly(ethylene glycol) in trimethylolpropane triacrylate for cellokayadhesionokayresistant surfaces. *Journal of Biomedical Materials Research*, 29(2):207–215, 1995.

[40] Toshiro Sato, Robert G. Vries, Hugo J. Snippert, Marc Van De Wetering, Nick Barker, Daniel E. Stange, Johan H. Van Es, Arie Abo, Pekka Kujala, Peter J. Peters, and Hans Clevers. Single Lgr5 stem cells build crypt-villus structures in vitro without a mesenchymal niche. *Nature*, 459(7244):262–265, may 2009.

[41] Cell Stem Cell. Advances in Organoid Technology: Hans Clevers, Madeline Lancaster, and Takanori Takebe. *Cell Stem Cell*, 20(6):759–762, jun 2017.

[42] Shuang Li, Min Wang, and Junmei Zhou. Brain Organoids: A Promising Living Biobank Resource for Neuroscience Research, apr 2020.

[43] Jonghun Kim, Gareth J. Sullivan, and In-Hyun Park. How well do brain organoids capture your brain? *iScience*, 24(2):102063, feb 2021.

[44] Augustin Chen, Zhenming Guo, Lipao Fang, and Shan Bian. Application of Fused Organoid Models to Study Human Brain Development and Neural Disorders, may 2020.

[45] X. Cui, Y. Hartanto, and H. Zhang. Advances in multicellular spheroids formation. *Journal of the Royal Society Interface*, 14(127), 2017.

[46] Linus Kloker, Can Yurttas, and Ulrich Lauer. Three-dimensional tumor cell cultures employed in virotherapy research. *Oncolytic Virotherapy*, Volume 7:79–93, sep 2018.

[47] Steven A. Sloan, Spyros Darmanis, Nina Huber, Themasap A. Khan, Fikri Birey, Christine Caneda, Richard Reimer, Stephen R. Quake, Ben A. Barres, and Sergiu P. Paşca. Human Astrocyte Maturation Captured in 3D Cerebral Cortical Spheroids Derived from Pluripotent Stem Cells. *Neuron*, 95(4):779–790.e6, aug 2017.

[48] Fikri Birey, Jimena Andersen, Christopher D. Makinson, Saiful Islam, Wu Wei, Nina Huber, H. Christina Fan, Kimberly R.Cordes Metzler, Georgia Panagiotakos, Nicholas Thom, Nancy A. O'Rourke, Lars M. Steinmetz, Jonathan A. Bernstein, Joachim Hallmayer, John R. Huguenard, and Sergiu P. Pasca. Assembly of functionally integrated human forebrain spheroids. *Nature*, 545(7652):54–59, may 2017.

[49] Takaaki Kirihara, Zhongyue Luo, Siu Yu A. Chow, Ryuji Misawa, Jiro Kawada, Shinsuke Shibata, Farad Khoyratee, Carole Anne Vollette, Valentine Volz, Timothée Levi, Teruo Fujii, and Yoshiho Ikeuchi. A Human Induced Pluripotent Stem Cell-Derived Tissue Model of a Cerebral Tract Connecting Two Cortical Regions. *iScience*, 14:301–311, apr 2019.

[50] Yu-Ting L. Dingle, Molly E. Boutin, Anda M. Chirila, Liane L. Livi, Nicholas R. Labriola, Lorin M. Jakubek, Jeffrey R. Morgan, Eric M. Darling, Julie A. Kauer, and Diane Hoffman-Kim. Three-Dimensional Neural Spheroid Culture: An In Vitro Model for Cortical Studies. *Tissue Engineering Part C: Methods*, 21(12):1274–1283, dec 2015.

[51] John D. Blair, Dirk Hockemeyer, and Helen S. Bateup. Genetically engineered human cortical spheroid models of tuberous sclerosis. *Nature Medicine*, 24(10):1568–1578, oct 2018.

[52] Goodwell Nzou, R. T. Wicks, E. E. Wicks, S. A. Seale, C. H. Sane, A. Chen, S. V. Murphy, J. D. Jackson, and A. J. Atala. Human cortex spheroid with a functional blood brain barrier for high-throughput neurotoxicity screening and disease modeling. *Scientific Reports*, 8(1):1–10, dec 2018.

[53] Han-Kyu Lee, Clara Velazquez Sanchez, Mei Chen, Peter J. Morin, John M. Wells, Eugene B. Hanlon, and Weiming Xia. Three Dimensional Human Neuro-Spheroid Model of Alzheimer's Disease Based on Differentiated Induced Pluripotent Stem Cells. *PLOS ONE*, 11(9):e0163072, sep 2016.

[54] M. L. Oyen. Mechanical characterisation of hydrogel materials. *International Materials Reviews*, 59(1):44–59, jan 2014.

[55] Shahid Bashir, Maryam Hina, Javed Iqbal, A. H. Rajpar, M. A. Mujtaba, N. A. Alghamdi, S. Wageh, K. Ramesh, and S. Ramesh. Fundamental concepts of hydrogels: Synthesis, properties, and their applications, nov 2020.

[56] Raphael M. Ottenbrite, Kinam Park, and Teruo Okano, editors. *Biomedical Applications of Hydrogels Handbook*. Springer New York, New York, NY, 2010.

[57] E.M. Weijers. Fibrin matrices for tissue engineering: Naturally occurring fibrinogen variants alter cellular characteristics, 2011.

[58] Tamer A.E. Ahmed, Emma V. Dare, and Max Hincke. Fibrin: A Versatile Scaffold for Tissue Engineering Applications. *Tissue Engineering Part B: Reviews*, 14(2):199–215, jun 2008.

[59] Francesco Rosso, Gerardo Marino, Antonio Giordano, Manlio Barbarisi, Domenico Parmeggiani, and Alfonso Barbarisi. Rosso F, Marino G, Giordano A, Barbarisi M, Parmeggiani D, Barbarisi A. Smart materials as scaffolds for tissue engineering,Journal of Cellular Physiology (2005) 203(3) 465–470. *Journal of Cellular Physiology*, 209(3):1054–1054, dec 2006.

[60] Ailish Breen, Timothy O'Brien, and Abhay Pandit. Fibrin as a delivery system for therapeutic drugs and biomolecules, jun 2009.

[61] Kuen Yong Lee and David J Mooney. Alginate: properties and biomedical applications. *Progress in polymer science*, 37(1):106–126, jan 2012.

[62] Gemma Palazzolo, Nicolas Broguiere, Orlando Cenciarelli, Harald Dermutz, and Marcy Zenobi-Wong. Ultrasoft Alginate Hydrogels Support Long-Term Three-Dimensional Functional Neuronal Networks. *Tissue Engineering Part A*, 21(15-16):2177–2185, aug 2015.

[63] K. E. Crompton, J. D. Goud, R. V. Bellamkonda, T. R. Gengenbach, D. I. Finkelstein, M. K. Horne, and J. S. Forsythe. Polylysine-functionalised thermoresponsive chitosan hydrogel for neural tissue engineering. *Biomaterials*, 28(3):441–449, 2007.

[64] William P Daley, Sarah B Peters, and Melinda Larsen. Extracellular matrix dynamics in development and regenerative medicine. *Journal of cell science*, 121(Pt 3):255–64, 2008.

[65] Takashi Hoshiba, Guoping Chen, Chiho Endo, Hiroka Maruyama, Miyuki Wakui, Eri Nemoto, Naoki Kawazoe, and Masaru Tanaka. Decellularized extracellular matrix as an in vitro model to study the comprehensive roles of the ECM in stem cell differentiation. *Stem Cells International*, 2016, 2016.

[66] Disha Sood, Karolina Chwalek, Emily Stuntz, Dimitra Pouli, Chuang Du, Min Tang-Schomer, Irene Georgakoudi, Lauren D. Black, and David L. Kaplan. Fetal Brain Extracellular Matrix Boosts Neuronal Network Formation in 3D Bioengineered Model of Cortical Brain Tissue. *ACS Biomaterials Science and Engineering*, 2(1):131–140, 2016.

[67] Cornelia Vasile, Daniela Pamfil, Elena Stoleru, and Mihaela Baican. New developments in medical applications of hybrid hydrogels containing natural polymers, mar 2020.

[68] Buket Ucar and Christian Humpel. Collagen for brain repair: Therapeutic perspectives, apr 2018.

[69] Pallavi Madhusudanan, Gayathri Raju, and Sahadev Shankarappa. Hydrogel systems and their role in neural tissue engineering, jan 2020.

[70] Theresa A. Ulrich, Elena M. De Juan Pardo, and Sanjay Kumar. The mechanical rigidity of the extracellular matrix regulates the structure, motility, and proliferation of glioma cells. *Cancer Research*, 69(10):4167–4174, may 2009.

[71] J. Matthew Barnes, Laralynne Przybyla, and Valerie M. Weaver. Tissue mechanics regulate brain development, homeostasis and disease, 2017.

[72] Jessica M Stukel and Rebecca Kuntz Willits. Mechanotransduction of Neural Cells Through Cell-Substrate Interactions. *Tissue engineering. Part B, Reviews*, 22(3):173–82, 2016.

[73] Ning Wang. Review of cellular mechanotransduction, may 2017.

[74] William J. Tyler. The mechanobiology of brain function. *Nature Reviews Neuroscience*, 13(12):867–878, dec 2012.

[75] Shenglian Yao, Shukui Yu, Zheng Cao, Yongdong Yang, Xing Yu, Hai-Quan Mao, Lu-Ning Wang, Xiaodan Sun, Lingyun Zhao, and Xiumei Wang. Hierarchically aligned fibrin nanofiber hydrogel accelerated axonal regrowth and locomotor function recovery in rat spinal cord injury. *International Journal of Nanomedicine*, Volume 13:2883–2895, may 2018.

[76] Steven R. Caliari and Jason A. Burdick. A practical guide to hydrogels for cell culture. *Nature Methods*, 13(5):405–414, 2016.

[77] Elias H. Barriga and Roberto Mayor. Adjustable viscoelasticity allows for efficient collective cell migration, sep 2019.

[78] Thomas R. Cox and Janine T. Erler. Remodeling and homeostasis of the extracellular matrix: Implications for fibrotic diseases and cancer, mar 2011.

[79] Adam J. Engler, Shamik Sen, H. Lee Sweeney, and Dennis E. Discher. Matrix Elasticity Directs Stem Cell Lineage Specification. *Cell*, 126(4):677–689, aug 2006.

[80] Penelope C. Georges, William J. Miller, David F. Meaney, Evelyn S. Sawyer, and Paul A. Janmey. Matrices with compliance comparable to that of brain tissue select neuronal over glial growth in mixed cortical cultures. *Biophysical Journal*, 90(8):3012–3018, 2006.

[81] Hong Nam Kim and Nakwon Choi. Consideration of the Mechanical Properties of Hydrogels for Brain Tissue Engineering and Brain-on-a-chip, mar 2019.

[82] Mireille Bélanger and Pierre J. Magistretti. The role of astroglia in neuroprotection, 2009.

[83] Sara Mederos, Candela González-Arias, and Gertrudis Perea. Astrocyte–Neuron Networks: A Multilane Highway of Signaling for Homeostatic Brain Function. *Frontiers in Synaptic Neuroscience*, 10:45, nov 2018.

[84] Tara Deemyad, Joel Lüthi, and Nelson Spruston. Astrocytes integrate and drive action potential firing in inhibitory subnetworks. *Nature Communications*, 9(1):1–13, dec 2018.

[85] Ovijit Chaudhuri, Justin Cooper-White, Paul A. Janmey, David J. Mooney, and Vivek B. Shenoy. Effects of extracellular matrix viscoelasticity on cellular behaviour, aug 2020.

[86] Christopher U. Brown, Timothy L. Norman, Vincent L. Kish, Thomas A. Gruen, and J. David Blaha. Time-dependent circumferential deformation of cortical bone upon internal radial loading. *Journal of Biomechanical Engineering*, 124(4):456–461, aug 2002.

[87] Madeline A. Lancaster, Magdalena Renner, Carol Anne Martin, Daniel Wenzel, Louise S. Bicknell, Matthew E. Hurles, Tessa Homfray, Josef M. Penninger, Andrew P. Jackson, and Juergen A. Knoblich. Cerebral organoids model human brain development and microcephaly. *Nature*, 501(7467):373–379, aug 2013.

[88] Christopher M. Madl, Bauer L. Lesavage, Ruby E. Dewi, Cong B. Dinh, Ryan S. Stowers, Margarita Khariton, Kyle J. Lampe, Duong Nguyen, Ovijit Chaudhuri, Annika Enejder, and Sarah C. Heilshorn. Maintenance of neural progenitor cell stemness in 3D hydrogels requires matrix remodelling. *Nature Materials*, 16(12):1233–1242, dec 2017.

[89] Kelly M. Schultz, Kyle A. Kyburz, and Kristi S. Anseth. Measuring dynamic cell-material interactions and remodeling during 3D human mesenchymal stem cell migration in hydrogels. *Proceedings of the National Academy of Sciences of the United States of America*, 112(29):E3757–E3764, jul 2015.

[90] Sara Mattana, Silvia Caponi, Francesco Tamagnini, Daniele Fioretto, and Francesca Palombo. Viscoelasticity of amyloid plaques in transgenic mouse brain studied by Brillouin microspectroscopy and correlative Raman analysis. *Journal of Innovative Optical Health Sciences*, 10(6), nov 2017.

[91] Kihan Park, Gabrielle E. Lonsberry, Marla Gearing, Allan I. Levey, and Jaydev P. Desai. Viscoelastic Properties of Human Autopsy Brain Tissues as Biomarkers for Alzheimer's Diseases. *IEEE Transactions on Biomedical Engineering*, 66(6):1705–1713, jun 2019.

[92] Mikail Rubinov and Olaf Sporns. Complex network measures of brain connectivity: Uses and interpretations. *NeuroImage*, 52(3):1059–1069, sep 2010.

[93] Farzad V. Farahani, Waldemar Karwowski, and Nichole R. Lighthall. Application of graph theory for identifying connectivity patterns in human brain networks: A systematic review, jun 2019.

[94] Daniele Poli, Vito P. Pastore, and Paolo Massobrio. Functional connectivity in in vitro neuronal assemblies. *Frontiers in Neural Circuits*, 9(OCT):57, oct 2015.

[95] André M. Bastos and Jan Mathijs Schoffelen. A tutorial review of functional connectivity analysis methods and their interpretational pitfalls, jan 2016.

[96] Ildefons Magrans de Abril, Junichiro Yoshimoto, and Kenji Doya. Connectivity inference from neural recording data: Challenges, mathematical bases and research directions, jun 2018.

[97] Olav Stetter, Demian Battaglia, Jordi Soriano, and Theo Geisel. Model-Free Reconstruction of Excitatory Neuronal Connectivity from Calcium Imaging Signals. *PLoS Computational Biology*, 8(8):e1002653, aug 2012.

[98] Xiuli Liu, Tingwei Quan, Shaoqun Zeng, and Xiaohua Lv. Identification of the direction of the neural network activation with a cellular resolution by fast two-photon imaging. *Journal of Biomedical Optics*, 16(8):080506, 2011.

[99] Thomas Schreiber. Measuring information transfer. *Physical Review Letters*, 85(2):461–464, jul 2000.

[100] Jana Katharina Wrosch, Vicky Von Einem, Katharina Breininger, Marc Dahlmanns, Andreas Maier, Johannes Kornhuber, and Teja Wolfgang Groemer. Rewiring of neuronal networks during synaptic silencing. *Scientific Reports*, 7(1):11724, dec 2017.

[101] Hideaki Yamamoto, Satoshi Moriya, Katsuya Ide, Takeshi Hayakawa, Hisanao Akima, Shigeo Sato, Shigeru Kubota, Takashi Tanii, Michio Niwano, Sara Teller, Jordi Soriano, and Ayumi Hirano-Iwata. Impact of modular organization on dynamical richness in cortical networks. *Science Advances*, 4(11):eaau4914, nov 2018.

[102] Arjan Hillebrand, Prejaas Tewarie, Edwin Van Dellen, Meichen Yu, Ellen W S Carbo, Linda Douw, Alida A Gouw, Elisabeth C W Van Straaten, Cornelis J Stam, C J S Designed, and C J S Performed. Direction of information flow in large-scale resting-state networks is frequency-dependent. *PNAS*, 113(14):3867–3872, 2016.

[103] Kathleen Vincent, Joseph S. Tauskela, and Jean-Philippe Thivierge. Extracting functionally feedforward networks from a population of spiking neurons. *Frontiers in Computational Neuroscience*, 6(OCTOBER 2012):86, oct 2012.

[104] Louis-David Lord, Angus B. Stevner, Gustavo Deco, and Morten L. Kringelbach. Understanding principles of integration and segregation using whole-brain computational connectomics: implications for neuropsychiatric disorders. *Philosophical Transactions of the Royal Society A: Mathematical, Physical and Engineering Sciences*, 375(2096):20160283, jun 2017.

[105] Wei He, Paul F. Sowman, Jon Brock, Andrew C. Etchell, Cornelis J. Stam, and Arjan Hillebrand. Increased segregation of functional networks in developing brains. *NeuroImage*, 200:607–620, oct 2019.

[106] Mangor Pedersen, Amir H. Omidvarnia, Jennifer M. Walz, and Graeme D. Jackson. Increased segregation of brain networks in focal epilepsy: An fMRI graph theory finding. *NeuroImage: Clinical*, 8:536–542, jun 2015.

[107] Aron K. Barbey. Network Neuroscience Theory of Human Intelligence, jan 2018.

[108] N. Laurens, P. Koolwijk, and M. P. de Maat. Fibrin structure and wound healing., may 2006.

[109] John W. Weisel. The mechanical properties of fibrin for basic scientists and clinicians. *Biophysical Chemistry*, 112(2-3 SPEC. ISS.):267–276, dec 2004.

[110] Stefan Jockenhoevel, Gregor Zund, Simon P. Hoerstrup, Khaled Chalabi, Jörg S. Sachweh, Lütfü Demircan, Bruno J. Messmer, and Marko Turina. Fibrin gel - advantages of a new scaffold in cardiovascular tissue engineering. *European Journal of Cardio-thoracic Surgery*, 19(4):424–430, apr 2001.

[111] Paul A Janmey, Jessamine P Winer, and John W Weisel. Fibrin gels and their clinical and bioengineering applications, 2009.

[112] Zhenxia Zhang, Shenglian Yao, Sheng Xie, Xiumei Wang, Feiyan Chang, Jie Luo, Jingming Wang, and Jun Fu. Effect of hierarchically aligned fibrin hydrogel in regeneration of spinal cord injury demonstrated by tractography: A pilot study. *Scientific Reports*, 7(1):1–9, jan 2017.

[113] Ziyuan Yu, Hongru Li, Peng Xia, Weijian Kong, Yuxin Chang, Chuan Fu, Kai Wang, Xiaoyu Yang, and Zhiping Qi. Application of fibrin-based hydrogels for nerve protection and regeneration after spinal cord injury. *Journal of Biological Engineering*, 14(1):22, dec 2020.

[114] Rémi Parenteau-Bareil, Robert Gauvin, and François Berthod. Collagen-Based Biomaterials for Tissue Engineering Applications. *Materials*, 3(3):1863–1887, mar 2010.

[115] Jeanie L. Drury and David J. Mooney. Hydrogels for tissue engineering: Scaffold design variables and applications. *Biomaterials*, 24(24):4337–4351, 2003.

[116] D. I. Zeugolis and M. Raghunath. Collagen: Materials analysis and implant uses. In *Comprehensive Biomaterials*, volume 2, pages 261–278. Elsevier, oct 2011.

[117] Marina Protasoni, Simone Sangiorgi, Andrea Cividini, Gloria Tiffany Culuvaris, Giustino Tomei, Carlo Dell'Orbo, Mario Raspanti, Sergio Balbi, and Marcella Reguzzoni. The collagenic architecture of human dura mater: Laboratory investigation. *Journal of Neurosurgery*, 114(6):1723–1730, jun 2011.

[118] Raquel de la Cruz and David Díaz Díaz. Self-Healing Collagen-Based Hydrogel for Brain Injury Therapy. pages 1–24. Springer, Berlin, Heidelberg, 2020.

[119] Marco Franchi, Alessandra Trirè, Marilisa Quaranta, Ester Orsini, and Vittoria Ottani. Collagen structure of tendon relates to function, mar 2007.

[120] Ali Karami, Hamid Tebyanian, Reza Sayyad Soufdoost, Ebrahim Motavallian, Aref Barkhordari, and Mohammad Reza Nourani. Extraction and Characterization of Collagen with Cost-Effective Method from Human Placenta for Biomedical Applications. *World journal of plastic surgery*, 8(3):352–358, sep 2019.

[121] Ivan de Curtis. Neuronal interactions with the extracellular matrix. *Current Opinion in Cell Biology*, 3(5):824–831, oct 1991.

[122] Ibidi. Collagen Type I, Rat Tail | 3D Cell Culture Gels & Coating | ibidi, 2021.

[123] B. D. Walters and J. P. Stegemann. Strategies for directing the structure and function of three-dimensional collagen biomaterials across length scales, 2014.

[124] Steven R Caliari and Jason A Burdick. A practical guide to hydrogels for cell culture. *NATURE METHODS*, 13(5), 2016.

[125] Mei Liu, Xin Zeng, Chao Ma, Huan Yi, Zeeshan Ali, Xianbo Mou, Song Li, Yan Deng, and Nongyue He. Injectable hydrogels for cartilage and bone tissue engineering, may 2017.

[126] Magdalini Tsintou, Kyriakos Dalamagkas, and Alexander Seifalian. Injectable Hydrogel versus Plastically Compressed Collagen Scaffold for Central Nervous System Applications. *International Journal of Biomaterials*, 2018, 2018.

[127] Buket Ucar and Christian Humpel. Collagen for brain repair: Therapeutic perspectives. *Neural Regeneration Research*, 13(4):595–598, 2018.

[128] Vanessa Gil and José Antonio Del Río. Analysis of axonal growth and cell migration in 3D hydrogel cultures of embryonic mouse CNS tissue. *Nature Protocols*, 7(2):268–280, 2012.

[129] W. Ma, W. Fitzgerald, Q. Y. Liu, T. J. O'Shaughnessy, D. Maric, H. J. Lin, D. L. Alkon, and J. L. Barker. CNS stem and progenitor cell differentiation into functional neuronal circuits in three-dimensional collagen gels. *Experimental Neurology*, 190(2):276–288, dec 2004.

[130] Miriam Aischa Al EnezyokayUlbrich, Hanna Malyaran, Robert Dirk Lange, Norina Labude, René Plum, Stephan Rütten, Nicole Terefenko, Svenja Wein, Sabine Neuss, and Andrij Pich. Impact of Reactive Amphiphilic Copolymers on Mechanical Properties and Cell Responses of FibrinokayBased Hydrogels. *Advanced Functional Materials*, 30(38):2003528, sep 2020.

[131] Huan Peng, Kristin Rübsam, Chaolei Hu, Felix Jakob, Ulrich Schwaneberg, and Andrij Pich. Stimuli-Responsive Poly(N-Vinyllactams) with Glycidyl Side Groups: Synthesis, Characterization, and Conjugation with Enzymes. *Biomacromolecules*, 20(2):992–1006, feb 2019.

[132] Thermo Fisher Scientific. B-27 Supplements | Thermo Fisher Scientific - DE, 2021.

[133] Thermo Fisher Scientific. N-2 Supplement (100X), 2021.

[134] J. Nakai, M. Ohkura, and K. Imoto. A high signal-to-noise ca2+ probe composed of a single green fluorescent protein. *Nature Biotechnology*, 19(2):137–141, 2001.

[135] Jasper Akerboom, Tsai Wen Chen, Trevor J. Wardill, Lin Tian, Jonathan S. Marvin, Sevinç Mutlu, Nicole Carreras Calderón, Federico Esposti, Bart G. Borghuis, Xiaonan Richard Sun, Andrew Gordus, Michael B. Orger, Ruben Portugues, Florian Engert, John J. Macklin, Alessandro Filosa, Aman Aggarwal, Rex A. Kerr, Ryousuke Takagi, Sebastian Kracun, Eiji Shigetomi, Baljit S. Khakh, Herwig Baier, Leon Lagnado, Samuel S.H. Wang, Cornelia I. Bargmann, Bruce E. Kimmel, Vivek Jayaraman, Karel Svoboda, Douglas S. Kim, Eric R. Schreiter, and Loren L. Looger. Optimization of a GCaMP calcium indicator for neural activity imaging. *Journal of Neuroscience*, 32(40):13819–13840, oct 2012.

[136] Lin Tian, S. Andrew Hires, Tianyi Mao, Daniel Huber, M. Eugenia Chiappe, Sreekanth H. Chalasani, Leopoldo Petreanu, Jasper Akerboom, Sean A. McKinney, Eric R. Schreiter, Cornelia I. Bargmann, Vivek Jayaraman, Karel Svoboda, and Loren L. Looger. Imaging neural activity in worms, flies and mice with improved GCaMP calcium indicators. *Nature Methods*, 6(12):875–881, 2009.

[137] Tsai-Wen Chen, Trevor J Wardill, Yi Sun, Stefan R Pulver, Sabine L Renninger, Amy Baohan, Eric R Schreiter, Rex a Kerr, Michael B Orger, Vivek Jayaraman, Loren L Looger, Karel Svoboda, and Douglas S Kim. Supplymentary!!! - Ultrasensitive fluorescent proteins for imaging neuronal activity. *Nature*, 499(7458):295–300, 2013.

[138] Marius Pachitariu, Carsen Stringer, Mario Dipoppa, Sylvia Schröder, L. Federico Rossi, Henry Dalgleish, Matteo Carandini, and Kenneth Harris. Suite2p: beyond 10,000 neurons with standard two-photon microscopy. *bioRxiv*, page 061507, jun 2016.

[139] Welcome to suite2p's documentation! — suite2p 0.7.2 documentation.

[140] *Pschyrembel klinisches Wörterbuch 2012*. De Gruyter, 263 edition, 2012.

[141] Tapan P. Patel, Karen Man, Bonnie L. Firestein, and David F. Meaney. Automated quantification of neuronal networks and single-cell calcium dynamics using calcium imaging. *Journal of Neuroscience Methods*, 243:26–38, mar 2015.

[142] Brian Karrer, Elizaveta Levina, and M. E.J. Newman. Robustness of community structure in networks. *Physical Review E - Statistical, Nonlinear, and Soft Matter Physics*, 77(4):046119, apr 2008.

[143] Cross-correlation - MATLAB xcorr - MathWorks Deutschland.

[144] Corning. *Corning Matrigel Matrix*. 2013.

[145] Sigma-Aldrich. ECM-Gel aus Engelbreth-Holm-Swarm murine sarcoma liquid, BioReagent, suitable for cell culture | Sigma-Aldrich, 2021.

[146] Corning Incorporated Life Sciences. Background 1. What is Corning Matrigel matrix? Amounts of Growth Factors (GF) Present in Corning Matrigel Matrix vs. Growth Factor Reduced (GFR) Corning Matrigel Matrix Growth Factor Range of GF Concentration in Corning Matrigel Matrix Average GF Concentr. Technical report, 2019.

[147] O R Implied, Including But, N O T Limited, T O Those, O F Merchantability, O R Fitness, F O R A Particular, I N No, Event Shall, Thewell Bioscience, Whether I N Contract, O R Under, A N Y Statute, O R On, A N Y Other, Basis For, Multiple Or, Consequential Damages, I N Connection, With Or, From This Document, Including But, N O T Limited, T O The, U S E Thereof, Whether Or, and N O T Foreseeable. ready-to-use tunable hydrogel for 3D cell culture and beyond. (June), 2018.

[148] Jooyoung Lee, Boa Song, Ramesh Subbiah, Justin J. Chung, U. Hyeok Choi, Kwideok Park, Sang-Heon Kim, and Seung Ja Oh. Effect of chain flexibility on cell adhesion: Semi-flexible model-based analysis of cell adhesion to hydrogels. *Scientific Reports*, 9(1):2463, dec 2019.

[149] Esther A. Ryan, Lyle F. Mockros, John W. Weisel, and Laszlo Lorand. Structural origins of fibrin clot rheology. *Biophysical Journal*, 77(5):2813–2826, nov 1999.

[150] Haison Duong, Benjamin Wu, and Bill Tawil. Modulation of 3D fibrin matrix stiffness by intrinsic fibrinogen-thrombin compositions and by extrinsic cellular activity. *Tissue Engineering - Part A*, 15(7):1865–1876, jul 2009.

[151] J. P. Collet, D. Park, C. Lesty, J. Soria, C. Soria, G. Montalescot, and J. W. Weisel. Influence of fibrin network conformation and fibrin diameter on fibrinolysis speed: Dynamic and structural approaches by confocal microscopy. *Arteriosclerosis, Thrombosis, and Vascular Biology*, 20(5):1354–1361, 2000.

[152] Kyung Eun Sung, Gui Su, Carolyn Pehlke, Steven M Trier, Kevin W Eliceiri, Patricia J Keely, Andreas Friedl, and David J Beebe. Control of 3-dimensional collagen matrix polymerization for reproducible Human Mammary Fibroblast cell culture in microfluidic devices. *Biomaterials*, 30(27):4833–4841, 2009.

[153] Karin A. Jansen, Albert J. Licup, Abhinav Sharma, Robbie Rens, Fred C. MacKintosh, and Gijsje H. Koenderink. The Role of Network Architecture in Collagen Mechanics. *Biophysical Journal*, 114(11):2665–2678, jun 2018.

[154] K HLAVACKOVASCHINDLER, M PALUS, M VEJMELKA, and J BHATTACHARYA. Causality detection based on information-theoretic approaches in time series analysis. *Physics Reports*, 441(1):1–46, mar 2007.

[155] Joon Lee, Shamim Nemati, Ikaro Silva, Bradley A. Edwards, James P. Butler, and Atul Malhotra. Transfer Entropy Estimation and Directional Coupling Change Detection in Biomedical Time Series. *BioMedical Engineering Online*, 11(1):1–17, apr 2012.

[156] Alan J. Man, Hillary E. Davis, Aki Itoh, Jonathan Kent Leach, and Peter Bannerman. Neurite outgrowth in fibrin gels is regulated by substrate stiffness. *Tissue Engineering - Part A*, 17(23-24):2931–2942, 2011.

[157] S M O'Connor, D a Stenger, K M Shaffer, and W Ma. Survival and neurite outgrowth of rat cortical neurons in three- dimensional agarose and collagen gel matrices. *Neurosci Lett*, 304:189–93. ST – Survival and neurite outgrowth of ra, 2001.

[158] Ruchi Parekh and Giorgio A. Ascoli. Neuronal Morphology Goes Digital: A Research Hub for Cellular and System Neuroscience, mar 2013.

[159] Bin Zhou, YunokayXia Zuo, and RuookayTian Jiang. Astrocyte morphology: Diversity, plasticity, and role in neurological diseases. *CNS Neuroscience & Therapeutics*, 25(6):665–673, jun 2019.

[160] Penelope C. Georges, William J. Miller, David F. Meaney, Evelyn S. Sawyer, and Paul A. Janmey. Matrices with compliance comparable to that of brain tissue select neuronal over glial growth in mixed cortical cultures. *Biophysical Journal*, 90(8):3012–3018, apr 2006.

[161] Jing Xie, Min Bao, Stéphanie M.C. Bruekers, and Wilhelm T.S. Huck. Collagen Gels with Different Fibrillar Microarchitectures Elicit Different Cellular Responses. *ACS Applied Materials and Interfaces*, 9(23):19630–19637, jun 2017.

[162] Jenna L. Wilson, Mohamad Ali Najia, Rabbia Saeed, and Todd C. Mcdevitt. Alginate encapsulation parameters influence the differentiation of microencapsulated embryonic stem cell aggregates. *Biotechnology and Bioengineering*, 111(3):618–631, mar 2014.

[163] Donghui Jing, Abhirath Parikh, and Emmanuel S. Tzanakakis. Cardiac cell generation from encapsulated embryonic stem cells in static and scalable culture systems. *Cell Transplantation*, 19(11):1397–1412, 2010.

[164] Niklas Schwarz, Ulrike B.S. Hedrich, Hannah Schwarz, P. A. Harshad, Nele Dammeier, Eva Auffenberg, Francesco Bedogni, Jürgen B. Honegger, Holger Lerche, Thomas V. Wuttke, and Henner Koch. Human Cerebrospinal fluid promotes long-term neuronal viability and network function in human neocortical organotypic brain slice cultures. *Scientific Reports*, 7(1), dec 2017.

[165] Heiko J. Luhmann, Anne Sinning, Jenq-Wei Yang, Vicente Reyes-Puerta, Maik C. Stüttgen, Sergei Kirischuk, and Werner Kilb. Spontaneous Neuronal Activity in Developing Neocortical Networks: From Single Cells to Large-Scale Interactions. *Frontiers in Neural Circuits*, 10(MAY):40, may 2016.

[166] Masanori Shimono and John M. Beggs. Functional Clusters, Hubs, and Communities in the Cortical Microconnectome. *Cerebral Cortex*, 25(10):3743–3757, oct 2015.

[167] J H Downes, M W Hammond, D Xydas, M C Spencer, and V M Becerra. Emergence of a Small-World Functional Network in Cultured Neurons. *PLoS Comput Biol*, 8(5):1002522, 2012.

[168] Michela Chiappalone, Marco Bove, Alessandro Vato, Mariateresa Tedesco, and Sergio Martinoia. Dissociated cortical networks show spontaneously correlated activity patterns during in vitro development. *Brain Research*, 1093(1):41–53, jun 2006.

[169] Zoltán Molnár, Heiko J. Luhmann, and Patrick O. Kanold. Transient cortical circuits match spontaneous and sensory-driven activity during development. *Science*, 370(6514):eabb2153, oct 2020.

[170] Yehezkel Ben-Ari. Developing networks play a similar melody. *Trends in Neurosciences*, 24(6):353–360, jun 2001.

[171] Yu-Ting L. Dingle, Molly Elizabeth Boutin, Anda M. Chirila, Liane L. Livi, Nicholas R. Labriola, Lorin M. Jakubek, Jeffrey R. Morgan, Eric M. Darling, Julie a. Kauer, and Diane Hoffman-Kim. 3D Neural Spheroid Culture: An In Vitro Model for Cortical Studies. *Tissue Engineering Part C: Methods*, 00(00):ten.TEC.2015.0135, 2015.

[172] Paul Charlesworth, Ellese Cotterill, Andrew Morton, Seth G.N. Grant, and Stephen J. Eglen. Quantitative differences in developmental profiles of spontaneous activity in cortical and hippocampal cultures. *Neural Development*, 10(1):1, jan 2015.

[173] Sarah Feldt Muldoon, Eric W. Bridgeford, and Danielle S. Bassett. Small-World Propensity and Weighted Brain Networks. *Scientific Reports*, 6(1):22057, feb 2016.

[174] Ed Bullmore and Olaf Sporns. Complex brain networks: Graph theoretical analysis of structural and functional systems, mar 2009.

[175] Jukka Pekka Onnela, Jari Saramäki, János Kertész, and Kimmo Kaski. Intensity and coherence of motifs in weighted complex networks. *Physical Review E - Statistical, Nonlinear, and Soft Matter Physics*, 71(6):065103, jun 2005.

[176] Jyh-jang Sun, Werner Kilb, and Heiko J Luhmann. Self-organization of repetitive spike patterns in developing neuronal networks in vitro. *European Journal of Neuroscience*, 32(8):1289–1299, oct 2010.

[177] Chapter 7 – Network Science by Albert-László Barabási.

[178] Richard F. Betzel, Maxwell A. Bertolero, and Danielle S. Bassett. Non-assortative community structure in resting and task-evoked functional brain networks, jun 2018.

[179] Merav Antman-Passig, Shahar Levy, Chaim Gartenberg, Hadas Schori, and Orit Shefi. Mechanically Oriented 3D Collagen Hydrogel for Directing Neurite Growth. *Tissue Engineering Part A*, 23(9-10):403–414, may 2017.

[180] Rocío Fernandez-Serra, Rebeca Gallego, Paloma Lozano, and Daniel González-Nieto. Hydrogels for neuroprotection and functional rewiring: A new era for brain engineering, may 2020.

[181] Niamh Moriarty, Abhay Pandit, and Eilís Dowd. Encapsulation of primary dopaminergic neurons in a GDNF-loaded collagen hydrogel increases their survival, re-innervation and function after intra-striatal transplantation. *Scientific Reports*, 7(1):1–14, dec 2017.

[182] Brendon M. Baker, Britta Trappmann, William Y. Wang, Mahmut S. Sakar, Iris L. Kim, Vivek B. Shenoy, Jason A. Burdick, and Christopher S. Chen. Cell-mediated fibre recruitment drives extracellular matrix mechanosensing in engineered fibrillar microenvironments. *Nature Materials*, 14(12):1262–1268, dec 2015.

[183] Peter Kirwan, Benita Turner-Bridger, Manuel Peter, Ayiba Momoh, Devika Arambepola, Hugh P.C. Robinson, and Frederick J. Livesey. Development and function of human cerebral cortex neural networks from pluripotent stem cells in vitro. *Development (Cambridge)*, 142(18):3178–3187, sep 2015.

[184] Rebekah Corlew, Martha M. Bosma, and William J. Moody. Spontaneous, synchronous electrical activity in neonatal mouse cortical neurones. *Journal of Physiology*, 560(2):377–390, oct 2004.

[185] Rustem Khazipov and Heiko J. Luhmann. Early patterns of electrical activity in the developing cerebral cortex of humans and rodents, jul 2006.

[186] Min D. Tang-Schomer, James D. White, Lee W. Tien, L. Ian Schmitt, Thomas M. Valentin, Daniel J. Graziano, Amy M. Hopkins, Fiorenzo G. Omenetto, Philip G. Haydon, and David L. Kaplan. Bioengineered functional brain-like cortical tissue. *Proceedings of the National Academy of Sciences of the United States of America*, 111(38):13811–13816, sep 2014.

[187] Steven M. Wellman and Takashi D.Y. Kozai. Understanding the Inflammatory Tissue Reaction to Brain Implants to Improve Neurochemical Sensing Performance, dec 2017.

[188] Takashi D Y Kozai, Andrea S Jaquins-Gerstl, Alberto L Vazquez, Adrian C Michael, and X Tracy Cui. Brain Tissue Responses to Neural Implants Impact Signal Sensitivity and Intervention Strategies.

[189] Natalia Lago, Ken Yoshida, Klaus P. Koch, and Xavier Navarro. Assessment of biocompatibility of chronically implanted polyimide and platinum intrafascicular electrodes. *IEEE Transactions on Biomedical Engineering*, 54(2):281–290, 2007.

[190] Amy E. Rochford, Alejandro Carnicer-Lombarte, Vincenzo F. Curto, George G. Malliaras, and Damiano G. Barone. When Bio Meets Technology: Biohybrid Neural Interfaces. *Advanced Materials*, 1903182:1–17, 2019.

[191] Dmitry Kireev, Viviana Rincón Montes, Jelena Stevanovic, Kagithiri Srikantharajah, and Andreas Offenhäusser. N3-MEA Probes: Scooping Neuronal Networks. *Frontiers in Neuroscience*, 13(APR):320, apr 2019.

[192] Matthew Mcdonald, David Sebinger, Lisa Brauns, Laura Gonzalez-Cano, Yotam Menuchin-Lasowski, Olympia-Ekaterini Psathaki, Angelika Stumpf, Thomas Rauen, Hans Schöler, and Peter D Jones. A mesh microelectrode array for non-invasive electrophysiology within neural organoids. *bioRxiv*, page 2020.09.02.279125, sep 2020.

[193] David A. Soscia, Doris Lam, Angela C. Tooker, Heather A. Enright, Michael Triplett, Piyush Karande, Sandra K.G. Peters, Ana Paula Sales, Elizabeth K. Wheeler, and Nicholas O. Fischer. A flexible 3-dimensional microelectrode array for: In vitro brain models. *Lab on a Chip*, 20(5):901–911, mar 2020.

Acknowledgments

This work would not have been possible without the support and help of many great people. I would therefore like to thank:

Prof. Dr. A. Offenhäusser - for entrusting me with this project, his supervision and all scientific discussions. Thanks for the opportunity to join the IBI-3, which is an inspiring, and always fun place to work.

Prof. Dr. M. Spehr - for being my second referee.

Prof. Dr. A. Pich - for making a great cooperative work possible. Thanks for all the inspiring scientific discussions and input.

Miriam Al-Enezy Ulbrich - for an awesome collaborative work! Thanks for all scientific discussions, but also for funny times in the lab. I enjoyed working with you a lot and I wish you all the best!

Prof. Dr. M. Pieper - for providing assistance with Matlab coding. Thanks a lot for your support and answering all my mathematical and programming questions.

Prof. Dr. R. Merkel - for giving me the opportunity to use the confocal microscope at IBI - 1. Also, I would like to thank Sven Gerlach for the introduction to the microscope and always being around for questions.

Bettina Breuer - million thanks for isolating millions of cells! Thank you for pushing me and

Nicole Terefenko, Shannon Jung and Joscha Graeve - for your committed work at this project. Nicole Terefenko for the help in establishing Collagen into the hybrid hydrogel system. Shannon Jung for the support at the DWI Aachen, with all chemical and rheological characterizations. Joscha Graeve for the evaluation of Fibrin hydrogels and his current work on electrophysiological measurements. always being around. Big thanks!

Dr. Kathrin Zobel - for being my supervisor at the beginning of my time in Jülich. Thanks for giving me the opportunity to step into this deeply interesting topic, and for all the scientific discussions and input.

Dr. V. Maybeck - for all the inspiring scientific discussions and always being around for questions.

Thorsten Auth and BioSoft - for the opportunity to join the IHRS BioSoft graduate school. Thanks for all the rewarding presentations and advanced trainings. Also thanks to all fellows for inspiring discussions and fun times.

The whole IBI-3 - Especially I would like to thank Nafiseh, Kagithiri, Lena, Viviana, Ekatharina, Pegah, Frano, Chris, Timm, Jamal and Dominik, for scientific discussions, but also lots of nice lunch-breaks and funny times aside work.

My close friends - Especially I would like to thank Maren and Dominique for all the lunch-breaks and walks. Also I would like to thank Chris and Anni. Thank you all, for your private support, motivation and always being around.

Most of all I would like to thank my parents and my brother - for the support during my whole life! Thanks for always encouraging me to reach whatever I aim for. Also thanks to my brother and Hanna for proofreading.

Band / Volume 70
Nanoscale four-point charge transport measurements in topological insulator thin films
A. Leis (2021), ix, 153 pp
ISBN: 978-3-95806-580-2

Band / Volume 71
Investigating the Interaction between π-Conjugated Organic Molecules and Metal Surfaces with Photoemission Tomography
X. Yang (2021), xviii, 173 pp
ISBN: 978-3-95806-584-0

Band / Volume 72
Three-Dimensional Polymeric Topographies for Neural Interfaces
F. Milos (2021), 133 pp
ISBN: 978-3-95806-586-4

Band / Volume 73
Development, characterization, and application of compliantintracortical implants
K. Srikantharajah (2021), xiv, 155, xv-xvii pp
ISBN: 978-3-95806-587-1

Band / Volume 74
Modelling, implementation and characterization of a Bias-DAC in CMOS as a building block for scalable cryogenic control electronics for future quantum computers
P. N. Vliex (2021), xiv, 107, xv-xxviii pp
ISBN: 978-3-95806-588-8

Band / Volume 75
Development of Electrochemical Aptasensors for the Highly Sensitive, Selective, and Discriminatory Detection of Malaria Biomarkers
G. Figueroa Miranda (2021), XI, 135 pp
ISBN: 978-3-95806-589-5

Band / Volume 76
Nanostraw- Nanocavity MEAs as a new tool for long-term and high sensitive recording of neuronal signals
P. Shokoohimehr (2021), xi, 136 pp
ISBN: 978-3-95806-593-2

Band / Volume 77
Surface plasmon-enhanced molecular switching for optoelectronic applications
B. Lenyk (2021), x, 129 pp
ISBN: 978-3-95806-595-6

Band / Volume 78
Engineering neuronal networks in vitro: From single cells to population connectivity
I. Tihaa (2021), viii, 242 pp
ISBN: 978-3-95806-597-0

Band / Volume 79
Spectromicroscopic investigation of local redox processes in resistive switching transition metal oxides
T. Heisig (2022), vi, 186 pp
ISBN: 978-3-95806-609-0

Band / Volume 80
Integrated Control Electronics for Qubits at Ultra Low Temperature
D. Nielinger (2022), xviii, 94, xix-xxvi
ISBN: 978-3-95806-631-1

Band / Volume 81
Higher-order correlation analysis in massively parallel recordings in behaving monkey
A. Stella (2022), xiv, 184 pp
ISBN: 978-3-95806-640-3

Band / Volume 82
Denoising with Quantum Machine Learning
J. Pazem (2022), 106 pp
ISBN: 978-3-95806-641-0

Band / Volume 83
Hybrid hydrogels promote physiological functionality of long-term cultured primary neuronal cells in vitro
C. Meeßen (2022), x, 120 pp
ISBN: 978-3-95806-643-4

Information
Band / Volume 83
ISBN 978-3-95806-643-4

Mitglied der Helmholtz-Gemeinschaft

JÜLICH
Forschungszentrum